UNIVERSITY OF NAIROBI

DEPARTMENT OF MECHANICAL AND MANUFACTURING ENGINEERING

EXTRACTION AND EVALUATION OF THE FUEL PROPERTIES OF TYRE PYROLYSIS OIL

BY:

Job Bosire Omwoyo (F56/12755/2018)
B.Sc. Mechanical Engineering (The University of Nairobi)

A Thesis submitted in partial fulfillment of the requirements for the degree of Master of Science in Mechanical Engineering, in the Department of Mechanical and Manufacturing Engineering of The University of Nairobi

MAY 2022

DECLARATION

I declare that this thesis is my original work and has not been presented for a degree in any other university.

Job Bosire Omwoyo F56/12755/2018

Sign: BOSIRE Date: 22/08/2022

This thesis has been submitted for examination with our approval as university supervisors.

Dr. Richard Kyalo Kimilu Sign: Date: 22/08/2022

Department of Mechanical Engineering,

University of Nairobi,

P.O. Box 30197-00100,

Nairobi, Kenya.

Prof. John Mmari Onyari Sign: Date: 22/08/2022

Department of Chemistry,

University of Nairobi,

P.O. Box 30197-00100,

Nairobi, Kenya.

DEDICATION

I am proud to dedicate this thesis to my parents, Mr. and Mrs. Omwoyo and my brother Duncan Ndege for their support and patience during the entire period of my studies.

ACKNOWLEDGEMENT

This project's success can be owed to a few people who volunteered to help.

First and foremost, I want to thank my first supervisor, Dr. R. K. Kimilu, for suggesting the research topic for me as well as providing assistance and direction during the project. I'm particularly grateful to the second supervisor, Prof. J. M. Onyari, for his advice and valuable insights into the study. Even though it may have seemed impossible to some, I am grateful for the opportunity to participate in this research.

Second, I appreciate the help I received from the Mechanical and Manufacturing Engineering department's entire personnel, particularly Mr. Kigeni and Mr. Kimani, who worked relentlessly with me. I'm also grateful to Mr. Mwangi of the Department of Chemistry's Physical Chemistry Laboratory for supporting me with experimental setups.

Third, I appreciate the encouragement to progress with the project from Dr. Aganda when I was at a point of abandoning my studies. I also appreciate Dr. Kivindu who used to instruct me to work on the project on a daily basis.

Finally, special thanks go to my brother, Duncan Ndege and my parents for their inspiration and financial support. Even if it was very strenuous on their side and I overstayed in school, they never gave up on supporting me.

UNIVERSITY OF NAIROBI

Declaration of Originality Form

This form must be completed and signed for all works submitted to the University for Examination.

Name of Student JOB BOSIRE OMWOYO
Registration Number F56/12755/2018
Faculty ENGINEERING
Department MECHANICAL ENGINEERING
Course Name MSC MECHANICAL ENGINEERING
Title of the work

EXTRACTION AND EVALUATION OF THE FUEL PROPERTIES OF TYRE PYROLYSIS OIL

DECLARATION

1. I understand what plagiarism is and I am aware of the University's policy in this regard
2. I declare that this THESIS is my original work and has not been submitted elsewhere for examination, award of a degree or publication. Where other people's work, or my own work has been used, this has properly been acknowledged and referenced in accordance with the University of Nairobi's requirements.
3. I have not sought or used the services of any professional agencies to produce this work.
4. I have not allowed and shall not allow anyone to copy my work with the intention of passing it off as his/her own work.
5. I understand that any false claim in respect of this work shall result in disciplinary action in accordance with University Plagiarism Policy.

Signature BOSIRE
Date 10/05/2022

ANTI-PLAGIARISM STATEMENT

This thesis has been written by me in my own words, except for the quotations from published and unpublished sources which have clearly been indicated and acknowledged. I am aware that the incorporation of material from other works or paraphrase of such material without acknowledgement will be treated as plagiarism, subject to the custom and usage of the subject, according to the regulation on conduct of examinations.

Name	Signature	Date
Job Bosire Omwoyo	BOSIRE	25/4/2022

TABLE OF CONTENTS

DECLARATION i
DEDICATION ii
ACKNOWLEDGEMENT iii
ANTI-PLAGIARISM STATEMENT v
LIST OF SYMBOLS x
LIST OF FIGURES xi
LIST OF TABLES xiii
ABSTRACT xiv
LIST OF ABBREVIATIONS xii
CHAPTER ONE: INTRODUCTION 1
1.1 Background information 1
1.2 Problem Statement 2
1.3 General Objective 3
1.3.1 Specific Objectives 3
1.4 Scope and Limitations 3
CHAPTER TWO: LITERATURE REVIEW 4
2.1 Introduction 4
2.2 Tyre Composition 4
2.3 Pyrolysis 5
2.3.1 Types of Pyrolysis 6
2.3.2 Products of Pyrolysis 8
2.3.3 Advantages and Disadvantages of Pyrolysis 10
2.4 Pyrolysis Reactors 10
2.5 Tyre pyrolysis oil production 12
2.6 Factors Affecting Products of Pyrolysis 13
2.7 Fuel characterization 16
2.7.1 Density 17
2.7.2 Kinematic viscosity 18
2.7.3 Calorific value 19

2.7.4 Cetane rating 20
2.7.5 Pour point 21
2.7.6 Flash point 21
2.7.7 Water 22
2.7.8 Sulphur Content 22
2.7.9 pH 22
2.7.10 Lubricity 23
2.8 Chemical Analysis 23
2.9 Summary of the Literature Review 24
CHAPTER THREE: METHODOLOGY 25
3.1 Introduction 25
3.2 Overview of the Design 25
3.3 Materials selection and design procedures 26
3.3.1 Heat Supplying Unit 26
3.3.2 Batch Type Reactor 26
3.3.3 Volatile Product Tube 32
3.3.4 Water Cooled Condensing Unit 35
3.3.5 Water Cooled Condensing Unit stand 37
3.3.6 Oil Collector 43
3.3.7 Pressure Connector tube 43
3.4 Extraction of Tyre Pyrolysis Oil 43
3.4.1 Raw Materials Collection and Preparation 44
3.4.2 Extraction and Collection of Tyre Pyrolysis Oil 44
3.5 Determination of Physical and Chemical Properties of Pyrolysis Oil 45
3.5.1 Specific Gravity 45
3.5.2 Kinematic Viscosity 46
3.5.3 Calorific Value 48
3.5.4 Flash Point 49
3.5.5 Sulphur Content 49
3.5.6 pH 49
3.5.7 Cetane Index 50

3.5.8 Fourier Transformation Infrared Spectroscopy (FT-IR) 50
3.5.9 Gas Chromatography and Mass Spectrometry (GC-MS) 50
3.6 Summary of the Chapter 51
CHAPTER FOUR: RESULTS AND DISCUSSIONS 52
4.1 Introduction 52
4.2 Design and Fabrication of the Pyrolysis System 52
4.2.1 Design Specifications of the Pyrolysis System 52
4.2.2 Reactor 53
4.2.3 Water Cooled Condenser 53
4.2.4 Condenser Stand 54
4.2.5 Volatile Product Tube 54
4.2.6 Pressure Gauge Tube 55
4.2.7 Assembled Structure of a Pyrolysis System 55
4.3 Oil Extraction 56
4.4 Physico-chemical properties 57
4.4.1 Specific Gravity 57
4.4.2 Kinematic viscosity 62
4.4.3 Calorific value 66
4.4.4 Flash point 68
4.4.5 Sulphur content 70
4.4.6 pH 71
4.4.7 Cetane Index 73
4.4.8 Fourier transformation infrared analysis (FTIR) 75
4.4.9 Gas chromatography and mass spectrometry (GC-MS) 80
4.5 Summary of the Chapter 91
CHAPTER FIVE: CONCLUSIONS AND RECOMMENDATIONS 92
5.1 Conclusions 92
5.2 Recommendations 93
REFERENCES 94
LIST OF PUBLICATIONS FROM THIS RESEARCH 119
APPENDIX A TECHNICAL DRAWINGS 120

APPENDIX B FABRICATED COMPONENTS 124
APPENDIX C GROSS COMBUSTION VALUES FOR SOME COMMONLY USED MATERIALS 126
APPENDIX D OPERATION AND MAINTENANCE OF THE PYROLYSIS SYSTEM. 127
APPENDIX E SAMPLE CALCULATIONS 131

LIST OF SYMBOLS

σ_a	$Axial\ stress.$
σ_c	$Circumferential\ stress.$
σ_{uts}	Ultimate tensile Strength
σ_y	Yield Stress
τ_w	$Shear\ Stress\ at\ the\ Wall$
μ	$Dynamic\ Viscosity$

LIST OF FIGURES

Figure 2. 1 Structural formulae for rubber compounds 5
Figure 2. 2 Steps of pyrolysis process. 5
Figure 2. 3 Pyrolysis products and applications 9
Figure 3. 1 The schematic diagram of the pyrolysis system that was fabricated..... 25
Figure 3. 2 The sketch of a condenser stand. 37
Figure 3. 3 Sketch of Ostwald Viscometer 47
Figure 4. 1 Batch type reactor (Part No. 001). 53
Figure 4. 2 Water Cooled Condenser with oil collector (Part No. 002). 53
Figure 4. 3 Condenser Stand (Part No. 003). 54
Figure 4. 4 Connection Tube (Part No. 004). 54
Figure 4. 5 Pressure Gauge Tube (Part No. 005). 55
Figure 4. 6 Physical structures designed and fabricated pyrolysis system. 55
Figure 4. 7 Variation of TPO yield with the percentage of sodium carbonate used. 56
Figure 4. 8 Variation of specific gravity with temperature for TPO and Diesel Fuel. 58
Figure 4. 9 Specific gravity regression lines for diesel fuel, TPO, and TPO with catalyst as a function of temperature. 60
Figure 4. 10 Specific gravity regression lines as a function of the amount of sodium carbonate utilized at various fuel temperatures. 61
Figure 4. 11 TPO and Diesel Fuel Kinematic Viscosity Variation with Temperature. 63
Figure 4. 12 Specific gravity regression lines for diesel fuel, TPO, and TPO with catalyst as a function of temperature. 64
Figure 4. 13 The effect of increasing the amount of sodium carbonate on viscosity at various temperatures. 66
Figure 4. 14 Variation of calorific value of TPO with the percentage of sodium carbonate.. 67
Figure 4. 15 Variation of Flash point value of TPO with the percentage of sodium carbonate. 69
Figure 4. 16 Variation of Sulphur content in TPO with the percentage of sodium carbonate.70
Figure 4. 17 Variation of pH value of TPO with the percentage of sodium carbonate. 72
Figure 4. 18 Variation of Cetane index of TPO with the percentage of sodium carbonate.... 74
Figure 4. 19 FTIR transmittance spectrum for diesel fuel. 76
Figure 4. 20 FTIR transmittance spectrum for tyres pyrolytic oil without catalyst. 76
Figure 4. 21 FTIR transmittance spectrum for TPO with 1.5% catalyst. 77
Figure 4. 22 FTIR transmittance spectrum for tyres pyrolytic oil with 2.5 % catalyst. 77
Figure 4. 23 FTIR transmittance spectrum for used tyres pyrolytic oil with 5 % catalyst. 77
Figure 4. 24 FTIR transmittance spectrum for used tyres pyrolytic oil with 7.5 % catalyst. .....**Error! Bookmark not defined.**
Figure 4. 25 FTIR transmittance spectrum for used tyres pyrolytic oil with 10 % catalyst. .. 78
Figure 4. 26 GC-MS chromatogram for tyre pyrolysis oil without catalyst. 83
Figure 4. 27 GC-MS chromatogram for tyre pyrolysis oil with 1.5 % catalyst. 84

Figure 4. 28 GC-MS chromatogram for tyre pyrolysis oil with 2.5 % catalyst..... 85
Figure 4. 29 GC-MS chromatogram for tyre pyrolysis oil with 5 % catalyst..... 86
Figure 4. 30 GC-MS chromatogram for tyre pyrolysis oil with 7.5 % catalyst..... 87
Figure 4. 31 GC-MS chromatogram for tyre pyrolysis oil with 10 % catalyst..... 88
Figure 4. 32 GC-MS chromatogram for diesel fuel..... 89

LIST OF TABLES

Table 2. 1 The percentage weight distribution of various tyre components 4
Table 3. 1 The mechanical properties of structural steel of 0.15 to 0.25 % carbon..... 28
Table 3. 2 Buckling of columns with different supports 40
Table 3. 3 Minimum weld properties..... 41
Table 3. 4 Stresses that are permitted by AISC code for mild steel weld metal..... 42
Table 3. 5 Fatigue strength reduction factor 42
Table 4. 1 Design specifications of the pyrolysis system 52
Table 4. 2 Mass percentage of pyrolysis products..... 56
Table 4. 3 Values of specific gravity at different temperatures for TPO and Diesel fuel 58
Table 4. 4 The linear square regression constants and coefficients for specific gravity as a function of temperature for the oil samples. 59
Table 4. 5 The regression coefficients and square regression constants for Specific gravity as a function of sodium carbonate used during pyrolysis for some temperatures..... 61
Table 4. 6 Values of kinematic viscosities at different temperatures for TPO and Diesel fuel 62
Table 4. 7 Constants of viscosity correlation and coefficients of determination..... 64
Table 4. 8 The regression coefficients and the square regression constants for kinematic viscosity as a function of sodium carbonate percentage used for different temperatures. 65
Table 4. 9 Table 4.9 Calorific values of Diesel fuel and TPO in relation to the percentage of sodium carbonate 67
Table 4. 10 Flash point values of Diesel fuel and TPO in relation to the percentage of sodium carbonate 68
Table 4. 11 Sulphur content in diesel and TPO in relation to the percentage of sodium carbonate 70
Table 4. 12 The pH values of diesel and TPO with the respective percentage of sodium carbonate 72
Table 4. 13 The Cetane index values of diesel and TPO with the respective percentage of sodium carbonate 73
Table 4. 14 The indicated functional groups in tyre pyrolysis oils and diesel fuel 79
Table 4. 15 Proportions of aromatics and aliphatic compounds in diesel fuel and tyre pyrolysis oils..... 90

ABSTRACT

The environmental degradation as a result of waste disposal and the energy crisis are some of the problems mankind is currently facing. It has resulted in the utilization of appropriate technologies that enable energy recovery from non-conventional sources. These may include recycling of waste material to get energy. Worn-out tyres are some of the waste material around us. Whereas they can't be remolded to any form, they contain high amounts of energy that can be recovered. The objective of this research was to extract and evaluate the fuel properties of oil obtained by pyrolising waste tyres. A batch type pyrolysis system was designed and fabricated. It was then used in the extraction of tyre pyrolysis oil.

Waste tyres were collected and cut into pieces with cross-sections of 2-3 cm wide and then fed into the reactor chamber. It was locked and then heated by a crucible furnace to a temperature between 530 ^{0}C and 570 ^{0}C. Heating was continued till no visible flow of gases was observed. This ensured that all possible gaseous and liquid products had exited the reactor, indicating completion of pyrolysis. The gases were condensed to obtain a liquid fraction of the pyrolysis gases, while the non-condensable fraction was fed back to the furnace as fuel. The collected pyrolytic oil was then weighed. To evaluate the effect of catalyst on the pyrolysis products, the same procedure was repeated with feed material being mixed with sodium carbonate as a catalyst in percentages of 1.5 %, 2.5 %, 5 %, 7.5 % and 10 %.

The chemical and physical properties of tyre pyrolysis oil were assessed. Evaluation of the effects of a catalyst on the collected oil samples was carried out as well. Specific gravity was found to increase with the increase in catalyst from 0.92167 to 0.95071 while calorific value, flash point, sulphur content, and Cetane index were decreased 40.431 to 39.182 MJ/kg, 51 to 32 ^{0}C, 8443 to 1689 mg/kg and 12.72 to 3.66 respectively. Kinematic viscosity was decreasing with the increase of catalyst up to when the catalyst was 2.5 % from 3.04924 to 2.51894 cSt and started to increase proportionally with it, while pH was increasing with the increase of catalyst up to when the catalyst was 5 % 6.93 to 8.12 and started to decrease.

The analysis of hydrocarbons present in the resulting tyre pyrolysis oil was carried out by the use of a gas chromatography and mass spectrometry (GC-MS) test. Functional groups were also analyzed using Fourier transformation analysis (FTIR). It was found from FTIR and GC-MS analyses, that the TPO samples produced by both catalytic and thermal pyrolysis were complex mixtures of aliphatic, aromatics, nitrogen and oxygen containing compounds with carbon content ranging between C_4 and C_{45}. The TPO was found to contain aliphatic compounds that were similar to the ones contained in diesel fuel.

The use of a catalyst was found to increase the oil yield and reduce the amount of Sulphur content in the oil. The change of the structure of the oil was found to make the oil not fit for its usage in a diesel engine when considering its Cetane index. Ways of improving the structure e.g. hydrogenation can be explored for its usability in a diesel engine.

LIST OF ABBREVIATIONS

AISC	American Institute of Steel Construction
Al_2O_3	Aluminium Oxide
ASTM	American Society of Testing Materials
AWS	American Welding Society
BR	butadiene rubber
BTX	Benzene, Toluene and Xylene
$CaCO_3$	Calcium Carbonate
CI	Compression Ignition
CO	Carbon Monoxide
CO_2	Carbon Dioxide
d	$Diameter\ of\ the\ cylinder.$
dr	$Change\ in\ Radius$
du	$Change\ in\ Velocity$
DF	Diesel Fuel
E	Young's Modulus
E_A	$Activation\ Energy$
FCC	Fluid Catalytic Cracking
FT-IR	Fourier Transformation Infrared
GCV	Gross Calorific Value
GC	Gas Chromatography
$H_{fussion}$	Specific latent heat of fusion.
H_{liquid}	Heat for raising temperature from melting point to flow temp per kg.
H_{solid}	Heat for raising the temperature of aluminum to melting point per kg.
H_T	Heat transferred
HC	Hydrocarbons
HFFR	High-Frequency Reciprocating Rig
HR	Heating Rate
H_2S	Hydrogen Sulfide
KCL	Potassium Chloride Plates

LCO	Light Cycle Oil
MgO	Magnesium Oxide
MS	Mass Spectrometry
Na_2CO_3	Sodium Carbonate
NR	Natural rubber
p	$Internal\ pressure.$
PAH	Polycyclic Aromatic Hydrocarbons
PP	Pour Point
Ru	$Universal\ Gas\ Constant$
$s.f.$	$Safety\ Factor.$
SBR	Styrene-butadiene rubber
T	$Temperature$
t	$Thickness\ of\ the\ cylinder$
TPO	Tyre Pyrolysis Oil
r	Radius
$r.f.$	$Retention\ Factor$
USY	Ultra-Stable Y-type Zeolite
VGO	Vacuum Gas Oil
WLO	Waste Lubrication Oil
ZSM	Zeolite Socony Mobil

CHAPTER ONE: INTRODUCTION

1.1 Background information

The environmental degradation and energy crisis are some of the problems mankind is currently experiencing. These issues are due to population growth, rapid industrialization and large amounts of waste material generated on a daily basis as a result of different activities. There is instability in world fuel markets and depletion of oil reserves. Hence, different attempts have been made to find alternatives to fossil fuels [1], [2]. This situation has resulted in the use of suitable technology for recovering fuels using non-conventional processes, and the process of recycling waste materials to get energy being one of them [3]. Used tyres are some of the waste material around us.

Worn out car tyres can be used to make footwear, but they are limited to sections that don't contain wires. Handles for some hand tools (e.g. panga machete, slasher and knifes) can be made up of pieces of tyres, but there are always pieces of tyres which will remain after their usage. They will need to be disposed of when they have no other use, and some individuals will burn them in order to reduce their quantity. Disposable tyres can also be used in landscaping in some areas, but the quantity of disposable tyres available exceeds what can be used. Tyres will always continue to be produced as long as there are vehicles running on the roads.

Natural rubber trees are a source of latex, which is the base material for tyres [4]. Latex is extracted by slicing a thin strip of bark and allowing it to seep into a collecting jar for several hours [5]. The rubber tree is mainly cultivated to produce latex, which is the basis material for various rubber products, e.g. tyres [6].

Rubber is an elastic material with the ability to greatly alter its dimensions dramatically when stress is applied and withdrawn [7], [8]. Rubber is also an isoprene polymer, which has double bonds between the monomers. Carbon black is another primary component of tyre rubber. In the manufacture of tyres, sulfur and other chemicals are used. Tyres contain approximately 20 different metal elements that cannot be destroyed by fire. Zinc is one of the metals present in tyres in large quantities, since zinc oxide is used in the process of vulcanization [4], [8].

Each year, an estimated 1,500,000,000 tyres are manufactured around the world, and the vast majority of them end up as waste tyres [9]–[11]. Tyres are made up of complex chemically cross-linked polymers. This makes remolding them into various shapes without significant degradation after they've been worn out difficult [12]–[14]. Disposed tyres present difficulties in land filling and do not degrade easily because their disposal and reprocessing are also difficult due to the same property that makes them attractive as tyres. The use of waste materials as a renewable energy source has become one of the possible ways of managing disposable tyres [15]. Worn out tyres can be retreaded and reused, but the resulting tyres are of low quality [16], and in the end, they will be disposed of as waste material [14].

Another feature of tyres is their tolerance to biological degradation [13], [17]–[19] which makes them resistant to harsh environmental conditions such as bacteria, friction, ozone exposure, and light [17]. Therefore, a threat to safety and environmental degradation is the indiscriminate discarding and stockpiling of worn out tyres. Tyres have a low density, with an empty space that accounts for approximately 75% of their total volume. Therefore, they occupy a greater amount of productive land space when piled up [20]. As a result, given the issues associated with disposing of used tyres, recycling them is the most viable option. Pyrolysis is one of the processes for decomposing used tyres into valuable materials and energy that is environmentally friendly [16], [21].

1.2 Problem Statement

The disposal of waste tyres is a problem to our environment. Landfilling of waste tyres is not a practical solution for rapidly increasing quantities of tyres since its decomposition is difficult. Some people have tried to burn the tyres in order to get the scrap metal, releasing harmful gases into the atmosphere and causing air pollution. The chemical energy that is contained in these tyres is not transformed to any useful form.

The calorific value of the tyres is between 33 and 40 MJ/kg [16], [22]–[27]. Hence, the energy that is available in them can be extracted and converted into a useful form. One of the ways of recovering energy from tyres is pyrolysis, in the form of tyre pyrolysis oil (TPO). Thermochemical decomposition of waste tyres may be carried out in a pyrolysis reactor. Product yield (in terms of solid, liquid and gas) can be varied by changing process parameters.

The tyre pyrolysis oil has been characterized by a high sulphur content which is above the required set standards for a diesel fuel [4], [14], [35]–[39], [27]–[34], which needs to be lowered [33], [36]–[38] and sodium carbonate was used in percentages of 1.5 %, 2.5 %, 5 %, 7.5 %, and 10 %. The sodium carbonate had an impact on the other fuel properties which needed to be assessed.

1.3 General Objective

The general objective of this project was to extract and carry out the evaluation of the fuel properties of tyre pyrolysis oil.

1.3.1 Specific Objectives

1. To design and fabricate a batch type pyrolysis system.
2. To determine the effect of a catalyst on the oil yield (sodium carbonate).
3. To evaluate the physico-chemical properties of the extracted TPO and compare them with diesel fuel.

1.4 Scope and Limitations

The scope of this research involved designing and fabricating a pyrolysis system, extraction of oil from tyres, and determination of the physico-chemical properties of TPO. Analysis of functional groups and hydrocarbons present in TPO was also carried out.

A study on lubricity could not be carried out since the High-Frequency Reciprocating Rig (HFFR) was not locally available. Cetane number could not be determined since the Cetane engine was not available, but Cetane index was determined, which was comparable to Cetane number. Elemental analysis was not carried out since the carbon/hydrogen/sulphur analyzer was not available locally as well. Storage stability could not be assessed since there was no equipment to carry out the test.

CHAPTER TWO: LITERATURE REVIEW

2.1 Introduction

Since the discovery of pyrolysis, researchers have been engaged in tyre pyrolysis in order to make better use of the resulting products. This chapter covers the composition of tyres, various reactors that have been used in pyrolysis, the pyrolysis process, factors affecting tyre pyrolysis, and tyre pyrolysis (TPO) characterization. Tyre pyrolysis has been done by looking at factors affecting tyre pyrolysis which end up dictating the type of reactors to be used. TPO characterization has also been done to assess the effects of the various factors during pyrolysis.

2.2 Tyre Composition

Natural rubber (NR), styrene-butadiene rubber (SBR) and butadiene rubber (BR) are the main components of tyres [37], [40]. Rubber is made up of two or three rubber compounds with additives. The tread consists of the blends SBR and NR, combined with oils, carbon black, and elements of vulcanization. The sidewall materials are made out of a combination of NR/BR. It is possible to differentiate the structural components of rubber from each other, but their principal structures are similar [41]. The percentage weight distribution of various tyre components is presented in Table 2.1.

Table 2. 1 The percentage weight distribution of various tyre components [42]

Tyre components	Percentage
Natural rubber	15-19
Carbon black	24-28
Synthetic rubber	25-29
Steel cords	9-13
Textile cords	5-6
Chemical additives	14-15

The principle components of the considered rubbers are hydrocarbons that mainly consist of carbon and hydrogen. These hydrocarbons form polymers made of multiple low molecular weight units or monomers, which have low molecular weight compounds. The structure of polymers usually consists of 1000-20000 repeated units of hydrocarbon monomers

that are either single or double bonded [40]. Natural rubber is a polymer composed of units of styrene, isoprene, isobutyl and butadiene, while SBR consists of units of styrene, alkane and alkene [41]. The structure of the rubber compounds is as shown in the schemes of Figure 2.1.

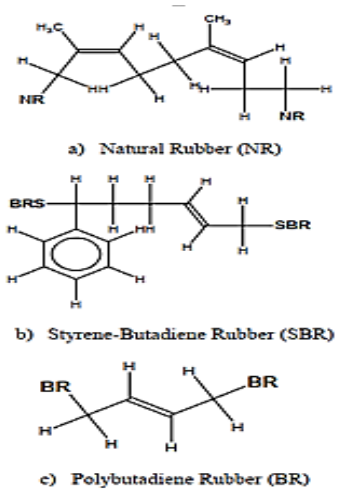

Figure 2. 1 Structural formulae for rubber compounds [43], [44]

2.3 Pyrolysis

Pyrolysis is a chemical reaction involving the breakdown of long chains of hydrocarbons into smaller chains using heat in the absence of oxygen [16], [45]–[47]. The products of this thermal decomposition are in liquid, solid and gaseous states [48]–[51]. Figure 2.2 shows the steps of the pyrolysis process.

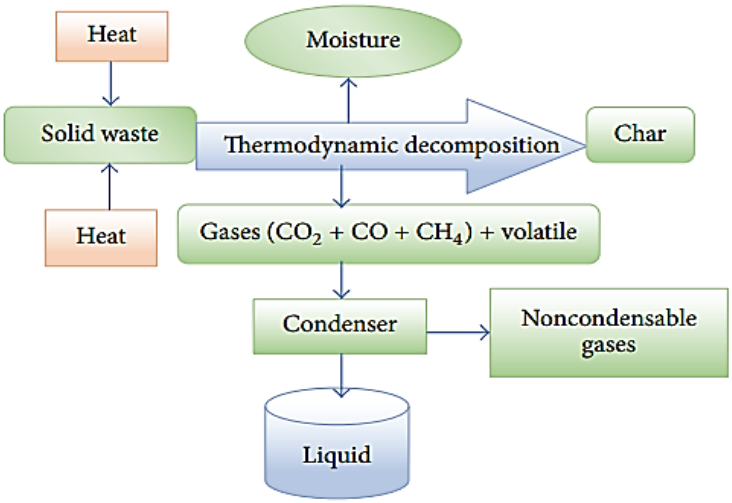

Figure 2. 2 Steps of pyrolysis process [52].

2.3.1 Types of Pyrolysis

The pyrolysis process can be conducted under various conditions of operation that can be used in its classification. They include the steps taken, the time of residence of the pyrolysis material in the reactor, the temperature of processing, the material fed, the size of the feed particle and the heating rate. Pyrolysis is therefore classified as follows:

Slow pyrolysis: It is usually characterized by a heating rate of (0.1-1) ^{0}C/sec, a reactor feed material residence period ranges from 450-550 seconds (7.5-9 minutes) and the size of the feed particle is (5-50) (mm) with operating temperature between (550-950) ^{o}C [53]. This method optimizes the production of charcoal and gas. The production of high-quality oil is unlikely [53], [54]. This is due to the long duration of residence that is advantageous to the secondary reaction, i.e. the primary cracking of the commodity takes place, adversely affecting the consistency and yield of bio-oil [51], [53].

Fast pyrolysis: The feed material is rapidly heated to the required temperature in an oxygen-free environment with a short duration of residence for the volatile product in the reactor [53], [55]. It has a heating rate of (10-200) ^{0}C/sec and a product residence time of (0.5-10) seconds. The feed particle size is less than 5 mm. The products of pyrolysis are cooled very fast after their elimination from the reaction chamber. The optimal reaction temperature is between 400–500 °C [55]. This process produces mainly liquid fuel [51], [54], [56]–[58]. Its investment costs are low and energy efficiency is high, particularly on small-scale setups [53].

Flash pyrolysis: Flash pyrolysis is defined by a residence duration of less than 0.5 seconds and a heating rate of 200 ^{0}C/s [53], [59]. These conditions prevent vapor from breaking into non-condensable gases, improving liquid product yield [59]. The feed material particle size is smaller than 0.2 mm, and the reaction temperature is greater than 1000 ^{0}C. It has low thermal stability, with solids in oil and pyrolytic water production [53].

Catalytic pyrolysis: The use of a catalyst is included in this pyrolysis process. When cracking large molecular weight hydrocarbons into smaller hydrocarbons, the catalyst improves the reaction kinetics of pyrolysis. Using a catalyst in the tyre pyrolysis process has a major impact on product structure, consistency, and yield [53]. The use of zeolite catalysts, ZSM-5 and USY [60], decreases the oil yield and increases the yield of gases [60], [61]. The use of Al_2O_3 as a catalyst leads to an increase in the yield of liquid with a decrease in the yield

of gas [62]. The catalyst can be added to the feedstock before it is introduced into the reactor, or it can be added after the feed has been heated in the reactor or another reactor downstream of the pyrolysis reactor.

Ablative pyrolysis: Ablation is a process that occurs when a solid is subjected to a high density of external heat flux, giving rise to continuous and rapidly eliminated solids, liquids and gases. In performing the rapid pyrolysis of the feed material such as tyres, ablation may be used. Concentrated radiation (contact or radiant ablative pyrolysis) is pressed against a hot surface or intercepted by the feed material [61], [63]. This process needs a highly sophisticated system and is less used.

Plasma pyrolysis: Plasma pyrolysis consists of four steps, including extremely quick particle heating from a plasma jet, immense volatile material emissions, ultra-fast homogeneous phase gasification, and rapid heating and exchange of mass. Thermal plasma pyrolysis has several advantages, including a high rate of heat transfer, desirable end-product properties, and a high capability for the removal and destruction of harmful substances. The resulting products of plasma pyrolysis are: char and gas. This is due to the discharge from plasma of vast amounts of highly active compounds, including free radicals, ions, activated atoms and molecules. From the volatile material of the tyres, heavy hydrocarbon compounds are released and easily cracked (decomposed), resulting in hydrogen and lighter hydrocarbons. Thermal plasma pyrolysis reactors need a high supply of energy to achieve high temperatures [64]. It is appropriate for the pyrolysis of harmful materials.

Molten salt pyrolysis: Salt, such as sodium carbonate, is employed in a turbulent and molten bed. Its primary feature is that hazardous materials are damaged by heat transfer and reaction/scrubbing media. Air under the molten salt's surface is used to inject shredded solid material. Before being released into the environment, hot gases (unreacted air, steam, and CO_2) pass through a molten salt bath, secondary reaction zone, and off-gas cleanup system. The remaining by-products react with inorganic compounds, which are trapped in the melt created by alkaline molten salt. The molten salt contains ash that has been removed from the reactor, cooled and can be deposited in landfills [65]. This type of pyrolysis may be appropriate for hazardous materials.

Co-pyrolysis: This process is characterized by the use of a mixture of reactants which can be either solids or solid and liquid. Solid materials, e.g. tyre crumb, and solvents like waste

lubrication oil (WLO) are fed to the reactor and heated to the required temperature [66]. Co-pyrolysis of tyres and WLO produces more oil than tyres alone. Although adding WLO to pyrolysis oil does not improve tyre deterioration, the density of co-pyrolysis oil is lower than that of commercial diesel. When scrap tyres are added to WLO, the heavy fractions deteriorate faster. An increase in temperature has no significant effect on the composition of co-pyrolysis oil or the distribution of co-pyrolysis oils. Co-pyrolysis oils are better than individual pyrolysis oils. Co-pyrolysis oils contain fewer aromatics compared to tyre-derived oils and fewer heavy fractions compared to WLO-derived oils [67]. Adding WLO to tyres increases linear hydrocarbons (HC) and decreases cyclic HC as observed in chromatography analysis [68].

2.3.2 Products of Pyrolysis

The products of pyrolysis and their composition depend on the feed type. For all polymer based inputs, the main pyrolysis products are significantly identical. The pyrolysis of tyres produces three different types of outputs/products.

Char (solid state): It is generated during the pyrolysis of numerous polymeric materials as a result of secondary polymerization events in the gaseous process [69]. Amorphous carbon and nonvolatile hydrocarbons make up the majority of it. Other components can be employed as additions and fillers and are intimately linked to the polymer matrix composition [70]. The capacity and ease of retrieving the char are proportional to the amount produced. The amount of carbon black previously employed in tyre formulation plus what is formed by the organic matrix's thermal degradation make up the char derived from tyre pyrolysis. The gross calorific value (GCV) of char obtained from tyres is approximately 28-34.32 MJ/kg [28], [71]–[75] making it a decent source of fuel [74]. Char can be used as a source of active carbon raw material and secondary carbon black [75].

Oil distillate (liquid state): This is an aqueous-phase blend of organic compounds with a composition which depends on the type of the process which was used to obtain it (fed material, pressure and temperature and process duration). It consists of low to high molecular weight hydrocarbons, aromatic, and cyclic compounds [69]. Pyrolysis oil can be utilized as a fuel or distilled to produce high-value compounds such as limonene, benzene, xylene (BTX), and toluene. It can also be utilized as an extender oil in rubber formulations; heavier fractions can be employed as road bitumen additives and as a feedstock for coke production. In the

petroleum refining industry, possible end-uses for pyrolysis oil include its usage as an oil feed material for fluid catalytic cracking (FCC) for manufacturing lighter fuels. In order to manufacture olefin-rich gases, thermal cracking is performed on light fuels. Coking is also possible for light fuels to manufacture light coke [76]. It is possible to upgrade liquid fuel to transport fuel or use it directly as a fuel [77]. The gross calorific value of tyre pyrolysis oil is (41-45) MJ/kg [16], [22], [78]–[87], [23], [88], [26], [34], [52], [71]–[74].

Syngas fraction (gaseous state): It is primarily composed of CH_4, H_2 and short chain hydrocarbons (up to C_4/C_5). This also has a non-condensable gaseous fraction of CO, CO_2 and H_2S [77], [88]–[90]. Hydrogen sulphide gas is present due to the sulfur presence included for tyre vulcanization [89]. It has a calorific value of (34-84) MJ/Nm^3 and is usually suitable for use as fuel [21], [22], [91], [31], [34], [71], [73], [78], [88]–[90]. Figure 2.3 shows the products of tyre pyrolysis and their applications.

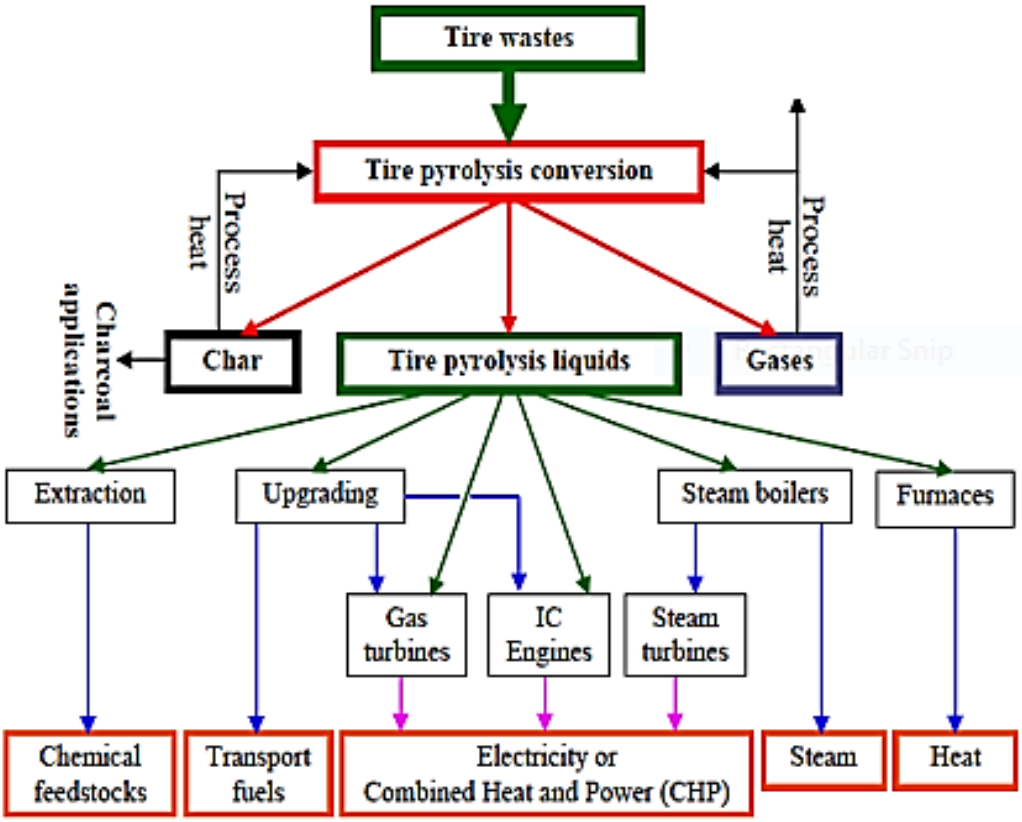

Figure 2. 3 Pyrolysis products and applications [22]

2.3.3 Advantages and Disadvantages of Pyrolysis

Advantages of Pyrolysis [92]

The pyrolysis process is much more appealing when compared with other thermo-chemical processes because it has the following attributes:

1. It is easy to be carried out in any desirable capacity.
2. Corrosive emissions can be reduced and avoided whereby heavy metals and alkali are retained in the residue of the process.
3. The generation of PAHs is less when compared to direct combustion.
4. Pyrolysis unit emissions have minimal impact on air pollution since the largest portion of the gases that are generated by pyrolysis are used as fuel for the system for heat generation at the reactor.
5. The products can be easily managed and exploited separately, in accordance with their final objectives.
6. Using pyrolysis products as secondary raw feed material results in a remarkable reduction in CO_2 emissions into the atmosphere.
7. It enables recycling of disposable tyres which cannot be recycled efficiently using other alternative means.

Disadvantages of Pyrolysis [92]

Problems with many pre-existing pyrolysis technologies include:

1. Non-continuous (using batch type) processes are not commercially viable.
2. There is coking and deposits of carbon on the surfaces of heat exchangers.
3. Sticking of sand particles in the reactor when a fluidized-bed is used.
4. The quality of fuel is unsatisfactory.
5. There is a relatively high content of sulphur in the end products.

2.4 Pyrolysis Reactors

The reactors that are most commonly used are explained as follows:

Batch type Reactors and Semi-Batch type Reactors: They can be built and operated easily. The difference between them, however, is significant. There is a constant flow of inert gas (usually nitrogen) at the reacting temperature in a semi-batch reactor that enables volatile

products to be extracted. The removal of volatile compounds using hot inert gases results, to some degree, in secondary reactions of the main cracking materials. This does not occur in a reactor of the batch type where secondary reactions should be promoted [93]. The batch type reactor is continually purged with an inert gas (nitrogen) at a fixed metered flow rate to remove the generated gases from the reactor and minimize secondary reactions such as thermal cracking, polymerization, and condensation [72], [94].

Fixed-Bed Reactors: The fixed-bed reactor is characterized by a low rate of heating due to its poor coefficient of heat transfer (HR). As a result, when a bigger sample mass is fed into the reactor, the sample temperature is not uniform, and the feedstock decomposes at different temperatures at the same time. The key application of fixed-bed reactors is to define regulating parameters affecting pyrolysis products [95]. Plastics are challenging to use as feed materials due to their low heat conductivity and high viscosity. This causes a serious problem when they are fed to this reactor. In some reactors, the molten polymer from a pressurized tank is fed into the reactor by a capillary tube [96]. Plastic is thermally cracked and the liquid or gaseous compounds that result are quickly fed into the fixed bed [97]. Fixed bed reactors are commonly employed by researchers in the execution of laboratory studies due to their ease of setup and operation. Most reactors are built out of stainless steel [98].

Fluidized-Bed Reactors: These reactors have a high heating rate (HR) and strong mixing, resulting in homogeneous temperature and feed composition [97]. Due to low thermal conductivity and high viscosity of polymers, temperature gradients exist in traditional reactors, preventing proper heat transfer, although the fluidized reactor has a significant advantage [97], [99]. Since the operation of fluidized bed reactors is difficult, only a few studies have been conducted with these reactors [61], [100]. The waste material is fed by gravity at a correctly metered rate through a rotary valve feeder. The pyrolysis's volatile products are cooled in a succession of water-cooled condensers, and the oils are then condensed in a series of cold traps that are kept at various temperatures with a mixture of solid CO-methanol and ice-water [72]. A fluidized bed reactor can be used for fast pyrolysis [61].

Spouted-Bed Reactor: It is an internal recycling reactor that operates with a sufficient catalyst/oil (C/O) ratio at low contact time (1-10) s (e.g. C/O = 6). It has outstanding hydrodynamic properties and effective heat transfer between the sputtered-bed phases. In addition to other features of the reactor’s conical geometry, such as its flexibility in solid and

gas flow rates under isothermal and stable bed conditions [101], it emerges that the plastic waste with normal FCC feed stocks should be subjected directly to cracking in FCC refinery units [102]. Before the reaction begins, the feed is commonly a mixture of 5–10 % plastic in an oil such as vacuum gas oil (VGO), light cycle oil (LCO), or even pure benzene, which is fed to the reactor with a catalyst. The valve is opened after the end of reaction to allow the release of products into the vacuum chamber, where the analysis is carried out [103].

Screw/Rotary Kiln Reactor: It is made up of an inclined cylinder which rotates two types of screw kilns; one is direct fired and the other is indirect fired [61], [63]. These reactors have a hopper at slightly higher pressure than atmospheric. In an inert atmosphere, (nitrogen) plastic or plastic-oil combinations are supplied and heated to temperatures between 250 and 300 ^{0}C using two external furnaces. Subsequently, the melted mixture is inserted into the reactor using a screw into the real reaction zone within a stainless steel tube [104], [105]. The heating system is essentially divided into two heating parts, where a tube is externally heated using two furnaces, the temperature of which can be independently adjusted [105]. When compared to a fixed-bed reactor, the rotary kiln is more effective at heating the feedstock. The inclined kiln's slow rotation achieves successful raw material mixing. There is widespread use of rotary kiln reactors, but they are typically used for slow/conventional pyrolysis, which carries out large product portions of char, liquid and gas under a low HR [95].

Microwave: Thermal energy is applied very rapidly to the input material and uniformly by the microwave, and reaction time is short. The heating efficiency of a microwave is high, and input material with low thermal conductivity can be easily heated. However, any vulcanized rubber fed to the reactor must have a sufficient polar structure to achieve microwave energy absorption at a rate which is appropriate for de-vulcanization [88]. It can be used for fast pyrolysis.

2.5 Tyre pyrolysis oil production

Tyres for pyrolysis are usually cut into pieces of approximately 4 cm^3 and fed to the reactor [22], [27], [84], [106]. The optimum temperature for TPO production is 550 ^{0}C at atmospheric pressure [23], [24], [35], [73], [80], [81], [89], [107]–[109]. Nitrogen gas is usually used as an inert gas which flows continuously through the reactor to carry the gaseous fraction of the products that are being generated during the process of pyrolysis [2], [18], [64], [70], [72],

[84], [94], [95], [106], [108], [19], [22], [25], [27], [35], [45], [51], [57]. Helium can also be used to create an inert environment [110]. The inclusion of nitrogen gas in the non-condensable gases during pyrolysis process, it lowers the gross calorific value of the resulting mixture since it does not participate in combustion.

A simple reactor can be improvised (batch type reactor) where the inert gas is not necessarily required. The choice of the reactor depends on the cost and how the process of pyrolysis is to be carried out. The amount of TPO extracted from tyres ranges between 34% and 58% of the feed material weight [4], [12], [84], [90], [94], [106], [107], [111]–[113], [27], [31], [52], [53], [73], [78], [81], [82]. Tyre pyrolysis is black in colour [114].

2.6 Factors Affecting Products of Pyrolysis

The yield of pyrolytic products is affected by the following operating conditions:

Reactor temperature: Reactor temperature variation affects the ratio of the three pyrolysis products to some extent. At a temperature of 375 ^{0}C, the rubber in a tyre begins to decompose by forming the products of pyrolysis. The solid rubber begins to decrease as liquid and gas begin to form. When pyrolysis temperature is increased, the amount of oil and non-condensable gases that are generated increase while charcoal reduces. The oil yield increases with increase in pyrolysis temperature, up to 550 ^{0}C and starts to decrease with an increase in temperature. Higher temperatures promote pyro-gas yields, while medium temperatures favor char and pyro-oil production. At higher temperatures, a secondary cracking reaction occurs, leading to the breaking of the liquid molecules into gas [22], [24], [25], [29], [46], [56], [57], [115], [116] hence, an increase in pyro-gas yield [117], [118]. There are also simultaneous reactions of thermal cracking which occur at high temperatures which can alter product selectivity hence reducing condensable gases [92]**.**

Particle size of feedstock: A smaller particle size has more reaction surface area to volume ratio. This results in a higher heating rate and a faster reaction taking place compared to a larger particle of the same material [22], [56], [107], [115], [119]. The condensable gases produced will have enough time, which will favor the secondary reactions taking place in the reactor for smaller sizes of feed [107], [117]. In a large particle, heat can only be transferred to a certain depth for a complete reaction when compared to smaller particles within the permissible pyrolysis period. As a result, the larger particle's nucleus becomes carbonized or

does not fully decompose, resulting in lower gas and liquid yields and higher char yields [56], [117], [120]. The optimum size of particles that is required when producing oil is 4 cm^3 [22], [84] with cross-sections of approximately 2-3 cm wide [38], [71], [108]. Heat and mass transfer rates within a particle define the pyrolytic reaction rate, and the apparent kinetic constant is inversely related to particle size [22], [120]. On the other hand, when grinding, to obtain smaller particle sizes requires more energy, and when using smaller-sized particles, the kinetic constant is not affected [121].

Reactor type: The operation temperature and heating rate are dictated by the type of reactor used. The fixed-bed reactor is distinguished by a low heating rate (HR) and is rarely implemented in scale-up systems due to its low coefficient of heat transfer and inefficiency. In feedstock heating, the rotary kiln's efficiency is higher compared to the fixed-bed reactor. A high HR and strong mixing of the feedstock are achieved by fluidized-bed reactors [95].

Feed material composition: The feed material composition determines the properties of the pyrolysis materials. It can also affect the efficiency of the catalysts [92], [95]**.** The composition and brand of a tyre will affect the composition of the resulting tyre pyrolysis oil [90], [117].

Residence time/inert gas flow: As the inert gas flow rate is increased, the residence time for vapor decreases, thereby increasing the rate at which pyrolysis vapor products are evacuated from the reactor. The increase in time residence of gases would result in secondary cracking of primary products of pyrolysis, which would enable a shift in the ratio of gas/liquid resulting in more gases and fewer end products of oil [18], [22], [56], [115], [117], [122]–[124]. Long contact time between char and volatiles leads to a secondary reaction of pyrolysis, resulting in a decrease in the yield of volatiles [18], [22], [56], [117], [122]–[124]. Excessive use of inert gas (nitrogen) leads to dilution of the non-condensable gases that will be collected.

Catalyst: Catalysts of various types have been used in the pyrolysis of waste tyres, with zeolite catalysts being the most commonly used. Due to their shape selectivity and acidity, they promote TPO cracking, resulting in an increase in gaseous products. As a result, the use of various zeolites, such as ZSM-5 and Y, is linked to the production of chemicals which are valuable, such as light olefins and aromatics [9], [11]. When alkaline catalysts such as NaOH, Na_2CO_3, and MgO are used, there is an increase in TPO yield [4], [9], [53] and a change in its structure [53], [111]. As a result, there is increased selectivity towards valuable fractions and

chemicals obtained using suitable catalysts, strengthening the commercial interest and prospects of waste tyre catalytic pyrolysis [9], [46], [95], [118], [125], [126]. Some feed to the reactor may have contaminants that may inhibit the effect of a catalyst if it is in small quantities and the catalyst may not have an effect if it is below its threshold level [125]. The effect of a catalyst can be witnessed when the process of pyrolysis is carried out at a lower temperature and it can achieve the same conditions when compared with another reaction at a higher temperature and vice versa [4], [46], [127].

Although alkaline catalysts may not be as active as acidic catalysts for C–C bond cleavage, they are active for alkylation, isomerization, hydrogenation, and reactions that involve the heteroatom migration of the double bonds in unsaturated compounds [128], [129]. Their reactive sites are also known as Lewis and Brønsted base sites because the former donate electron pairs to reactants while the latter accept protons from the reactants [130]. The active sites of alkaline catalysts are generated during high-temperature forms of treatment, with metal oxides resulting in the removal of impurities adsorbed under the atmospheric conditions, such as H_2O or CO_2, and carbonates and hydroxides leading to thermal decomposition [128], [131].

Alkaline catalysts have demonstrated good results for catalytic pyrolysis of biomass, resulting in deoxygenation and decarboxylation reactions and some improvements in the quality of the obtained bio-oil [128]. Furthermore, alkaline catalysts have demonstrated good activity for plastic catalytic cracking, for example, polystyrene, because they enhance cracking initiation through random scission (like in thermal pyrolysis) or carbanions formation through the removal of hydrogen atoms from polystyrene adsorbed on-base sites, thereby accelerating the depolymerization of plastics [132]. Taking a similar mechanism of cracking initiation, pyrolysis of tyres using alkaline catalysts undergoes secondary reactions such as alkylation, isomerization, and cleavage of the carbon-heteroatom bonds [129].

The reactor Pressure: An increase in the pressure of the reactor during the pyrolysis process will result in an increase in pyrolysis oil viscosity that will be extracted [17], [133]. The reactor pressure can be reduced (often associated with vacuum pyrolysis) by reducing the residence time of the volatile fraction of pyrolysis products. This reduces the occurrence of secondary reactions on the volatiles, thus increasing the yield of oil [91], [111]–[113], [133], [134]. The reduction of secondary reactions decreases the deposition of gas on solid chars [91]. A lower pressure system would also result in a reduction in process temperature (according to

the ideal gas law, $PV=n\hat{R}_uT$). When the procedure is carried out at a low pressure and temperature, there is a decrease in energy demand [91].

2.7 Fuel characterization

A compression ignition (CI) engine fuel produces power when it is atomized, mixed with air in the cylinder and ignited at a high pressure. The fuel should ignite at the appropriate time and release the required energy per unit volume during combustion. The fuel should also be able to flow easily and burn readily at the required temperature and pressure [135].

In a compression ignition (CI) engine, the piston completes four separate strokes while turning the crankshaft. A stroke refers to the full travel of the piston along the cylinder, in either direction. The four separate strokes are termed as follows [136], [137].

1. Suction stroke: Suction occurs when intake valves open, allowing air to enter. The piston travels from the top dead center to the bottom dead center, making one stroke and rotating the crank 180°. As they descend, they create a significant depression in the combustion chamber; this depression, combined with the injection of fuel by an injector, causes the chamber to fill up.
2. Compression stroke: When the valves close and the piston rises, the fuel inside the combustion chamber is compressed. The pressures reached at the end of this phase in diesel engines are high allowing the mixture to self-ignite.
3. Expansion stroke: The high temperature and pressure formed at the end of compression, causes ignition spontaneously in diesel engines. Following combustion, gases at extremely high pressure and temperature formed inside the chamber, pushing the piston down to the bottom dead center. Because all of the pistons are linked by the crankshaft, when one goes up, the other goes down, and the mechanism moves forward.
4. Exhaust stroke: As a result of the combustion of the fuel, the piston rises, expelling the gases through the opening of the exhaust valves, which evacuate the gas from the cylinder, preparing it for a new cycle. The combustion residues are introduced into the exhaust manifold, which is connected to the exhaust system, including the muffler and possibly the silencer.

Several components aid the four-cycle process. As the pistons reciprocate, they drive or are driven by connecting rods that run through the crank shaft, which drives or is driven by the

flywheel. The pistons are propelled in the first, second, and fourth strokes of the cycle by the momentum generated in the revolving flywheel, as well as by the moment of inertia, that enables a smooth operation. Finally, the camshaft facilitates the opening and closing of the intake and exhaust valves via a linkage connected to the crankshaft [136], [137].

There should be no excessive pollution when the fuel is used. It is also desirable for the fuel to be safe in terms of toxicity and flammability [138]. Some of the important characteristic parameters of tyre pyrolysis oil that need to be determined before the fuel is used in running an engine are described in this section.

2.7.1 Density

A fuel's density is given as the proportion of its mass to the volume occupied at a specific temperature. Usually, fuel density is measured using a density meter at a normal temperature of 15 ^{0}C. The knowledge of density can be applied to quantity estimates and the evaluation of ignition quality [135]. The density of TPO is generally higher compared to diesel fuel [12], [23], [114], [127], [139]–[142], [26], [28], [32], [53], [78], [80], [84], [106] and use of a catalyst e.g. sodium carbonate can increase the density of TPO [4]. The density is directly proportional to the number of double bonds and inversely proportional to chain length [143]–[146]. Density is a very significant characteristic property of the fuel, as it is used to calculate the quantity of fuel supplied by injection pumps into the engine cylinders [135].

When working in a cold environment, it is desirable to first warm up the fuel, and it is required to have an adequate amount of volatile and low density components in order to enable the starting of the vehicle easily. The fuels should also have denser elements that will provide power once the engine reaches its operating temperature. The needed fuel density is determined by the engine size, load variations, speed characteristics, starting, design, and atmospheric conditions. Engines that operate at a high rate of change in speed and load, such as trucks and buses, may require more volatile and less dense fuels to obtain better performance, particularly in terms of smoke emissions. However, denser fuels, such as diesel, have a higher energy content than less dense fuels, and they provide superior fuel economy [135]. Particulate emissions are proportional to the fuel's density [146], [147].

In a direct injection (DI) engine, adequate atomization improves mixing and completes combustion, and is thus an important factor in engine emissions and its efficiency [148].

Atomization is important in engine combustion because it determines spray characteristics and the fuel/air mixing [149], [150]. The liquid fuel should be atomized to increase its surface area that is exposed to the hot gases and enable its rapid evaporation and the process of mixing with the oxidant [150]. An increase in fuel density has a negative impact on atomization [148], [149].

The atomization of fuel, its motion, evaporation, and the mixing with air all have a significant impact on combustion performance and emissions. Spray dynamics and combustion characteristics are critical in determining, for example, flame stability behavior at widely varying loads, safe and efficient energy utilization, and pollutant formation and destruction mechanisms [150]. Proper atomization and spraying improves fuel's energy efficiencies while drastically reducing pollutant emissions [150]–[152].

2.7.2 Kinematic viscosity

The kinematic viscosity of a fluid is a measure of its internal friction, which opposes dynamic changes in fluid motion at a given temperature [153], [154]. It affects the boundary characteristics of lubrication of the fuel [155]. The kinematic viscosity of TPO is closely comparable to that of jet fuel and is significantly lower in most cases than that of diesel fuel [4], [23], [26], [32], [35], [78], [80], [84], [114], [139]. However, Rofiqul *et al.*, [27] and Razmi *et al.*, [142] found it to be higher and the use of a catalyst in pyrolysis, e.g. MgO and $CaCO_3$, can lower it [129]. In general, different fluids have different temperature-viscosity relationships, and because viscosity is temperature-dependent, all viscosity values should be presented alongside the corresponding temperature values [135].

A viscometer is used to determine the viscosity of a fluid, and the Stokes or Centistokes unit is the most commonly used unit. The amount of pre-heating required after storage, handling, and adequate atomization is determined by the kinematic viscosity of the fuel. Highly viscous fuels are difficult to pump, atomize poorly, and burn slowly [1], [156]–[160]. Difficulty in pumping can damage the fuel pump and poor atomization can cause starting of the engine to be difficult [1], [135]. Insufficient atomization can result in carbon deposition on cylinder walls or burner tips, and it is normally improved by pre-heating [156].

Kinematic viscosity is directly proportional to the organic liquids' chain length [144]–[146], [161]–[165]. Kinematic viscosity is also inversely proportional to the degree of

unsaturation and it is controlled by the configuration of the double bond, with the trans-configuration having a higher viscosity than the cis-configuration [144], [145], [162], [165], [166]. Branching also increases liquid viscosity because it reduces carbon chain interaction by preventing neighboring molecules from approaching each other [167]. Viscosity has also been found to be proportional to lubricity (low viscosity poor lubricity) [168].

Fuel viscosities greater than 5.5 centistokes at 40°C are usually used in slow-moving engines and may require preheating before injection. Each engine has a minimum required viscosity to avoid power loss owing to the injection pump and its leakage. The highest fuel viscosity required is determined by factors such as fuel temperature, injection structural features, engine size, and design [135]. Low viscosity will result in more leaks past the injection pump's piston [1].

The fuel itself is used to lubricate most components of an engine such as pumps and fuel injectors [47], [169] and reduce frictional losses to preserve energy [47], [170]. The sliding areas within the pump rely upon the fuel's lubricity and fuels of low viscosities are not good lubricants [168]. The long chain polymer-based fuels have been found to provide an enhanced lubrication by reducing friction drastically [171], [172].

2.7.3 Calorific value

The fuel's calorific value is the amount of thermal energy emitted when fully burnt. It indicates the energy contained in a given fuel per unit mass. The suitability of a material or substance to be used as fuel is also determined by its calorific value [153]. It is measured in joules per unit mass of a material (kilograms).

A bomb calorimeter is commonly used to determine a fuel's calorific value [173]. The gross calorific value for TPO has been found to be slightly less compared to diesel fuel [12], [16], [53], [71]–[74], [78]–[82], [22], [83]–[88], [127], [129], [140], [23], [26], [27], [29], [31], [34], [52]. According to Diez *et al.* [34], the TPO's calorific value varies proportionally to pyrolysis temperatures between 350 ^{0}C-500 ^{0}C.

When comparing saturated and unsaturated hydrocarbon fuels, un-saturated hydrocarbon fuels have a lower calorific value, and this condition could be due to the following factors: First, functional groups in the molecular structure such as C=C and C-OH limit both vapour emission and energy release from the combustion reaction [174]–[177]. Second, the

oxidation of light hydrocarbon molecules into end products, such as CO_2, necessitates the addition of oxygen-containing moieties as well as the breaking of C-C bonds [174], [178]. The increase in chain length increases the calorific value and it decreases with an increase in unsaturation [144], [146], [164], [166].

2.7.4 Cetane rating

The ability of a diesel engine fuel to ignite at the required pressure and temperature in the cylinder following fuel injection is the most important quality [179]. The igniting quality of a fuel is determined by its Cetane rating [173]. This is made up of the Cetane number and the Cetane index. The Cetane number may be measured directly when fuel is burned in a Cooperative Fuel Research (CFR) engine under normal test settings [180], whereas the Cetane index is calculated from the fuel parameters, such as its distillation temperature or chemical structure [12], [26], [32], [180].

Cetane number: The Cetane number is a measure of the ignition quality of a fuel. It describes the engine's rough or smooth operation as a function of the fuel's ignition delay and the rate at which pressure rises. Ignition quality is defined as the amount of time that passes between the commencement of fuel injection into the cylinder and the start of combustion; the shorter the period, the better the ignition quality. If the ignition delay is excessively long, a considerable volume of fuel may be injected before combustion begins, causing the combustion to proceed with an accelerated intensity and a rapid rise in pressure. When it comes to starting and running in a cold environment and at a low speed, a high Cetane number implies smoothness [181]. The presence of unsaturated hydrocarbons and branching lowers the fuel's Cetane number, causing poor combustion [164], [166], [182]. It is also proportional to the chain length [144], [164], [166] and inversely proportional to unsaturation [144], [166]. Decreasing the Cetane number results in an increase in particulate emissions [147].

Cetane index: The Cetane index is used when no direct determination of the traditional Cetane number is possible. It is possible to achieve a good estimate of Cetane rating of the fuel by calculating the Cetane index (CI). The Cetane index can be approximated using Equation 2.1 [12], [26], [32], [179], [180].

$$CI = 454.74 - 1641.416D + 774.74D^2 - 0.544T_{50} + 97.803[log_{10}(T_{50})]^2 \quad \text{Eq. 2.1}$$

Where $CI = Cetane\ Index$

$D = Fuel\ Density\ at\ 15\ degrees\ centigrade$
$T_{50} = 50\ \%\ Recovery\ Temperature\ (degrees\ centigrade)$

2.7.5 Pour point

The pour point (PP) is the temperature at which a fuel freezes and ceases to flow freely, resulting in the formation of a semi-solid. The pour point is a measurement of the lowest temperature at which fuel can be safely transferred until it turns into a gel in the liquid state. In low-temperature conditions, fuels with a high pouring point are difficult to use. It is important to heat these fuels before the engine starts [135].

The pour point (PP) is an essential fuel property which needs to be determined in places that experience very low temperatures. Fuels must be combined with appropriate additives in these locations in order to supply the requisite energy and performance, hence eliminating difficulties associated with low temperatures [135]. The pour point for TPO is higher compared to diesel fuel, hence TPO will have more problems at lower temperatures compared to diesel fuel [12], [27], [53], [78], [84], [106].

2.7.6 Flash point

The flash point is defined as the temperature at which a liquid fuel releases enough flammable vapor from its surface to ignite in the presence of a flame [162], [179], [183]. It differs from the fire point whereby at a flash point, once the source of ignition is eliminated, the flame goes off, but at a fire point, the flame continues when the source of ignition has been withdrawn [184]. It has no effect on the combustion performance of the engine, but it is a critical quality for its safety in handling and storage. When compared to fuels with a low flash point, fuels with a high flash point are safer to store and handle [179], [185]. The chain length of the fuel's hydrocarbons is directly proportional to the fuel's flash point [162]. The flash point is used to determine the flammability of liquid fuels [183].

The flash point of tyre pyrolysis oil has been found to be lower than diesel fuel. This indicates that it can ignite at a lower temperature compared to diesel fuel [12], [13], [141], [186], [23], [26], [27], [78], [80], [84], [106], [139]. Use of Na_2CO_3 and $CaCO_3$ as catalysts causes an increase in the flash point of the extracted pyrolysis oil [4], [129]. When MgO_2 is utilized as a catalyst in the synthesis of TPO, it also results in an increase in TPO's flash point

[129]. Hydrocarbons with branched molecules of the same carbon number have a lower boiling point and flash point than linear molecules [187].

2.7.7 Water

One of the key characteristics used to determine a fuel's efficiency is its ability to complete combustion. Water vapor is produced during the burning of most regularly used organic fuels, and its energy content can be recovered by condensing it. Moisture, on the other hand, has a detrimental impact on combustion efficiency, thus it should be kept to a minimum in the fuel [188].

Tyre pyrolysis oil contains more water content compared to the maximum that is recommended for diesel fuel [12], [26], [32], [80]. Demirbasa *et al.* [4] found TPO to contain water that was within the allowable limit when using sodium carbonate as a catalyst. The water content in the TPO can also be reduced when the feed material to the reactor is dry.

2.7.8 Sulphur Content

In a diesel engine, sulphur has no effect on combustion. Burning sulphur, on the other hand, produces sulphur oxides, which dissolve in condensed water formed by the combustion of hydrogen to produce sulphuric acid. As a result of the increased sulphur content, corrosion effects on turbo blowers, silencers, and exhaust pipes are likely to occur [179]. The presence of sulphur in fuel causes environmental pollution whenever the fuel is used.

TPO has been found to contain sulphur that is above the required set standards [4], [27]–[32], [35], [36], [134]. However, the use of catalyst can reduce the sulphur content in the resulting TPO [4], [129]. The sulphur content is also directly proportional to the pyrolysis temperature [34], [71].

2.7.9 pH

The pH of a substance is a measure of its alkalinity or acidity. The degree of alkalinity or acidity is expressed in a pH scale. This scale extends from 0 to 14, with 7 being a neutral point [87]. TPO has been found to be acidic [78], [84] but Martínez *et al.* [81] found it to be slightly alkaline. Acidity may be reduced by the use of a basic catalyst, e.g. sodium carbonate [4].

2.7.10 Lubricity

Fuels used in engines should attain the required lubricity to enable lubrication of the injection systems to prevent extreme system wearing. Some methods employed in reducing sulphur from fuel (desulphurization) can also result in a decrease in its natural lubricating qualities. Certain additives that are used to increase fuel lubricity cause certain negative effects when applied in appropriate quantities or when blended with other additives on the basis of lubricity improvement [135].

A high lubricity level ensures that the engines' injection system is adequately lubricated under most operating situations [135]. The lubricity of TPO is usually less when it is compared to diesel fuel [27], [32], [80]. Therefore, in order to achieve the necessary lubricity, TPO needs to be blended with diesel or additives.

2.8 Chemical Analysis

Gas Chromatography Mass Spectrometry (GC-MS): The objective of the GC-MS test is to establish the types and nature of the present compounds (hydrocarbons) [107], [125], [142]. TPO has been found to be a very complex mixture that is made up of C_5–C_{16} organic compounds with a high concentration of unsaturated compounds [22], [32], [71], [76], [81] while Laresgoiti *et al.* [38], Banar *et al.* [83] and Kan *et al.* [37] found that carbon content ranged between (C_7–C_{32}). It mainly contains aliphatic and aromatic compounds [22], [32], [78], [83], [90], [110], [141] such as n-undecane, n-pentadecane, n-heptadecane, n-hexadecane, n-tetradecane, and some other high molecular weight alkanes, phenanthrenes, alkylated napthalenes, and alkenes (especially limonene) [83].

Fourier Transformation Infrared (FT-IR): The FT-IR is not the most appropriate analytical tool for determining aromatic, polar and saturated components [22], [27], [73], [83], [84], [106]. Nevertheless, it enables the identification of functional groups which reveal the chemical characteristics of the liquids [22], [39], [73], [83], [84], [90], [97] and specifies the types of bonds [39]. TPO has been found to contain aromatic, aliphatic and hydroxyl compounds [22], [73].

2.9 Summary of the Literature Review

Batch/Semi-Batch type pyrolysis reactors have been found to be easy to design and operate compared to other reactors [93]. The amount of TPO that can be extracted from tyres ranges between 34 % and 58 % of the weight of the feed material. In order to achieve optimum oil production, a size of approximately 4 cm^3 and a temperature of 550 ^{0}C at atmospheric pressure are required [22], [84]. Nitrogen gas is usually used to create an inert environment, but a simple reactor can be improvised (batch type reactor) where the feed material is squeezed inside the reactor and the inert gas will not be needed for pyrolysis.

TPO has been functionally analyzed and found to have a carbon content ranging from C_5 to C_{24}.TPO has some chemical and physical properties in common with diesel fuel, but it has a high sulphur content. Aylon *et al.* [189] found that temperature and solid mass flow rate affected the product chemical properties of TPO. Diez *et al.* [114] found the calorific value of oil to be proportional to the pyrolysis temperatures used, from 36 MJ/kg up to 40 MJ/kg (between 350 ^{0}c and 550 ^{0}c).

CHAPTER THREE: METHODOLOGY

3.1 Introduction

This chapter outlines the design procedure and materials required in order to construct a pyrolysis system for 6 kg feed per batch, extraction of pyrolysis oil using various proportions (0 %, 1.5 % 2.5 %, 5 %, 7.5 % and 10 %) of sodium carbonate as a catalyst and determination of physico-chemical properties of the pyrolytic oil. The design procedure of every component of the pyrolysis system was followed and the finalized design was effectively communicated in the form of a detailed drawing with the required dimensions. The pyrolysis system was fabricated and then used in the extraction of various oil samples from tyres. The evaluation of the fuel properties of the oil samples was carried out and compared to diesel fuel.

3.2 Overview of the Design

Figure 3.1 shows a schematic diagram of the pyrolysis system that was designed and fabricated.

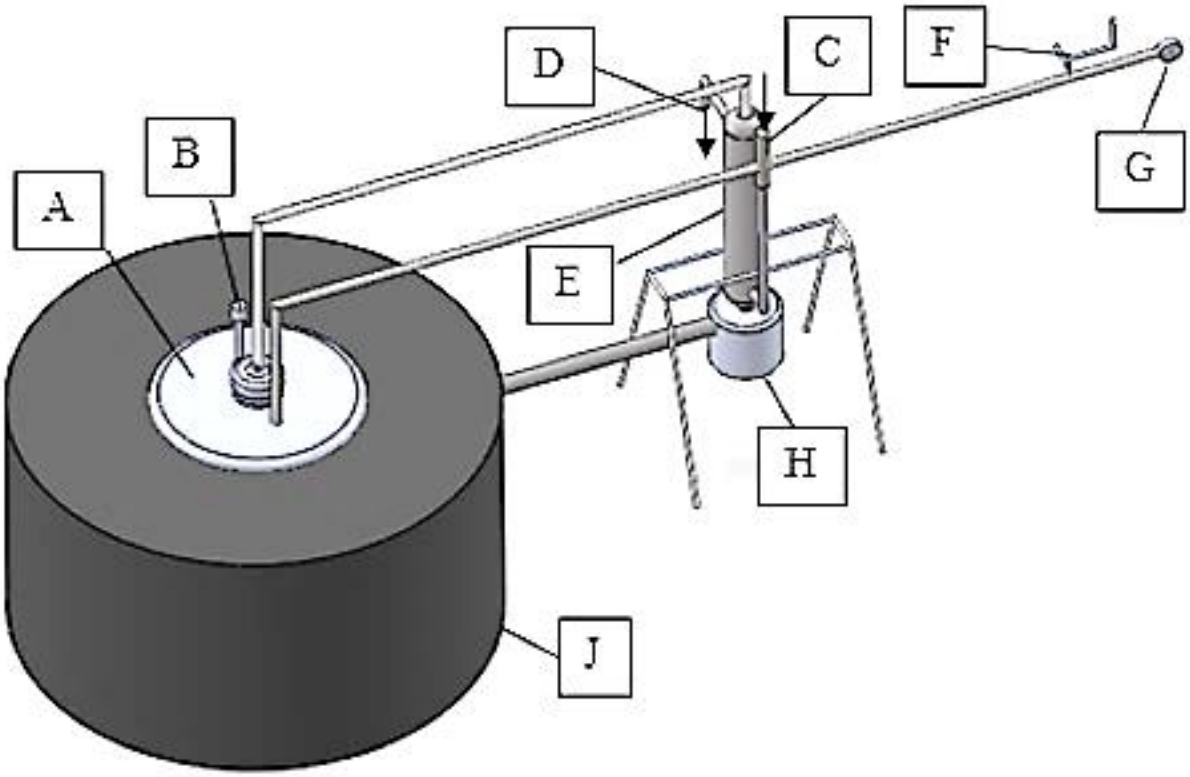

Figure 3. 1 The schematic diagram of the pyrolysis system that was fabricated.

The list of the labelled components in Figure 3.1 is as follows:

- A – Reactor
- B – Thermocouple
- C – Water Inlet
- D – Water Outlet
- E – Condenser
- F – Pressure Relief Valve
- G – Pressure Gauge
- H – Oil Collector
- J – Heat Supplying Unit

3.3 Materials selection and design procedures

This research involved three stages. They included the design and fabrication of the pyrolysis system, the extraction of tyre pyrolysis oil, and finally the oil's characterization.

The following items and materials were sourced for use in fabrication of the pyrolysis system.

3.3.1 Heat Supplying Unit

A crucible furnace was used as a source of heat. Its materials were able to withstand the operating temperatures. The thermal expansion of its components was within acceptable limits and did not interfere with the structure of the reactor. It was able to supply the required amount of heat to the reactor.

3.3.2 Batch Type Reactor

The reactor is where the feed material is converted into various products. It consisted of a cylindrical reactor type where the pyrolysis reaction took place. This reactor was not self-sustained; therefore, it needed an external source of heat to maintain its operation. This reactor was located in the heat supplying unit where it was heated to the required temperature.

The following were the characteristics of the reactor material:

1. It was able to withstand operating temperatures and pressures that could be developed.
2. It was able to transfer the required amount of heat (its material was a good conductor of heat) to the feed material.
3. Stability in the operating atmosphere: did not oxidize when subjected to the high operating temperatures and did not corrode when exposed to the resulting gases.

4. It had acceptable mechanical strength and the ability to withstand thermal and mechanical shocks.
5. It was air tight with one exit for the removal of products.

The reactor was made up of a mild steel cylinder. A 6 kg cooking gas cylinder was considered for use over buying sheet metal because more time was required to fabricate sheet metal than to modify a cooking gas cylinder. Its height was 16 cm and its diameter was 15 cm. The maximum pressure the reactor could withstand and the heat to be transferred were considered.

1. **Pressure consideration**

General design assumptions of the reactor material:

1. The material used was homogeneous.
2. The material's cross sectional area was assumed to be uniform.
3. Failure could only occur after the normal yield stress had been exceeded.

The mechanical properties of structural steel containing 0.15 to 0.25 percent carbon are shown in Table 3.1.

Table 3. 1 The mechanical properties of structural steel of 0.15 to 0.25 % carbon [190]

Property	Lb/in^2	Mpa
Young's Modulus (E)	30 ×10^6	207×10^3
Yield Stress (σ_y)	30 ×10^3 - 40 ×10^3	207 – 276
Ultimate tensile Strength (σ_{uts})	55 ×10^3 - 65 ×10^3	379 – 448

The following Equations were used in finding the maximum pressure the cylinder can withstand given its size and mechanical properties. Longitudinal and circumferential stresses were considered using Equation 3.1 and 3.2, respectively [191].

1. Considering longitudinal stresses.

$$p = \frac{4t\sigma_a r.f.}{d \times s.f.} \qquad \text{Eq. 3.1}$$

2. Considering circumferential stresses.

$$p = \frac{2t\sigma_a r.f.}{d \times s.f.} \qquad \text{Eq. 3.2}$$

Where $\sigma_a - \ Axial\ stress.$

$\sigma_c - \ Circumferential\ stress.$

$p -$ $Internal\ pressure.$

$d -$ $Diameter\ of\ the\ cylinder.$

$t -$ $Thickness\ of\ the\ cylinder.$

$r.f. - Retention\ Factor.$

$s.f. = Safety\ Factor.$

The retention factor of mild steel at a temperature of 600 ^{0}C is about 0.2 [192]. It was also assumed to be equal to 0.2 for copper since their crystalline temperatures lie within the same range.

Calculation of the maximum pressure that the cylinder can withstand when considering longitudinal stresses

$$p = \frac{4t\sigma_a r.f.}{d \times s.f.} = \frac{4 \times 0.0025 \times 250 \times 10^6 \times 0.2}{0.25 \times 2} = 1.0 \times 10^6 \text{Pa or 10 Bar}$$

Calculation of the maximum pressure that the cylinder can withstand when considering circumferential stresses.

$$p = \frac{2t\sigma_a r.f.}{d \times s.f} = \frac{2 \times 0.0025 \times 250 \times 10^6 \times 0.2}{0.25 \times 2} = 5.0 \times 10^5\ Pa\ or\ 5\ Bar$$

Thus, the allowable pressure was to be limited to 5 bar. To achieve this, a pressure gauge and a release valve were installed to monitor any pressure build up within the reactor.

2. Calculation of the heat supply to the reactor

In the calculation of heat transfer to the reactor, two alternatives were considered in determining the power supplied to the reactor by the furnace. The following available information was used:

1 The crucible furnace takes three hours to melt 20 kg of aluminium metal for casting.

2 The crucible furnace consumes approximately 6 kg of diesel fuel per hour. The calorific value of diesel was assumed to be 45 MJ/kg. The furnace efficiency was also assumed to be 80 %.

The first alternative is that the crucible furnace takes three hours to melt 20 kg of aluminium metal. This information was used to determine power supply to the reactor by the furnace.

$$H_T = \frac{M(H_{solid} + H_{fussion} + H_{liquid})}{Time} \qquad \text{Eq. 3.3}$$

where M = Mass of aluminum

H_T = Heat transferred

H_{solid} = Heat for raising tempareture of aluminum to melting point per kg.

$H_{fussion}$ = Specific latent heat of fussion.

H_{liquid} = Heat for raising temperature from melting point to flow temp per kg.

$Time$ = Total time taken in heating aluminum

$$H_{solid} = C_p(t_{melt} - t_{initial}) \quad \text{Eq. 3.4}$$

$$H_{solid} = 920(660 - 15) = 593{,}400\, J/kg$$

$$H_{fussion} = 293.4\, J/kg$$

$$H_{liquid} = C_p(t_{flow} - t_{melt}) \quad \text{Eq. 3.5}$$

The flowing/pouring temperature of aluminium is 750 ºC [193]–[196].

$$H_{liquid} = 920(750 - 660) = 82{,}800\, J/kg$$

Heat supply into the crucible can be determined using Equation 3.3;

$$H_T = \frac{20(\ 593{,}400\ + 293.4\ + 82800\ )}{3 \times 3600} = \mathbf{1252.7656\ watts}$$

This is the heat that is supplied to the aluminium through the crucible that has a thermal conductivity of 3.8 w/m^2.K. Heat that could be conducted by the designed reactor that is made up of mild steel with a thermal conductivity of 50 w/m^2.K is higher and was calculated as follows [197].

$$\mathbf{Q_{crusible} = U\Delta T = 1252.7656\ Watts}$$

$$U_{crusible} = \frac{1}{R} = \frac{2\pi LK}{ln\frac{r_2}{r_1}} + \frac{KA}{x} \quad \text{Eq. 3.6}$$

$$= \frac{2\pi \times 0.37 \times 3.8}{ln\frac{0.175}{0.145}} + \frac{3.8 \times \pi \times 0.14}{0.04} = \frac{88.7603W}{k}$$

The heat transfer coefficient through the reactor can be calculated as follows [197].

$$U_{reactor} = \frac{k \times A}{thickness} = \frac{k\ (\pi r^2 + \pi rL)}{thickness} \quad \text{Eq. 3.7}$$

$$U_{reactor} = \frac{50(\pi 0.15^2 + \pi \times 0.15 \times 0.15)}{0.0016} = 4417.8647 W/^o c$$

Heat that is supplied to the reactor was calculated as follows.

$$Q_{reactor} = 1.2527656 \times \frac{4417.8647}{88.7603} = \mathbf{62.3539\ kW}$$

The second alternative is that the crucible furnace consumes approximately 6 kg of diesel fuel per hour. The calorific value of diesel was assumed to be 45 MJ/kg. The power supplied by the furnace was calculated as follows, assuming a furnace efficiency of 80 %.

$$Q_{reactor} = \frac{Mass \times \text{Calorific value} \times \text{efficiency}}{Time} \qquad \text{Eq. 3.8}$$

$$Q_{reactor} = \frac{6 \times 45 \times 10^6 \times 0.8}{3600} = \mathbf{60\ kW}$$

The two approaches gave comparable values, and the heat load of **62.3539 kW** was used to calculate the time required to supply heat to the reactor and the required specification of the condenser.

3. Determination of the duration required to carry out the pyrolysis process

The activation energy of tyre pyrolysis was calculated in order to determine the rate at which products of pyrolysis were generated. Then the time required for pyrolysis was approximated. The time required to achieve the required temperature was five minutes.

The TPO production was done at a temperature of 550 ^{0}C at atmospheric pressure [23], [24], [73], [80], [81], [89], [107]–[109]. Also, vacuum pyrolysis can be carried out at 500 ^{0}C at 20 kPa [36], [76], [198]. Equation 3.9 was used in the calculation of the activation energy of tyre pyrolysis [199].

$$E_A = \frac{(R_u\, T_1\, T_2)}{(T_1 - T_2)} ln \frac{k_1}{k_2} \qquad \text{Eq. 3.9}$$

Where; $E_A = Activation\ Energy$

$R_u = Universal\ Gas\ Constant$

$T_1 = Reaction\ Temperature\ at\ Condition\ 1$

$T_2 = Reaction\ Temperature\ at\ Condition\ 2$

$k_1 = Reaction\ Constant\ at\ Condition\ 1$

$k_2 = Reaction\ Constant\ at\ Condition\ 2$

The reaction constant in this case is pressure and the activation energy was calculated as follows;

$$E_A = \frac{(8314 \times 773 \times 823)}{(823 - 773)} ln \frac{100{,}000}{80{,}000} = 23.604982\ MJ/kg$$

The rate of product generation from the reactor was calculated as follows.

$$Rate\ of\ Products' Generation\ = \frac{H_{reactor}}{E_A} = \frac{62.3539 \times 10^3}{23.604982 \times 10^6} = 2.6416 \times 10^{-3} kg/s$$

The time required to supply heat to the designed reactor was calculated as follows;

$$Heating\ Time = \frac{Mass\ of\ Feed\ Material}{Rate\ of\ Products'\ Generation} + Duration\ to\ Achieve\ Required\ Temp.$$

$$= \frac{6.5kg}{2.6056 \times 10^{-3} kg/s} + 300 = 2572\ seconds = 42.87\ min$$

Thus, the time taken to heat the feed material was forty five minutes.

3.3.3 Volatile Product Tube

The volatile product tube was made up of mild steel that was connected to the reactor outlet and a copper tube at some distance from the reactor. A mild steel tube was located at the reactor outlet since it could withstand higher temperatures than copper, and copper was included since it had a high thermal conductivity, which is ten times compared to mild steel. The copper tube was used to increase the cooling of the produced gases. The selected metals could not react with the hot gases.

The total length of the volatile product tube was 1.65 m, assuming that the maximum allowable pressure loss along the tube is 100 Pa. The minimum radius of the tube was determined. The calculations were done as follows using fluid flow expression in a round tube [200].

$$\tau_w = \mu \frac{du}{dr} \qquad \text{Eq.3.10}$$

Where $\tau_w = Shear\ Stress\ at\ the\ Wall$

$\mu = Dynamic\ Viscosity$

$du = Change\ in\ Velocity$

$dr = Change\ in\ Radius$

Also,

$$\tau_w \times area\ of\ the\ wall = Pressure\ Drop \times cross - sectional\ area \qquad \text{Eq. 3.11}$$

Or,

$$\tau_w = \frac{Pressure\ Drop \times cross - sectional\ area}{area\ of\ the\ wall}$$

Assuming the pressure loss along the volatile product tube to be 100 Pa then the shear stress will be given as,

$$\tau_w = \frac{100\times\pi r^2}{\pi r l} = \frac{100\times r}{1.65} = 60.61r \qquad \text{Eq. 3.12}$$

Where; $\tau_w = Shear\ Stress$

$r = Radius\ of\ the\ Area$

$l = Length\ of\ the\ Volatile\ Product\ Tube$

Using Equation 3.12 as a replacement for τ_w in Equation 3.10, we have;

$$60.61r = \mu\frac{du}{dr} \qquad \text{Eq. 3.13}$$

The mass of the products generated per unit time is 2.6056×10^{-3} kg/s. Assuming 70 % of it to be volatile, the mass that will flow through the tube was calculated as follows;

$$Volatile\ Production\ rate = Total\ rate \times \frac{70}{100} = 2.6056 \times 10^{-3} \times \frac{70}{100}$$

$$= 1.82392 \times 10^{-3}\ kg/s$$

Assuming their density in liquid form is 950 kg/m^3, the volume flow rate will be;

$$Volume\ flowrate = \frac{Mass}{Density} = \frac{1.82392\times10^{-3}}{950} = 1.92 \times 10^{-6}\ m^3/s \qquad \text{Eq. 3.14}$$

When a liquid changes from a liquid to a gaseous state at a constant pressure, its volume changes by approximately a thousand times. Therefore, the volume flowrate in gaseous form will be multiplied by a thousand to get $1.92 \times 10^{-3}\ m^3/s$. The velocity will be determined as:

$$The\ Average\ Velocity = \frac{Volume\ Flowrate}{cross - sectional\ Area} = \frac{1.92 \times 10^{-3}}{\pi \times r^2} m/s$$

Eq. 3.15

The maximum velocity will be experienced at the centre of the tube and it is twice the average velocity.

$$The\ Maximum\ Velocity = The\ Average\ Velocity \times 2 = \frac{1.92 \times 10^{-3}}{\pi \times r^2} \times 2$$

$$= \frac{3.84 \times 10^{-3}}{\pi \times r^2} m/s$$

The velocity at the wall, is zero (no slip condition). Therefore, the change in velocity from the wall to the Centre perpendicular to the direction of flow is $du = \frac{3.84\times10^{-3}}{\pi\times r^2}\ m^3/s$ and $dr = r$. Replacing them in Equation 3.13, we have.

$$60.61r = \mu \frac{3.84 \times 10^{-3}}{\pi \times r^2 \times r}$$

The value of μ was assumed to be $60 \times 10^{-6} \frac{kg}{ms}$ .This is the highest value that a gas may not exceed.

Thus,

$$r^4 = 60 \times 10^{-6} \times \frac{3.84 \times 10^{-3}}{60.61 \times \pi}$$

$$r = 0.004898\, m = 4.898\, mm$$

The tubes that were available were 10 mm diameter copper with 0.5 mm thickness and 18 mm diameter mild steel with 1mm thickness. If there was blockage towards the end of the tubes, the tube might bust, so the maximum pressure the tube could withstand was calculated as follows, where longitudinal and circumferential forces were considered.

1. **For mild steel**

The maximum pressure that the tube can withstand when considering longitudinal stresses and circumferential stresses were calculated respectively.

$$p_{longitidinal} = \frac{4t\sigma_a r.f.}{d \times s.f.}$$

$$p_{longitidinal} = \frac{4 \times 0.001 \times 250 \times 10^6 \times 0.2}{0.018 \times 2} = 5.5556 \times 10^6 \text{ Pa} \quad \text{or} \quad 55.556 \text{ Bar}$$

$$p_{circumferential} = \frac{2t\sigma_a r.f.}{d \times s.f}$$

$$p_{circumferential} = \frac{2 \times 0.001 \times 250 \times 10^6 \times 0.2}{0.018 \times 2} = 2.7778 \times 10^6 \text{Pa} \quad \text{or} \quad 27.778\, bar$$

2. **For copper tube**

Using Equations 3.16 and 3.17, the maximum pressure that the tube can withstand when considering longitudinal and circumferential stresses was determined as follows:

$$p_{longitidinal} = \frac{4 \times t \times \sigma_a r.f.}{s.f. \times d} = \frac{4 \times 0.0005 \times 40 \times 10^6 \times 0.2}{2 \times 0.009}$$

$$= 8.8889 \times 10^5\, Pa \quad or\ 8.8889\, bar$$

$$p_{circumferential} = \frac{2 \times t \times \sigma_a r.f.}{s.f. \times d} = \frac{2 \times 0.001 \times 40 \times 10^6 \times 0.2}{2 \times 0.009}$$

$$= 4.4444 \times 10^5 Pa \quad or\ 4.4444\ bar$$

3.3.4 Water Cooled Condensing Unit

A condensing unit was required for cooling the gases to the required temperature for condensation and sub cooling. The condensate (oil) was then collected for analysis. The condenser was made up of a material (copper) that could not react with the hot gases.

The material used for the condensing tubes was copper tube enclosed in a mild steel shell. The copper tube was used because of its good thermal conductivity and could not react with the gases from the reactor. It was capable of remaining stable at the required operating temperature. Operating pressure and heat to be transferred were considered in the design process.

1. **Consideration of Pressure**

If there could be blockage towards the end of the tubes, the tubes could bust, so the maximum pressure the tube could withstand was determined, where longitudinal and circumferential forces were considered. As determined in Section 3.3.3, the maximum allowable longitudinal and circumferential stresses for the copper tube were 8.89 and 4.44 bar, respectively.

2. **Heat transfer consideration**

The condenser consisted of tubes in a shell-type water-cooled condenser. The coil was made up of copper due to its good conductivity of heat, and was locally available. The shell was made up of mild steel.

The rate of heat supply to the reactor was used to determine the length of tubes required at the condenser.

The total Length of Condenser Tube Required

The flow of water was counter flow to the flow of the volatile fraction of pyrolysis products. To determine the total length of the condenser tubes, the effectiveness method was employed [197], [201].

$$Effectiveness\ \varepsilon_c = \frac{Actual\ heat\ transfer}{Maximum\ possible\ heat\ transfer} \qquad \text{Eq. 3.16}$$

$$\varepsilon_c = \frac{T_{h1} - T_{h2}}{T_{h1} - T_{c2}}$$

Where, $T_{h1} = Temperature\ of\ the\ hot\ gases\ at\ inlet\ to\ the\ condenser$

$T_{h2} = Temperature\ of\ the\ hot\ gases\ at\ outlet\ to\ the\ condenser$

$T_{c2} = Temperature\ of\ the\ cooling\ water\ at\ inlet\ to\ the\ condenser$

The temperature of hot gases was assumed to be 600 ^{0}C, its outlet temperature was assumed to be 35 ^{0}C and the temperature of cooling water at the inlet point was assumed to be 30 ^{0}C and exit at 40^{0}C.

$$\varepsilon_c = \frac{600\ -\ 35}{600\ -\ 30} = 0.9912$$

The effectiveness can also be expressed as shown in Equation 3.17 [201].

$$Effectiveness = \frac{1-\ exp\{-NTU(1-R)\}}{1-R[exp\{-NTU(1-R)\}]} \qquad \text{Eq. 3.17}$$

Where $NTU = Number\ of\ Transfer\ Units$

$R = Tempearture\ Ratio$

The temperature ratio can be expressed as follows:

$$R = \frac{C_{min}}{C_{max}} = \frac{40\ -\ 30}{600\ -\ 35}\ =\ 0.0215$$

Where,

$C_{min} = Minimum\ Capacity\ Rate\ for\ a\ Fluid\ with\ a\ Higher\ Temperature\ Change$

$C_{max} = Maximum\ Capacity\ Rate\ for\ a\ Fluid\ with\ a\ Lower\ Temperature\ Change$

Let $exp\{-NTU(1-R)\}$ be represented by B

Therefore, $\varepsilon_c = \frac{1-B}{1-RB}$

Substituting, $0.9912 = \frac{1-B}{1-0.0215B}$

$B = 0.4129$

The value of B was used to determine the number of transfer units (NTU)

$$NTU = -\ln\frac{B}{1-R} = -\ln\frac{0.4129}{1-0.0215} =\ 0.8628$$

$$C_{min} = \frac{Heat}{T_{h1} - T_{h2}} = \frac{62.3539}{600\ -\ 35}\ =\ 0.11037\ kW/K$$

$$C_{max} = \frac{Heat}{T_{c1} - T_{c2}} = \frac{62.3539}{80\ -\ 30}\ =\ 1.2471\ kW/K$$

$$mass\ flowrate\ of\ water = \frac{C_{max}}{C_{p.water}} = \frac{1.2471}{4.2}\ =\ 0.2969\ kg/sec$$

The coefficient of heat transfer was determined as follows in order to use it in the calculation of the required surface area of the condenser.

$$U = \frac{1}{resistance} = \frac{1}{\frac{x}{k} + \frac{x}{k}} = \frac{1}{\frac{0.001}{380} + \frac{0.05}{0.6}} = 12\ W/^{o}c$$

The required surface area of the condenser was then determined;

$$A = \frac{NTU \times C_{min}}{U_{condenser}} = \frac{0.8628\ \times 0.11037}{12} = 7.9356 \times 10^{-3} m^2$$

Having determined the required surface area, determination of the required length was done as follows;

For 8mm diameter;

$$L = \frac{A}{\pi d} = \frac{7.9356 \times 10^{-3}}{\pi \times 8 \times 10^{-3}} = \mathbf{0.3157\ m}.$$

Assuming a heat transfer efficiency of 20 % due to the bituminous fraction of the oil sticking on the inner surfaces of the condenser tubes. The total length required was **1.5785 m** and six tubes were used, each with a length of 0.3 m.

3.3.5 Water Cooled Condensing Unit stand

Figure 3.2 shows the sketch of a condenser stand. Failure along the horizontal sections will occur due to bending moments and failure along the vertical sections will occur due to buckling.

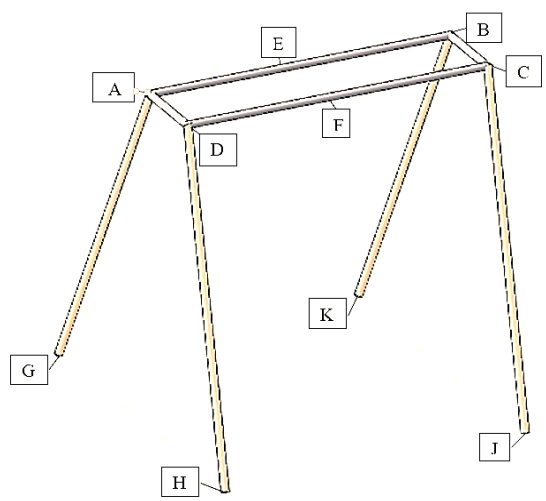

Figure 3. 2 The sketch of a condenser stand.

Bending Moment

Bending moments will be experienced along sections A-B and C-D when the weight of the condenser acts at points E and F. The following assumptions were used in the Equations for normal bending moment stresses in straight beams;

1. The material is homogeneous and has uniform cross-sectional area.
2. Stress and Strain obeys Hooke's Law.
3. Plane sections will remain plane before and after bending.
4. Application of the load is perpendicular to the bending plane.
5. In the plane of bending, the beam has a symmetry axis.

Bending, rather than wrinkling, sidewise buckling, or crushing, will cause the beam to fail. The bending moment equation was used.

$$\frac{\mathrm{M}}{I} = \frac{\sigma}{y} = \frac{\mathrm{E}}{\mathrm{R}} \qquad \text{Eq. 3.18}$$

Where M = moment of resistance.

I = moment of inertia of the section about neutral axis.

E = Young's Modulus

R = Radius of curvature of neutral axis.

σ = bending stress.

y = the perpendicular distance from the neutral axis.

Letting $Z = \frac{\mathrm{I}}{y}, \mathrm{M} = \sigma \mathrm{Z}$ Eq. 3.19

In the case of a circular cross-section area of diameter d

Section modulus $Z = \frac{\pi d^3}{32} = \frac{\mathrm{Ad}}{8}$ Eq. 3.20

This component will fail when the working stress is more than the yield stress. The working stress in this case is $\sigma_w = \frac{\sigma_y}{s.f.}$ Eq. 3.21

Where: s.f. is safety factor = 2

σ_y is minimum yield stress =207 MPa

Therefore,

$$\sigma_w = \frac{207}{2} = 103.5 \text{ MPa}$$

The bending stresses could be experienced along Section A-B and C-D. Starting from the bending moment Equation;

$$\frac{\mathrm{M}}{I} = \frac{\sigma}{y} = \frac{\mathrm{E}}{\mathrm{R}} \qquad \text{Eq. 3.22}$$

$$I = \frac{\sigma d^4}{64} = \frac{\sigma r^4}{4} \qquad \text{Eq. 3.23}$$

The bending moment was determined using Equation 3.24.

$$M = \frac{Mass \times gravitatinal\ acc. \times Perpendicular\ Distance}{4} \qquad \text{Eq. 3.24}$$

$$M = \frac{10\ \times 10 \times 0.2}{4} = 5\ Nm$$

The required diameter $d = 2r = 2\left(\frac{4M}{\sigma_w \pi}\right)^{1/3} = 2\left(\frac{4\times 5}{103.5\times 10^6\ \times \pi}\right)^{1/3} = 7.89\ mm$

The available size used is 8 mm diameter.

Failure Due To Buckling

Failure due to buckling may be experienced along A-G, D-H, C-J and B-K. Euler's buckling formula was used in the size of material selection.

Euler's buckling formula

In Euler's buckling formula, the following assumptions are made:

1. The column material is isotropic and homogeneous.
2. The compressive load acts along the column axis only.
3. The column is free from initial stress.
4. The column's weight is negligible.
5. The column is initially straight (no eccentricity of the axial load).
6. Fixed ends are rigid and pinned joints are frictionless.
7. The cross-sectional area of the column remains consistent throughout its length.
8. The normal stress is much higher than the bending stress.
9. The column's length is significantly more than its cross-sectional area.
10. The only way the column will fail is by buckling.

The critical buckling load formula that was derived by Euler

$$P_{cr} = \frac{IE\pi^2}{s.f. \times \mathrm{L}^2} \qquad [202] \qquad \text{Eq. 3.25(a)}$$

The equation only applies to columns that are simply supported. The method used to generate the equation, however, can be applied to various sorts of supports.

$$P_{cr} = \frac{IE\pi^2}{s.f. \times {L_{eff}}^2} \qquad [202] \qquad \text{Eq. 3.25(b)}$$

Where $I - Area\ Moment\ of\ Inertia\ of\ the\ Cross - section\ of\ the\ Column$

$E - Young's\ modulus\ of\ elasticity\ of\ column\ material$

$s.f. - Safety\ Factor$

${L_{eff}}^2 = The\ Effective\ Length\ of\ the\ Column$

Table 3.2 shows the buckling of columns with different supports. In the last row of Table 3.2, the effective length for each case is listed.

Table 3. 2 Buckling of columns with different supports [202]

	Case 1	Case 2	Case 3	Case 4[a]
	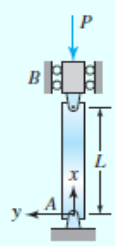	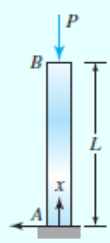	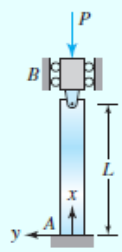	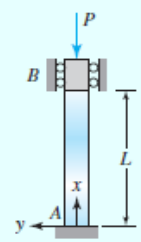
	Pinned at both ends	**One end fixed, other end free**	**One end fixed, other end pinned**	**Fixed at both ends**
Differential equation	$EI\frac{d^2v}{dx^2} + Pv = 0$	$EI\frac{d^2v}{dx^2} + Pv = Pv(L)$	$EI\frac{d^2v}{dx^2} + Pv = R_B(L-x)$	$EI\frac{d^2v}{dx^2} + Pv = R_B(L-x) + M_B$
Boundary conditions	$v(0) = 0$ $v(L) = 0$	$v(0) = 0$ $\frac{dv}{dx}(0) = 0$	$v(0) = 0$ $\frac{dv}{dx}(0) = 0$ $v(L) = 0$	$v(0) = 0$ $\frac{dv}{dx}(0) = 0$ $v(L) = 0$ $\frac{dv}{dx}(L) = 0$
Characteristic equation $\lambda = \sqrt{\frac{P}{EI}}$	$\sin \lambda L = 0$	$\cos \lambda L = 0$	$\tan \lambda L = \lambda L$[b]	$2(1 - \cos \lambda L) - \lambda L \sin \lambda L = 0$
Critical load P_{cr}	$\frac{\pi^2 EI}{L^2}$	$\frac{\pi^2 EI}{4L^2} = \frac{\pi^2 EI}{(2L)^2}$	$\frac{20.13EI}{L^2} = \frac{\pi^2 EI}{(0.7L)^2}$	$\frac{4\pi^2 EI}{L^2} = \frac{\pi^2 EI}{(0.5L)^2}$
Effective length L_{eff}	L	$2L$	$0.7L$	$0.5L$

The minimum required diameter of the vertical sections of the stand was calculated using the Euler buckling formula, in which the second area moment of inertia was determined first. The height of the stand was 1m. The sections were assumed to be fixed and pinned at the ends.

The second moment of inertia was calculated as follows:

$$I = \frac{P_{cr} \times {L_{eff}}^2 \times s.f.}{E \times \pi^2} = \frac{2.5(0.7 \times 1)^2 \times 2}{\pi^2 \times 210 \times 10^9} = 1.1821 \times 10^{-12}\ m^4$$

Thus, the required minimum diameter is given as:

$$d = \left(\frac{I \times 64}{\pi}\right)^{1/4} = \left(\frac{1.1821 \times 10^{-12} \times 64}{\pi}\right)^{1/4} = 4.9264\ mm$$

The used material was 8 mm diameter.

Determination of the welding material required

The American Welding Society (AWS) applies an E prefix to a four or five-digit numbering system for electrodes, with the first two or three digits designating the approximate tensile strength. The numeral after the last one denotes the welding position, such as flat, vertical, or overhead. On request, the AWS will provide the whole set of requirements. The following are some pertinent conversions between S.I and Imperial units.

1-pound force = 4.448 N

1 inch = 0.0254 metre

A conversion factor of 6,894 is used (from imperial in Kpsi to metric in Pa. you multiply by 6894).

Tables 3.3 and 3.4 show the minimum weld properties and values of permitted stresses in relation to the yield stresses by the AISC code for weld metal, respectively.

Table 3. 3 Minimum weld properties [203]

AWS electrode number	Tensile strength (kpsi)	Yield strength (kpsi)	% elongation
E60xx	62	50	17-25
E70xx	70	57	22
E80xx	80	67	19
E90xx	90	77	14-17
E100xx	100	87	13-16
E120xx	120	107	14

Table 3. 4 Stresses that are permitted by AISC code for mild steel weld metal [203]

Type of loading	Type of weld	Permissible stress	n
Tension	Butt	$0.60s_y$	1.67
Bearing	Butt	$0.9s_y$	1.11
Bending	Butt	$0.6\text{-}0.66s_y$	1.52-1.67
Simple compression	Butt	$0.6s_y$	1.67
Shear	Butt of fillet	$0.4s_y$	1.44

The safety factor n was computed using the energy theory. Factors that are implied by this code were easily calculated.

For tension n = (1/60), and for shear n = (0.577/0.40), if the distortion-energy theory is taken as the criterion of failure.

Table 3.5 shows the various values of fatigue strength reduction factors of a weld material of mild steel in different joints.

Table 3. 5 Fatigue strength reduction factor [203]

Type of weld	**k_f**
Reinforced butt weld	1.2
Toe of transverse fillet weld	1.5
End of parallel fillet weld	2.7
T-butt joint with sharp corners	2.0

For the condenser stand

Considering Shear Stress

The type of welding rod that was used was determined as follows [203];

$$s_y = \frac{\sigma_w \times k_f \times n}{0.6} \qquad \text{Eq. 3.26}$$

Reduction factor $K_f = 2.0$

Factor of safety n =1.44

$$\sigma_w = \frac{Mass \times Gravitationa\ Acc.}{Area} = \frac{16\ \times\ 10}{2 \times \frac{\pi \times 0.008^2}{4}} = 1591549\ N/m^2$$

$$s_y = \frac{\sigma_w \times\ k_f \times\ n}{0.6} = \frac{1591549 \times\ 2.0\ \times 1.44}{0.6} = 7{,}639{,}437\ N/m^2$$

$$s_{y(in\ table\ 3.3)} = \frac{7{,}639{,}437}{6894 \times 1000} = 1.10813 \text{ Kpsi}$$

Using the value of $s_y(in\ table\ 3.3)$ (1.10813 Kpsi), a weld of E60xx electrode will be able to withstand that stress.

3.3.6 Oil Collector

The reactor could be fed with a capacity of 6 kg, and the maximum amount of oil that can be extracted from tyres is 58 %. The density of oil was assumed to be 950 kg/m^3. The volume of the oil collector required was calculated as follows;

$$Volume\ of\ Oil\ Collector = \frac{Mass\ of\ Feed\ Material \times Maximum\ Oil\ Fraction}{Density\ of\ Oil} \qquad \text{Eq. 3.27}$$

$$Volume\ of\ Oil\ Collector = \frac{6.5 \times 0.58}{950} = 0.00397\ m^3 = 3.97\ litres$$

The calculated size was approximately 4 litres and a five litre container was adopted. Its material (PET plastic) was stable at the temperature at which the oil was collected. Its makeup material was also free from any reaction with the collected liquid.

3.3.7 Pressure Connector tube

This tube connected the pressure gauge to the reactor, and it was connected to a valve that was used to release pressure in case it built up. It was made up of mild steel since it has the ability to withstand the temperature that was used in pyrolysis. The available size that was to be fitted to the pressure gauge was 18 mm dimeter with 1mm thickness. It was cooled by water to ensure that the pressure gauge could not be spoiled by the high temperature of the reactor. The maximum longitudinal and circumferential stresses (pressure) it could withstand at the operating temperature were calculated in Section 3.3.3 as 55.556 and 27.778 bar, respectively.

3.4 Extraction of Tyre Pyrolysis Oil

Tyre pyrolysis necessitates a number of steps, beginning with the collection of raw materials, followed by preparation, placement in the reactor, and firing of the reactor to decompose the tyres into final pyrolysis products.

3.4.1 Raw Materials Collection and Preparation

Worn-out tyres were brought to the workplace. They were cleaned and dried then cut into pieces with cross-sections of 2-3 cm wide [38], [71], [108]. The optimum size that was required is 4 cm^3 [22], [84]. They were fed directly into the reactor of 6 kg capacity.

3.4.2 Extraction and Collection of Tyre Pyrolysis Oil

The sample material was placed in the reactor chamber, locked before the start of pyrolysis. A crucible furnace was used to heat the reactor chamber. The outlet of the reactor was located at the top for the condensable and non-condensable fractions that were directed to the condenser by the volatile product tube.

Heating was done up to a temperature of 550 °C under atmospheric pressure since this is the optimum temperature to extract oil [23], [24], [140], [204], [35], [73], [80], [81], [89], [107]–[109] at a rate of 2 ^{o}C/sec. The reactor temperature was maintained between 530 ^{0}C and 570 ^{0}C by switching the crucible furnace off at the upper limit and on at the lower limit for forty five minutes. The liquid and gaseous products were allowed to exit the reactor and the oil was collected while the non-condensable gases were combusted.

After the completion of the pyrolysis, heat supply to the reactor was stopped. The collected pyrolytic oil was weighed. The system was then prepared for the next run. This process was carried out thrice on each of the oil samples that were obtained with sodium carbonate catalyst (with 99% purity) of mass percentages of 0, 1.5, 2.5, 5, 7.5, and 10 with tyre mass percentages of 100, 98.5, 97.5, 95, 92.5 and 90 in the reactor's feedstock respectively. Figure 3.3 shows the schematic diagram of the process of pyrolysis and collection of oil.

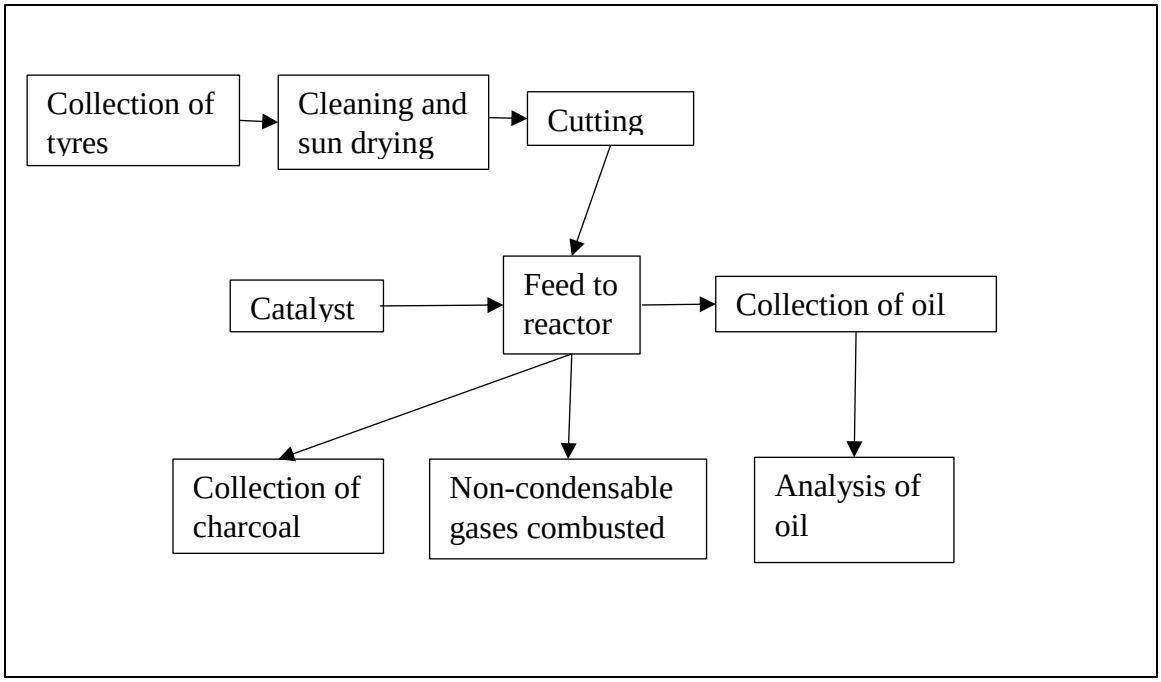

Figure 3. 3 the schematic diagram of the process of pyrolysis and collection of oil.

3.5 Determination of Physical and Chemical Properties of Pyrolysis Oil

The following chemical and physical properties were determined for the pyrolysis and diesel oils; specific gravity, kinematic viscosity, flash point, calorific value, Sulphur content, pH, Cetane number and composition. Detailed descriptions of each test are as outlined below.

3.5.1 Specific Gravity

The ratio of a substance's density to that of water is its specific gravity [205], [206]. The purpose of this experiment was to determine the effect of sodium carbonate and exposure to different temperature conditions on the specific gravity of the oil samples. The ASTM D 1298 method for calculating Specific Gravity, Density, or API Gravity of Crude Oil and Liquid Petroleum Products was utilized [185]. This experiment was carried out at the University of Nairobi's Chemistry Department Laboratory.

The following procedure was used in determining the specific gravity of the oil samples.

1. The density bottle was cleaned with tap water, rinsed using distilled water and then dried in the oven.

2. It was then weighed using an analytical weighing scale and its weight recorded.
3. The density bottle was filled with water, corked and then placed in the water bath that had been adjusted to a temperature of 15 ^{0}C for twenty minutes to attain thermal equilibrium.
4. The density bottle with water was then removed from the water bath and wiped to remove all the water drops on its surface. Then weighing was done using the analytical weighing scale five times, and its average value was determined and used in the calculation.
5. The mass of the water in the bottle was determined by calculating the difference in weight between the empty density bottle and the density bottle that was filled with water.
6. After determining the mass and water density at a given temperature, the volume of the water in the bottle was determined, hence calibrating the bottle.
7. The density bottle was emptied then cleaned using a thinner then filled with the fuel sample to be tested.
8. Steps 3, 4 and 5 were repeated for temperatures between 15 ^{0}C and 65 ^{0}C with an increment of 5 ^{0}C for each fuel sample. The specific gravity for each fuel sample was then determined.

The specific gravity was calculated using Equation (3.28) developed by Hannah *et al.* [207].

$$s.g. = \frac{M_O - M_e}{M_W - M_e} \qquad \text{Eq. 3.28}$$

Where $s.g = Specific\ Gravity$

$M_e = Mass\ of\ empty\ container$

$M_O = Mass\ of\ Oil + Mass\ of\ empty\ container$

$M_W = Mass\ of\ Water + mass\ of\ empty\ container$

The specific gravity of each fuel sample was determined at each temperature as the mass of fuel ratio to that of water at the same temperature.

3.5.2 Kinematic Viscosity

The ASTM D 445, Standard Test Method for determining Kinematic Viscosity of both Transparent and Opaque Liquids (including Dynamic Viscosity Calculation), was used. Figure

3.4 shows a sketch of Ostwald viscometer size D BS/U790 that was used to determine the viscosity.

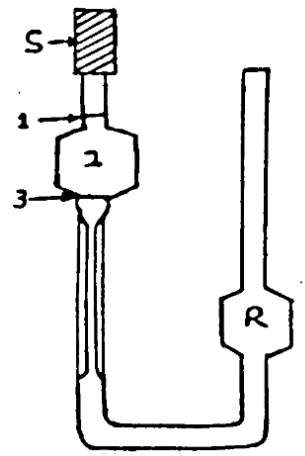

Figure 3. 4 Sketch of Ostwald Viscometer

Cleaning and rinsing of the viscometer was done before drying it in the oven. It was fastened in a vertical posture in a temperature-controlled water bath, with the marks "1" and "3" below the water level and clearly visible through the water bath. 15 ml distilled water was pipetted into the broader arm, allowing it to fill the upper bulb '2' halfway between the two marks while also leaving the lower bulb R at least 1/3 filled. With the help of a thermostatic thermometer, ice cold water was used in adjusting the water bath temperature and allowed for 15-20 minutes to attain its thermal equilibrium.

The oil sample was sucked up through 'S' to a level above mark '1' and then allowed to flow down through the tube. The time it took for the meniscus to move from '1' to '3' was then determined (Fig. 3.3) using a stop watch. The average time was calculated after doing this at least five times. This method was repeated in 5 °C increments at temperatures ranging from 15 °C to 60 °C. This procedure was done on all the test fuels, and the viscosity of the fuels was determined using Equation 3.29 developed by Pritchard *et al.* [200]. This test was carried out in the Chemistry department Laboratory of The University of Nairobi.

$$\upsilon_o = \frac{\upsilon_w t_o}{t_w} \qquad \text{Eq. 3.29}$$

Where υ_w – Kinematic viscosity of the oil

υ_o – Kinematic viscosity of water

t_o – Time taken for oil to flow from point 2 to 3

t_w- Time taken for water to flow from point 2 to 3

3.5.3 Calorific Value

ASTM D 4809, Standard Method for determining Heat of Combustion of Liquid Hydrocarbon Fuels (Precision Method), using a bomb colorimeter was used. This test was carried out in Chemistry department Laboratory of the University of Nairobi.

Procedure:

A bomb calorimeter was used in determining the calorific value of the oil samples and the procedure that was used is as follows [206];

1. The weight of the empty capsule was determined using an analytical weighing scale and it was recorded.
2. The capsule was filled with the sample oil and their weight was determined. The mass of the oil sample was calculated using the weight of the filled capsule and the empty capsule.
3. The cooling jacket of the calorimeter was filled with 1700ml of water.
4. The capsule with the oil was put in the crucible and placed in the firing apparatus of the calorimeter.
5. The bomb calorimeter was assembled after being charged with oxygen up to 25 atmospheres of the calorimeter. The stirrer was then switched on.
6. The temperature readings were taken at intervals of one minute for five minutes to make sure that the temperature of the bomb was stable, and then the bomb was fired.
7. Temperatures were taken at intervals of half a minute for the entire range of the temperature rise and at one minute intervals for five minutes after temperatures started to drop.

Calculations

Determination of the energy that was transferred to the cooling water was done using Equation (3.30) [206], [208]

$$Energy\ (cal/g) = \frac{2335 \times \Delta T}{mass\ of\ capsule\ and\ oil} \qquad \text{Eq. 3.30}$$

$$\Delta T = (maximum\ temperature\ attained) - (temperature\ at\ firing) \qquad \text{Eq. 3.30(a)}$$

2335 is the energy due to the calorimeter.

The energy contributed by combustion of the capsule was calculated as follows:

$$capsule\ energy\ (cal) = capsule\ mass\ (g) \times energy\ due\ to\ capsule \qquad \text{Eq. 3.30(b)}$$

The capsule energy was subtracted from the energy transferred to the cooling bath and the net energy contributed by the combustion of oil was determined.

The energy content was converted from cal. /g and expressed as MJ/Kg using the following converting factor: 1 calorie = 4.184 joules.

3.5.4 Flash Point

The Open Cup Test Method for determining Flash Point was used. The oil was placed in the tester's cup and heated slowly at a constant rate. At regular intervals, a source of ignition was delivered into the cup. The flash point was determined as the lowest temperature at which the vapor above the specimen ignited when the ignition source was applied [185]. This test was carried out in the Chemistry department Laboratory of the University of Nairobi.

3.5.5 Sulphur Content

ASTM D 129, Standard Method was used (General Bomb Method). Total sulphur in liquid and solid petroleum products that may be liquefied with moderate heating or dissolved in a suitable organic solvent can be determined by this test [185]. The sample was oxidized by combustion in a bomb calorimeter that contained oxygen under high pressure. The sulfur, as sulfate in the bomb washings, was then determined gravimetrically as barium sulfate. This test was carried out in Chemistry department Laboratory of the University of Nairobi.

3.5.6 pH

The pH of the fuel was determined using a Signal digital pH meter. The following procedure was followed;

1. The meter was calibrated by making a 100 ml solution of pH 7 and pH 4 using the provided tablet.
2. Calibration was achieved by using a calibration knob on the pH meter.
3. The tablet was then inserted into the samples of tyre pyrolysis oil that were tested.
4. The pH value was read directly from the digital display.

3.5.7 Cetane Index

ASTM D 976, Standard Test Method was used to calculate the Cetane index of the fuel samples [185]. Each fuel sample was heated to a temperature at which 50 % of the fuel evaporated. This process was done thrice for each sample and the average value was used for the calculation of Cetane index using Equation 3.26 [12], [26], [179], [180], [185].

$$CI = 454.74 - 1641.416D + 774.74D^2 - 0.544T_{50} + 97.803[log_{10}(T_{50})]^2 \quad \text{Eq. 3.31}$$

Where $CI = Cetane\ Index$

$D = Fuel\ Density\ at\ 15\ degrees\ centigrade$

$T_{50} = 50\ \%\ Recovery\ Temperature\ (degrees\ centigrade)$

3.5.8 Fourier Transformation Infrared Spectroscopy (FT-IR)

Fourier Transformation Infrared (FTIR) analysis was performed using the IRTracer-100 Shimadzu model equipment. The FTIR spectra of the oils were recorded using a Perkin Elmer synthesis monitoring system for characterization. The FTIR spectra were obtained with 8 cm^{-1} resolution in the 600–4000 cm^{-1} range.

3.5.9 Gas Chromatography and Mass Spectrometry (GC-MS)

Gas chromatography-mass spectrometry analysis was done using GCMS-QP2010 SE model equipment. The injection temperature was 200 °C and the column oven temperature was 35 °C. Split injection mode was used with linear flow control mode at 5.7 psi pressure. The total flow was 73.7 mL/min with a column and purge flow of 0.70 and 3.0 mL/min, respectively, at a linear velocity of 30.0 cm/sec at 100 split ratio. The High-Pressure Injection and Splitter Hold were off while the Carrier Gas Saver was on with a split ratio of 5 and a server time of 1 minute. The oven temperature program was maintained at 35 °C for 5 minutes, then a heating rate of 5 °C/minute to a temperature of 100 °C was done, followed by another heating rate of 50 °C/minute to a final temperature of 250 °C and held at 250 °C for 5 minutes. The Ion Source and Interface Temperatures were 200 and 250.00 °C, respectively, with a Solvent Cut Time of 2.00 minutes. The detector gain was 1.05 kV (+0.00 kV) with a mode relative to the tuning result. The time taken for running was 26 minutes, with a start time of 2:30 min. The ACQ mode was used to scan. The event time was 0.30 sec at a scanning speed of 1666 with a frequency of 35.00 at the start and 500.00 m/z at the end. The ion mass spectra were automatically determined and compared to the spectrum libraries using NIST search

software. The retention duration of standard solutions was used to validate the identity of the peaks and provide quantitative analysis.

3.6 Summary of the Chapter

The pyrolysis system was designed and fabricated, then it was used to extract oil from tyres. Extraction of TPO from tyres, and assessment of physico-chemical properties was carried out. Chemical analysis on hydrocarbons present and functional group analysis were carried out and compared to diesel fuel.

CHAPTER FOUR: RESULTS AND DISCUSSIONS

4.1 Introduction

This chapter contains the designed and fabricated components of the pyrolysis system and the evaluation of fuel properties of the extracted oil in comparison to diesel fuel.

4.2 Design and Fabrication of the Pyrolysis System

4.2.1 Design Specifications of the Pyrolysis System

Design specifications of the pyrolysis system were tabulated as shown in Table 4.1. Technical drawings are in appendix A

Table 4. 1 Design specifications of the pyrolysis system

Part No.	Item name	Min. design specification	Adopted specification	Safety Factor	No. of pieces	Material
001	Reactor	Diameter: 15 mm Length: 15 mm Shape: see Figure 4.1	Diameter: 15 mm Length : 15 mm	2	1	Mild steel
002	Condenser	Diameter: 89 mm Length: 650 mm Shape: see Figure 4.2	Diameter: 89 mm Length: 650 mm	2	1	Mild steel shell and copper tubes
003	Condenser stand	Length: 715 mm Width: 405 mm Height: 950 mm Shape: see Figure 4.3	Length: 715 mm Width: 405 mm Height: 950 mm	2	1	Mild steel bars
004	Connection tube	Length:1.65 m Diameter: 4.96 mm Shape: see Figure 4.4	Length: 1.65 m Diameter: 9 mm	2	1	Mild steel and copper tubes
005	Pressure gauge tube	Length: 2.3 m Diameter: 18 mm Shape: see Figure 4.5	Length : 2.3 m Diameter: 18 mm	2	1	Mild steel tube

4.2.2 Reactor

The reactor was made up of mild steel material. Its function was to house and transfer heat to the feed material. After reaction process the volatile products could leave the reactor through the volatile product tube. Figure 4.1 shows an isometric view of the batch type reactor.

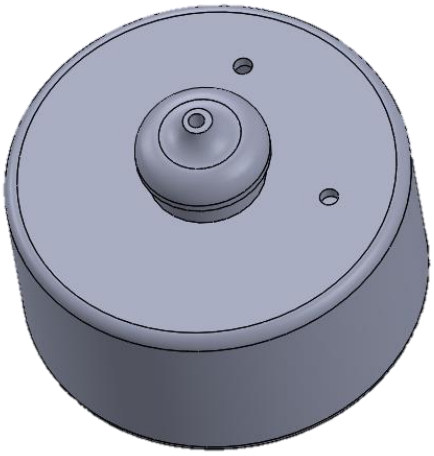

Figure 4. 1 Batch type reactor (Part No. 001).

4.2.3 Water Cooled Condenser

The condenser was made up of a galvanized steel shell, copper tubes, a reducing cup and a closing cup. Its function was to condense the condensable gases into oil. Figure 4.2 shows an isometric view of the water cooled condenser with oil collector.

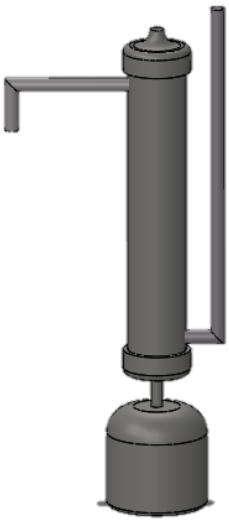

Figure 4. 2 Water Cooled Condenser with oil collector (Part No. 002).

4.2.4 Condenser Stand

It was made up of an 8mm diameter bar. Its function was to carry the condenser. Figure 4.3 shows an isometric view of the condenser stand.

Figure 4. 3 Condenser Stand (Part No. 003).

4.2.5 Volatile Product Tube

The volatile product tube was made up of four 6mm and one 16mm bolts, ¾" diameter mild steel tube and a 9mm copper tube. Its function was to carry both condensable and non-condensable gases from the reactor to the condenser. It could offer some cooling to the gases before their entry to the condenser. Figure 4.4 shows an isometric view of the connection tube.

Figure 4. 4 Connection Tube (Part No. 004).

4.2.6 Pressure Gauge Tube

The pressure gauge tube was made up of mild steel tubes, (3/4” and 1.5”) a valve and 18 mm bolt and nut. It connected the pressure gauge to the reactor. Figure 4.5 shows an isometric view of the pressure gauge tube.

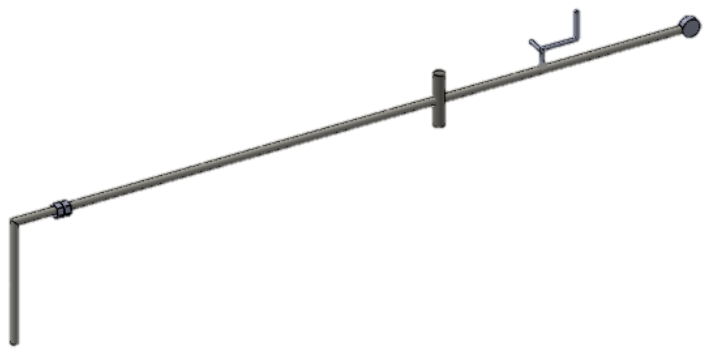

Figure 4. 5 Pressure Gauge Tube (Part No. 005).

4.2.7 Assembled Structure of a Pyrolysis System

After the designing process, the components were assembled as shown in Figure 4.6.

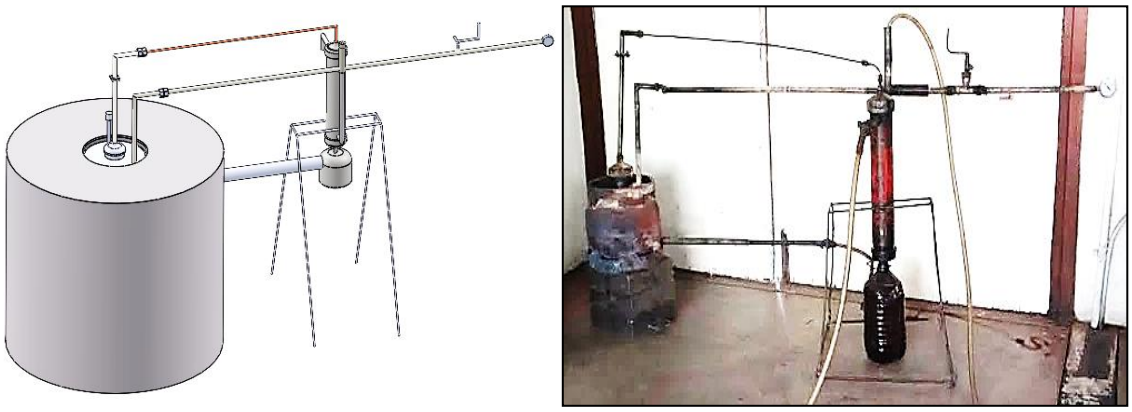

Figure 4. 6 Physical structures designed and fabricated pyrolysis system.

4.3 Oil Extraction

The produced TPO was black in colour with a strong smell. Six kilograms of feed material required four and half litres of diesel fuel for complete pyrolysis. The mass percentage of TPO yield in relation to the feed material was recorded in Table 4.2.

Table 4. 2 The mass percentage of TPO yield in relation to the feed material

Fuel sample	Percentage of oil yield
TPO 0.0 % sodium carbonate	35
TPO 1.5 % sodium carbonate	38
TPO 2.5 % sodium carbonate	39
TPO 5.0 % sodium carbonate	41
TPO 7.5 % sodium carbonate	42
TPO 10 % sodium carbonate	43

The results in Table 4.2 were used to plot a graph of TPO yield in relation to the percentage of sodium carbonate used as shown in Figure 4.7.

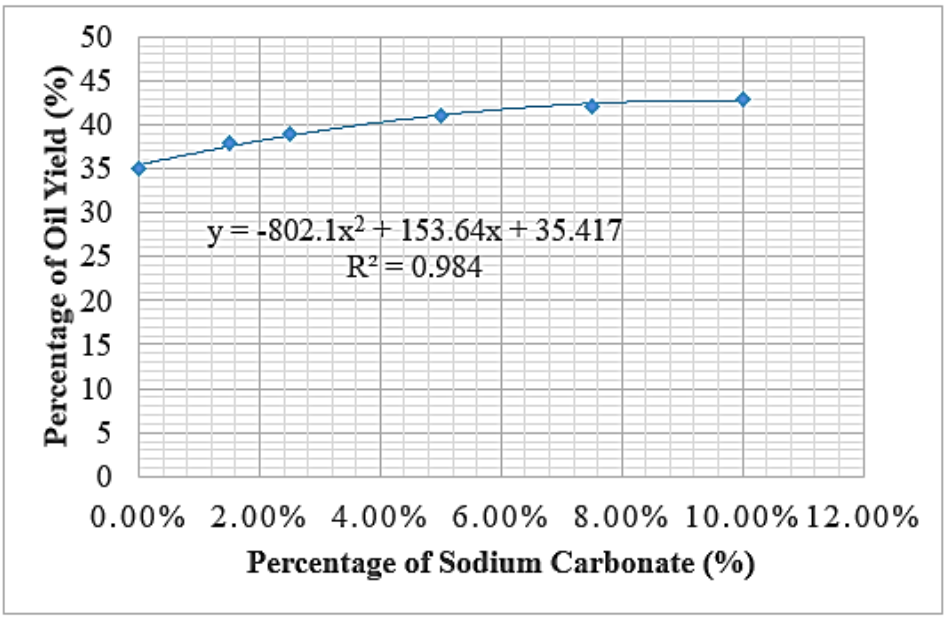

Figure 4. 7 Variation of TPO yield with the percentage of sodium carbonate used.

It was found from figure 4.7 that the TPO yield was 35 percent without a catalyst, and this was in agreement with Leonard [89] who reported 33 percent oil yield. There was an increase in TPO yield with an increase in catalyst up to 43 percent with a catalyst concentration

of 10 percent and this was in agreement with Demirbas et al. [4] who did pyrolysis at 485 ^{o}C using 10% catalyst (Na_2CO_3) and obtained 49.2 % weight of oil whereas they found the yield of oil to be 39.6 % when carrying out thermal pyrolysis under the same conditions. The difference in yield could have been a result of the size difference in the feed material. Demirbas et al. [4] used fine material while in this research size of 4 cm^3 was used. When using larger particles, the nucleus becomes carbonized or does not fully decompose, resulting in lower gas and liquid yields and higher char yields [56], [117], [120]. The introduction of a catalyst reduced the activation energy required for the pyrolysis process to take place, hence improving the reactivity of cracking of large molecular weight compounds resulting in an increase in oil yield [118], [126].

When the catalyst was increased beyond 5 percent, the increase in yield started stagnating. This could be due to the CO_2 that was generated during the process of pyrolysis, mixed with Na_2CO_3, which resulted in partial thermal and partial catalytic pyrolysis processes taking place simultaneously [118]. There was a reaction between the generated sulfur and sodium carbonate to form sodium sulfate with larger molecules compared to sodium carbonate, hence reducing the reaction surface area to volume ratio between the feed material and catalyst [14], [209]–[211].

4.4 Physico-chemical properties

4.4.1 Specific Gravity

The ratio of a fuel's density to that of water is its specific gravity and this was determined between a temperature of 15°C and 60°C at an increase of 5°C for each fuel. The results were presented as indicated in Table 4.3.

Table 4. 3 Values of specific gravity at different temperatures for TPO and Diesel fuel

Temperature	Percentage of sodium carbonate used						Diesel
	0.00 %	1.5 %	2.5 %	5.0 %	7.5 %	10.0 %	
15	0.92395	0.9369	0.94065	0.9444	0.94973	0.95506	0.84755
20	0.92167	0.93508	0.93795	0.94186	0.94577	0.95071	0.84371
25	0.91861	0.93299	0.93586	0.93986	0.94292	0.9481	0.84089
30	0.91502	0.93048	0.93369	0.9369	0.9402	0.94549	0.83793
35	0.91126	0.92836	0.93144	0.93371	0.9381	0.94248	0.8343
40	0.90675	0.92503	0.92954	0.93205	0.93576	0.93947	0.83127
45	0.90172	0.9214	0.92666	0.93041	0.93339	0.93636	0.82847
50	0.89768	0.91707	0.92227	0.92747	0.93035	0.93324	0.82638
55	0.89466	0.91298	0.919	0.92347	0.9268	0.93013	0.82337
60	0.89212	0.91011	0.91667	0.92119	0.9247	0.92737	0.82009

The results in Table 4.3 were used to plot a graph of specific gravity with temperature for TPO and diesel fuel as shown in Figure 4.8.

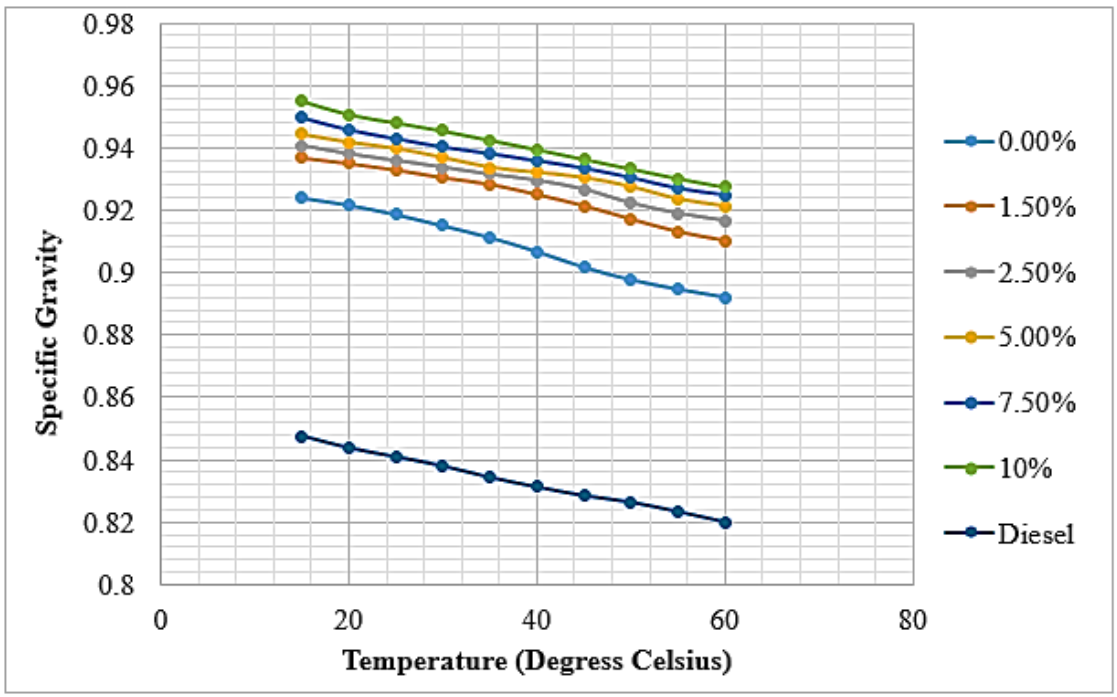

Figure 4. 8 Variation of specific gravity with temperature for TPO and Diesel Fuel.

It was observed in Figure 4.8 that the specific gravity is a temperature dependent property. When the temperature was increased from 15 to 60 °C the specific gravity was found to decrease from 0.92395 to 0.89412 for TPO (without a catalyst), while that of diesel

decreased from 0.84755 to 0.82009. The increase in temperature results to an increase in thermal or kinetic energy, and the molecules of fluids become more mobile, increasing the occupied volume, hence reducing the density. Also, the attractive forces between molecules of a liquid reduce with an increase in temperature, hence increasing the distance between them. TPO had a higher specific gravity than diesel fuel at all temperatures tested.

The specific gravity of TPO at 20 ^{0}C was 0.92167, which was above the limit that is recommended by KEBS (0.820 - 0.870 at a temperature of 20 ^{0}C) for diesel fuel (0.84371). The specific gravity of TPO was also found to be in agreement with Martinez *et al.* [80] but Islam *et al.* [22] found it to be 0.943 which was slightly more. Using a catalyst made the density of the tyre pyrolysis oil increase with the amount of catalyst, deviating it further from the recommended value. In order to attain the required specific gravity, a blend of diesel and TPO with proportions of 67 % and 33 % respectively, may be used to get a specific gravity of 0.86944. When 10 % catalyst (with 10 % sodium carbonate) is used, a blend of diesel 76 % and TPO 24 % can also be appropriate to get a specific gravity of 0.86939.

The linear regression square method was used to estimate the measured values of TPO's specific gravity that were produced using sodium carbonate, and Equation 4.1 was applied:

$$S.G. = mt + b \qquad \text{Eq. 4.1}$$

Where: *S.G.* = specific gravity,

t = temperature (°C),

m and *b* = correlation constants

Table 4.4 lists the regression constants and coefficients for DF, TPO, and TPO with catalyst, while Figure 4.9 depicts the linear least square regression lines.

Table 4. 4 The linear square regression constants and coefficients for specific gravity as a function of temperature for the oil samples.

Fuel sample	$m \times 10^{-4}$	b	R^2
TPO 0.0 % sodium carbonate	-8	0.9367	-0.99664
TPO 1.5 % sodium carbonate	-6	0.948	-0.99071
TPO 2.5 % sodium carbonate	-5	0.9493	-0.99368
TPO 5.0 % sodium carbonate	-5	0.9523	-0.99700
TPO 7.5 % sodium carbonate	-5	0.9569	-0.99790
TPO 10 % sodium carbonate	-6	0.9635	-0.99930
Diesel fuel	-6	0.9975	-0.99875

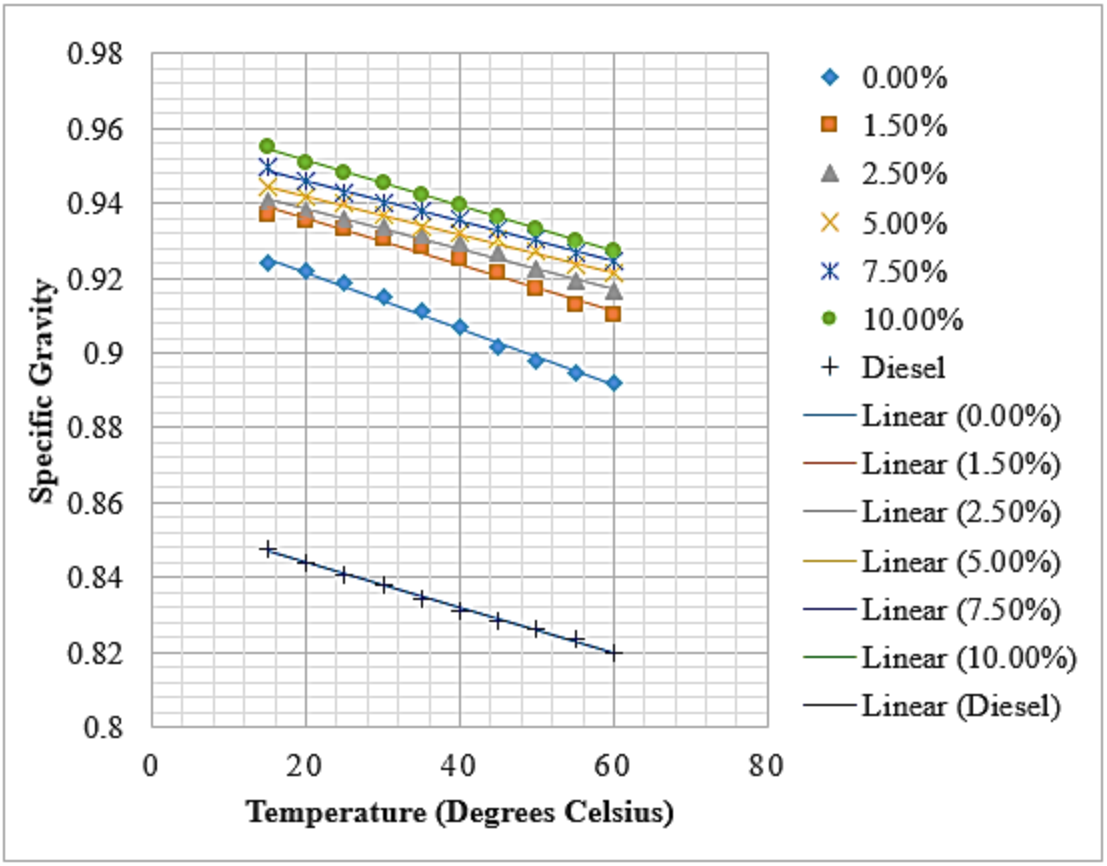

Figure 4. 9 Specific gravity regression lines for diesel fuel, TPO, and TPO with catalyst as a function of temperature.

Using the correlation constants in Table 4.4, the specific gravity of each fuel at various temperatures may be computed. The lowest regression coefficient R^2 was 0.99071, indicating that linear least square regression well reflected the connection between specific gravity and temperature.

The different values of specific gravity that were measured could possibly correlate as a function of the percentage sodium carbonate employed in oil extraction, as shown by Equation 4.2.

$$S.G. = cx^4 + dx^3 + ex^2 + fx^1 + gx^0 \qquad \text{Eq. 4.2}$$

Where *SG* is the fuel's specific gravity, *x* is the percentage of sodium carbonate used, and *c*, *d*, *e*, *f* and *g* are correlation constants. Table 4.5 contains the correlation coefficients and

regression constants, while Figure 4.10 depicts the least square regression lines at various temperatures.

Table 4. 5 The regression coefficients and square regression constants for Specific gravity as a function of sodium carbonate used during pyrolysis for some temperatures.

Temperature (^{0}C)	c	d	e	f	g	R^2
15	-1725.3	414.21	-33.894	1.2837	0.9240	1.0000
20	-1567.8	388.73	-33.047	1.2747	0.9217	0.9991
25	-1462.5	379.40	-33.793	1.3415	0.9187	0.9985
30	-1810.7	458.88	-39.71	1.4966	0.9151	0.9992
35	-2687.4	636.10	-51.053	1.7421	0.9113	0.9994
40	-2487.8	606.42	-50.986	1.8491	0.9068	1.0000
45	-2219.0	558.03	-49.387	1.9236	0.9017	0.9999
50	-1855.8	477.56	-43.888	1.8238	0.8977	0.9997
55	-1774.4	459.80	-42.374	1.7688	0.8946	1.0000
60	-1732.4	445.94	-41.226	1.7488	0.8921	0.9997

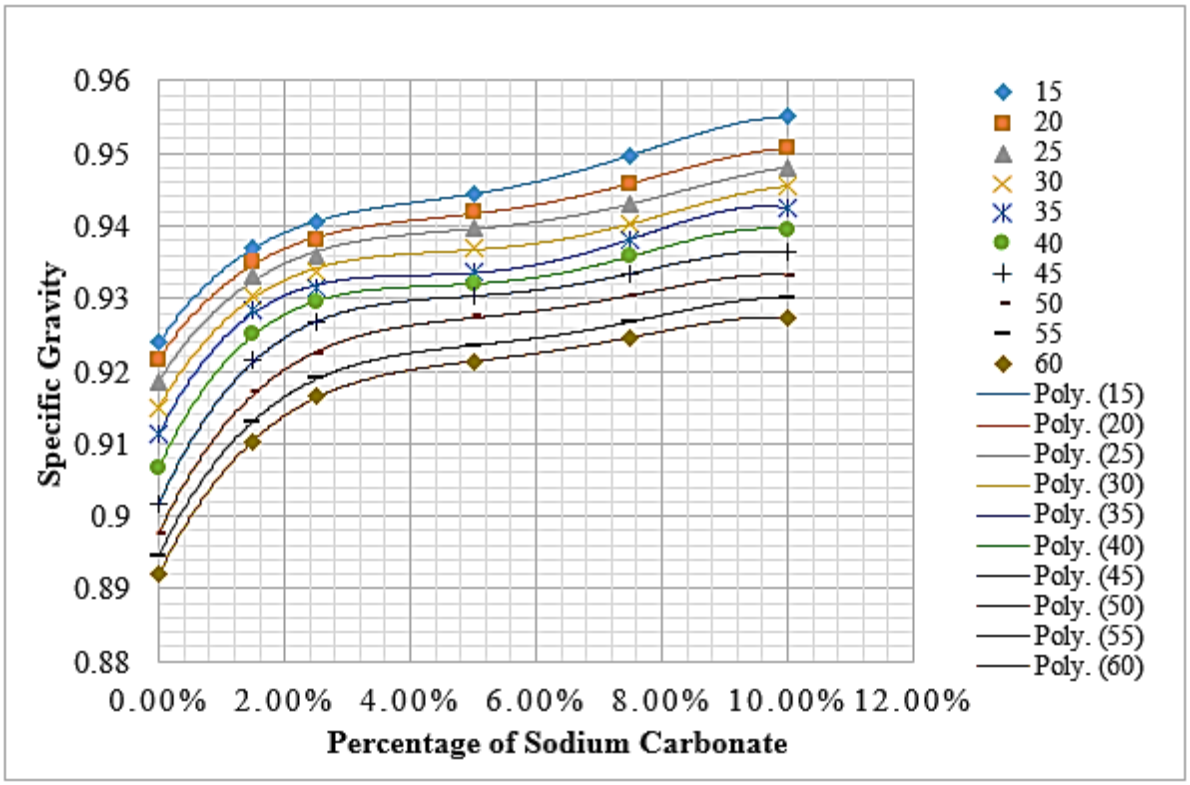

Figure 4. 10 Specific gravity regression lines as a function of the amount of sodium carbonate utilized at various fuel temperatures.

It was found from Figure 4.10 that using sodium carbonate (catalyst) resulted in an increase in specific gravity at all test temperatures, which agrees with Demirbas *et al.* [4]. The increase between 0 % and 1.5 % was rapid and then the rate of increase of specific gravity reduced but continued to increase with the increase of a catalyst. The carbon chain length is inversely proportional to the density of liquid hydrocarbons. During the increase in branching, there was an increase in the concentration of shorter carbon chain lengths and the number of double bonds in the tyre pyrolysis oil, thus contributing to the increase in specific gravity [143].

4.4.2 Kinematic viscosity

The kinematic viscosity of the test fuels was determined at each temperature, and the results are shown in Table 4.6.

Table 4. 6 Values of kinematic viscosities at different temperatures for TPO and Diesel fuel

Temperature	Percentage of sodium carbonate used						Diesel
	0.00 %	1.50 %	2.50 %	5.00 %	7.50 %	10.00 %	
15	7.05303	3.50833	2.33333	3.20833	4.50758	4.97273	4.13637
20	5.75379	3.10227	1.96212	2.78409	3.79167	4.34849	3.48561
25	4.69319	2.73106	1.80303	2.41288	3.30091	3.71212	2.9697
30	3.97728	2.43939	1.67045	2.20379	2.86364	3.24091	2.65159
35	3.51326	2.20075	1.53788	2.04167	2.56243	2.82993	2.38643
40	3.04924	2.05469	1.43182	1.85606	2.32031	2.51894	2.20076
45	2.79734	1.88257	1.35227	1.67045	2.15167	2.29727	2.04172
50	2.54545	1.66394	1.27272	1.55741	2.02728	2.1212	1.93566
55	2.41287	1.54485	1.16666	1.43181	1.91928	1.98864	1.85606
60	2.22121	1.4953	1.14015	1.43181	1.85122	1.88258	1.82955

The results in Table 4.6 were used to plot a graph of kinematic viscosity with temperature for TPO and diesel fuel as shown in Figure 4.11.

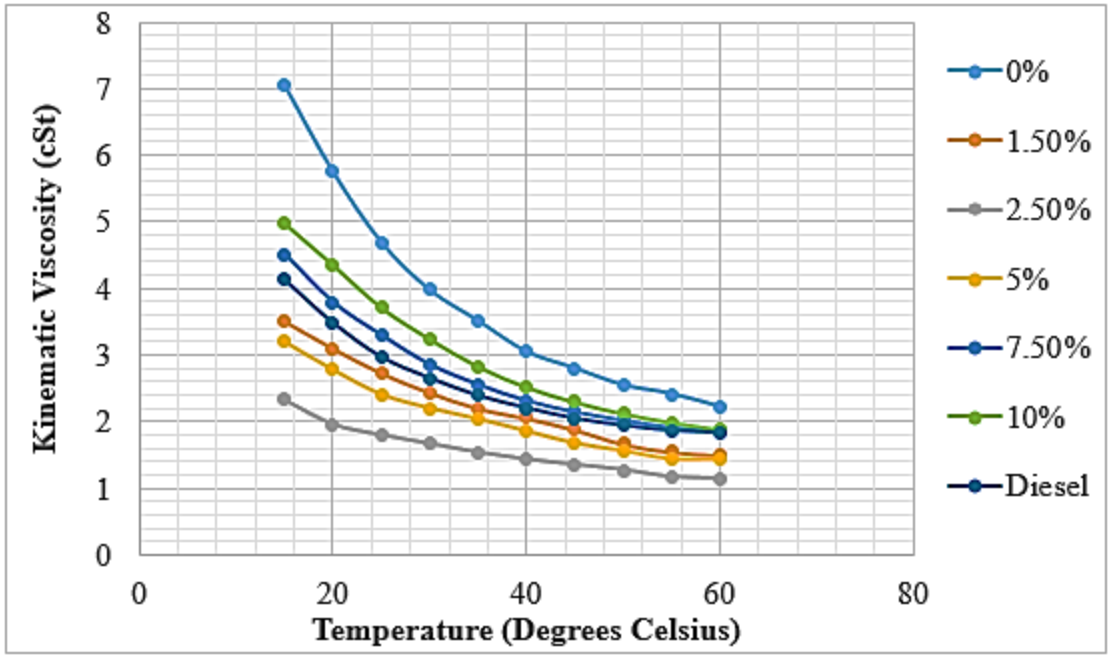

Figure 4. 11 TPO and Diesel Fuel Kinematic Viscosity Variation with Temperature.

It was observed from Figure 4.11 that kinematic viscosity is a temperature-dependent property. As the temperature was increased from 15 to 60 °C the kinematic viscosity decreased from 7.05303 cSt to 2.12121 cSt for TPO (without a catalyst) while that of diesel fuel decreased from 4.13637 cSt to 1.82955 cSt. TPO gave a high kinematic viscosity at all test temperatures when compared to diesel fuel. The temperature increase in the liquid causes a reduction in cohesive forces, resulting in a decrease in shear stress, which is responsible for the kinematic viscosity of TPO. The determined kinematic viscosity values were in agreement with Frigo *et al.* [32] and the kinematic viscosity was within the required range that is recommended by KEBS (1.9 - 6 cSt at a temperature of 40 ^{0}C).

A second order polynomial model in the form of Equation 4.3 was used to accurately fit the fluctuation in viscosity with temperature.

$$\upsilon = jt^2 + kt^1 + mt^0 \qquad \text{Eq. (4.3)}$$

Where kinematic viscosity υ is measured in centistokes, temperature t is measured in degrees Celsius, and j, k, and m are constants. Table 4.7 contains the various values of the constants for diesel fuel and TPO in relation to sodium carbonate, and Figure 4.12 depicts the least square regression lines for various temperatures.

Table 4. 7 Constants of viscosity correlation and coefficients of determination.

Fuel	$j \times 10^{-4}$	k	m	R^2
0.0 % sodium carbonate	28	-0.3054	10.814	0.9919
1.5 % sodium carbonate	7	-0.0999	4.8034	0.9971
2.5 % sodium carbonate	5	-0.0592	3.0362	0.9862
5.0 % sodium carbonate	8	-0.0960	4.4177	0.9946
7.5 % sodium carbonate	15	-0.1653	6.5677	0.9957
10 % sodium carbonate	15	-0.1804	7.3221	0.9989
Diesel fuel	14	-0.1516	6.0008	0.9931

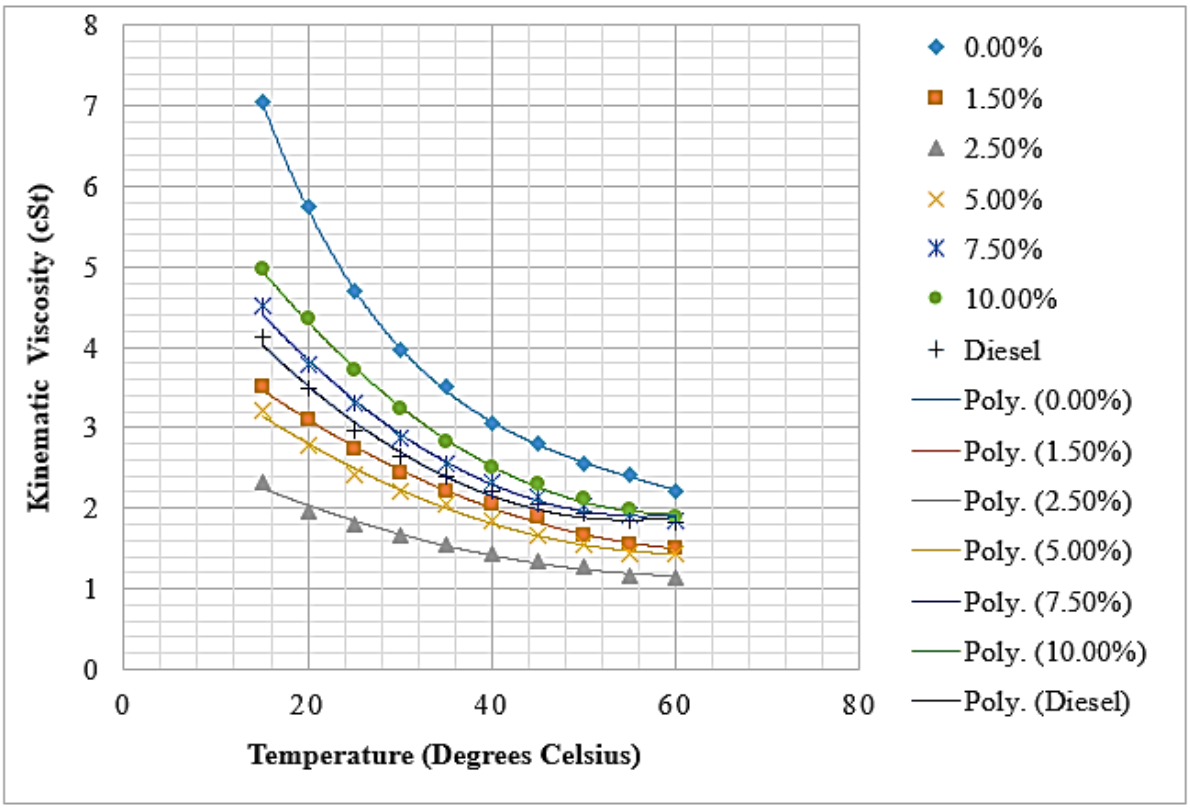

Figure 4. 12 Specific gravity regression lines for diesel fuel, TPO, and TPO with catalyst as a function of temperature.

It was found in Figure 4.12 that diesel fuel, TPO and TPO with catalyst had a polynomial kinematic viscosity-temperature relationship. Using the correlation constants in Table 4.7, the kinematic viscosity of each fuel at various temperatures could be calculated. The lowest regression coefficient R^2 was found to be 0.9919, indicating that the least square

regression accurately represented the relationship between kinematic viscosity and temperature.

Equation 4.4 expresses the variation in kinematic viscosity as a function of the percentage of catalyst utilized.

$$\upsilon = px^4 + qx^3 + sx^2 + nx^1 + yx^0 \qquad \text{Eq. (4.4)}$$

Where υ is kinematic viscosity, p, q, s, n, and y are the correlation constants. The correlation constants p, q, s, n, and y and the correlation coefficients R^2 were recorded in Table 4.8.

As shown in Figure 4.13, using sodium carbonate (catalyst), decreases the kinematic viscosity of TPO as the amount of catalyst increased at all test temperatures. The kinematic viscosity of TPO decreased with an increase in sodium carbonate up to 2.5 % and then started increasing with an increase in sodium carbonate.

Table 4. 8 The regression coefficients and the square regression constants for kinematic viscosity as a function of sodium carbonate percentage used for different temperatures.

Temperature	p	q	s	n	y	R^2
15	291890	-91366	9751.6	-374.520	7.0806	0.996
20	221869	-69493	7496.1	-291.070	5.7940	0.9868
25	112679	-42188	5111.7	-212.170	4.7263	0.9849
30	108209	-36871	4235.3	-170.750	4.0076	0.9800
35	107657	-34798	3820.8	-148.920	3.5410	0.9763
40	52036	-21378	2701.2	-114.010	3.0776	0.9629
45	21505	-14501	2174.8	-99.220	2.8185	0.9749
50	29310	-15581	2149.6	-92.851	2.5580	0.9890
55	17948	-13350	2009.4	-89.765	2.4241	0.9909
60	17743	-12318	1801.0	-78.203	2.2344	0.9832

The variation of viscosity with an increase in the percentage of sodium carbonate for various temperatures is shown in Figure 4.13.

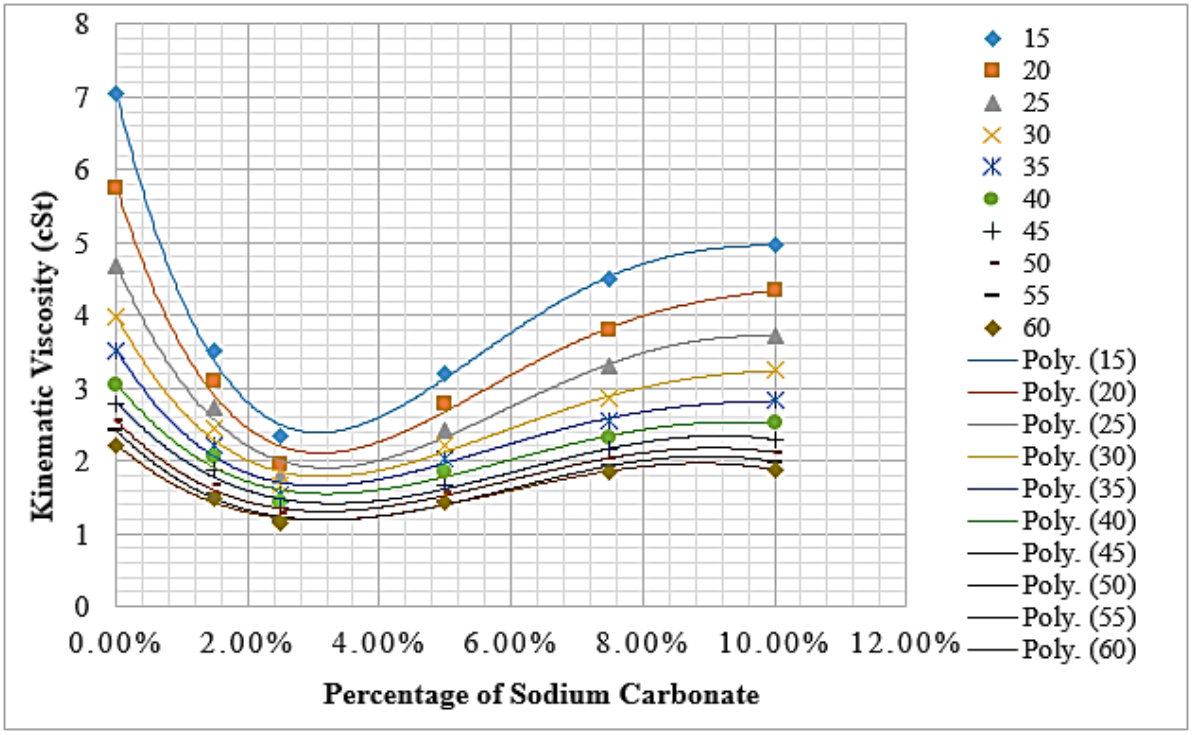

Figure 4. 13 The effect of increasing the amount of sodium carbonate on viscosity at various temperatures.

The kinematic viscosity at 40 ^{0}C varied between 3.04924 and 1.43182 cSt. When using 2.5% and 5% (1.43182 and 1.85606 cSt respectively) the kinematic viscosity was below the limit that is recommended by KEBS (1.9 - 6 cSt at a temperature of 40 ^{0}C).

The TPO without a catalyst had a higher concentration of long carbon chains, which were reduced with an increase in branching when the catalyst was introduced, and this resulted to a decrease in viscosity up to when 2.5 % catalyst was used [161], [162]. Viscosity is also decreased when the degree of unsaturation increases, and it is impacted by the configuration of the double bond, with the trans-configuration having a higher viscosity than the cis-configuration [162]. Branching reduced the contact between carbon chains by preventing neighboring molecules from approaching one another, causing viscosity to rise over 2.5 percent catalyst concentration [167].

4.4.3 Calorific value

The calorific values of diesel fuel and TPO in relation to the percentage of sodium carbonate were determined and recorded in Table 4.9.

Table 4. 9 Calorific values of Diesel fuel and TPO in relation to the percentage of sodium carbonate used to extract it.

Fuel	Calorific value, MJ/kg
TPO 0.0 % sodium carbonate	40.431
TPO 1.5 % sodium carbonate	40.280
TPO 2.5 % sodium carbonate	40.179
TPO 5.0 % sodium carbonate	39.927
TPO 7.5 % sodium carbonate	39.593
TPO 10.0 % sodium carbonate	39.182
Diesel fuel	43.144

The results in Table 4.9 were used to plot a graph of the calorific value of TPO with the percentage of sodium carbonate as shown in Figure 4.14.

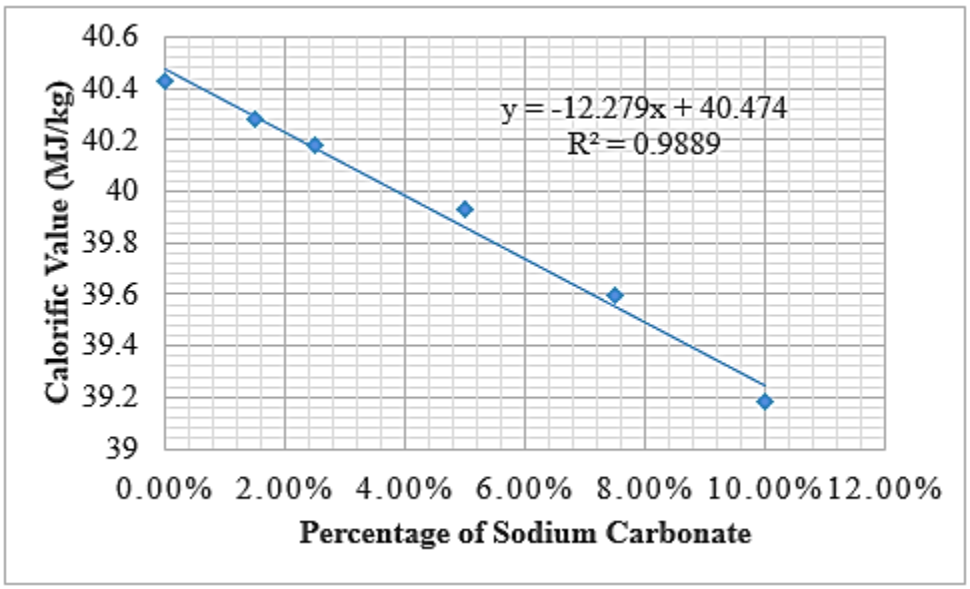

Figure 4. 14 Variation of the calorific value of TPO with the percentage of sodium carbonate.

The calorific value of a fuel refers to the amount of chemical energy released when the fuel is burned. TPO had a calorific value of 40.431 MJ/kg, while diesel fuel was 43.38 MJ/kg, a difference of 6.798 percent. This value of calorific value for TPO was in agreement with Islam *et al.* [78], Hürdoğan *et al.* [86] and Martinez *et al.* [80]. TPO had a higher specific gravity than diesel fuel (918.61 kg/m^3 and 840.89 kg/m^3 at 25 ^{0}C, respectively). Since the

injection pumps work on a volumetric basis, the energy content of TPO is 37.14 MJ/L and 36.48 MJ/L for diesel.

The calorific value of TPO was found to decrease slightly with the introduction of sodium carbonate from 40.431 to 39.182. The minimum value was achieved when 10 % of sodium carbonate was used. The calorific value of TPO was lower than diesel fuel due to unsaturation (presence of C=C bonds) in TPO and decreased with an increase in catalyst due to unsaturation, resulting in lower vapour emission and energy release (increase of endothermic process of reactants) from the combustion reaction [162], [174]–[178].

4.4.4 Flash point

The flash point values of diesel fuel and TPO in relation to the percentage of sodium carbonate were recorded in Table 4.10.

Table 4. 10 Flash point values of Diesel fuel and TPO in relation to the percentage of sodium carbonate used to extract it.

Fuel	Flash point ^{0}C
TPO 0.0 % sodium carbonate	51
TPO 1.5 % sodium carbonate	47
TPO 2.5 % sodium carbonate	45
TPO 5.0 % sodium carbonate	41
TPO 7.5 % sodium carbonate	37
TPO 10.0 % sodium carbonate	32
Diesel fuel	62

The results in Table 4.10 were used to plot a graph of Flash point values of TPO in relation to the percentage of sodium carbonate as shown in Figure 4.15.

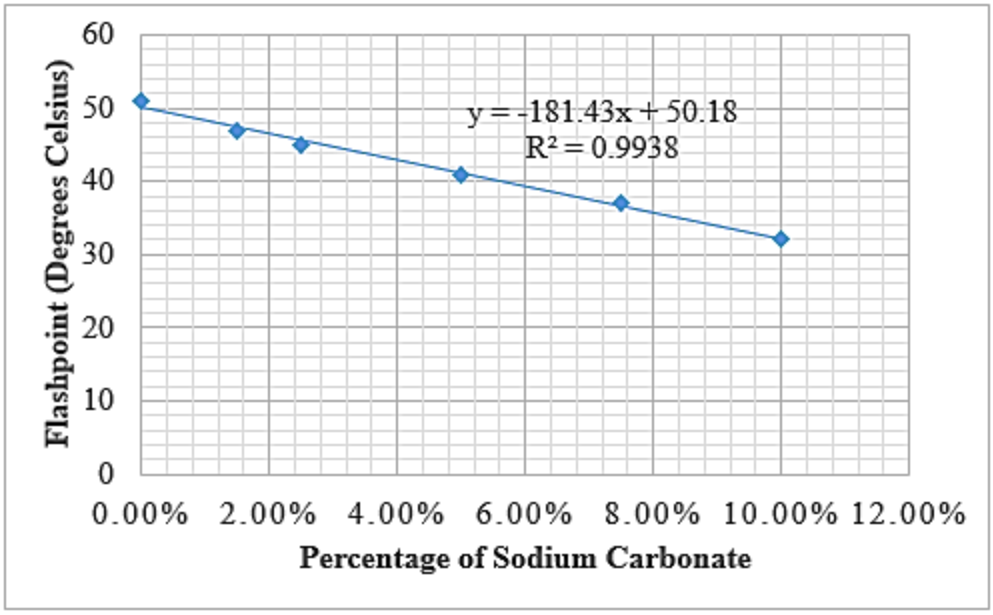

Figure 4. 15 Variation of Flash point value of TPO with the percentage of sodium carbonate.

The flash point of TPO was found to be 51 ^{0}C and that of diesel is 75 ^{0}C. The TPO's flash point was found to decrease with an increase of sodium carbonate from 51 ^{0}C to 32 ^{0}C (for 0 % to 10 % sodium carbonate). Islam *et al.* [52] also found the flash point of TPO to be 50 ^{0}C while Frigo *et al.* [32] found a higher value of 58 ^{0}C. When 10 % sodium carbonate was used, the resulting TPO was found to be more flammable compared to other extracted pyrolysis oil samples [183], [184]. The flash point value for TPO was below the recommended value for the diesel engine fuel. This indicated that it had the ability to ignite at a lower temperature than diesel [186].

Tyre pyrolysis oil is made up of a variety of compounds with a wide range of distillation temperatures, and there was an increase in volatility with an increase in sodium carbonate percentage resulting to a lower flash point [82], [106]. The TPO was made up of hydrocarbons that are more branched when compared to diesel fuel, and the level of branching was increased with an increase in sodium carbonate that was used in pyrolysis, therefore reducing the flash point as well as the boiling point of TPO [187]. There was an increase in concentration of shorter carbon chains with an increase in catalyst, which also contributed to a decrease in TPO's flash point [162].

4.4.5 Sulphur content

Table 4.11 indicates the sulphur content in TPO in relation to the percentage of sodium carbonate in the feed material to the reactor.

Table 4. 11 Sulphur content in diesel and TPO in relation to the percentage of sodium carbonate used to extract it.

Fuel	Sulphur content (mg/kg)
TPO 0.0 % sodium carbonate	8443
TPO 1.5 % sodium carbonate	6360
TPO 2.5 % sodium carbonate	5298
TPO 5.0 % sodium carbonate	3065
TPO 7.5 % sodium carbonate	2272
TPO 10.0 % sodium carbonate	1689
Diesel fuel	507

The variation of sulphur content in TPO with the percentage increase of sodium carbonate is presented in Figure 4.16.

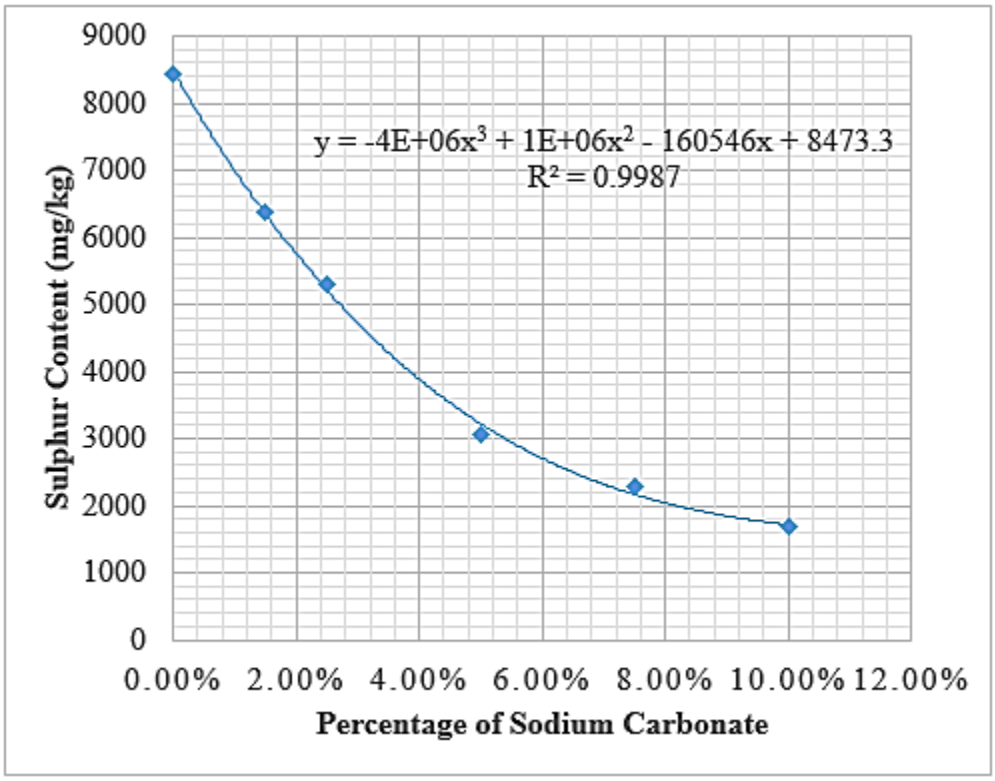

Figure 4. 16 Variation of sulphur content in TPO with the percentage of sodium carbonate.

The Sulphur content for TPO was 8443 mg/kg, this was in agreement with Martinez *et al.* [80] who reported a value of 8400 mg/kg, Yazdani *et al.* [39] found it to be 8500, Ucar *et al.* [67] found it to be 8300 mg/kg. Martinez *et al.* [81] and Roy *et al.* [76] found the sulphur content to be 8000 mg/kg. The sulphur content obtained was above the requirements of a diesel fuel according to KEBS regulatory standards. It is shown in Figure 4.16 that increasing the amount (%) of sodium carbonate, decreases the level of sulphur content in the TPO samples (with catalyst). This observation is in agreement with Demirbas *et al.* [4] and İlkılıç *et al.* [108]. The lowest sulphur content that was attained was 1689 mg/kg when 10 % of sodium carbonate was used.

The sodium carbonate reacted with the sulphur that was being generated during the pyrolysis process, forming sodium sulphate and carbon dioxide gas. Sulphur in the form of sodium sulphate was retained in the reactor as part of the solid fraction, hence resulting in its reduction in the resulting TPO [14], [209], [210]. The reduction in sulfur content was significant at low concentrations of sodium carbonate and the proportion at which it was reducing with an increase in sodium carbonate was gradually decreasing. This is due to the formation of sodium sulfate with larger molecules compared to sodium carbonate, hence restricting further diffusion of sulfur into the unreacted, inner cores of the sodium carbonate that was used [14], [209]–[211]. The rate of diffusion of sulfur to the inner core could also reduce, since its concentration gradient between the outer surface and the inner core of sodium carbonate was reducing.

4.4.6 pH

The pH values of TPO with the respective percentage of sodium carbonate, including diesel fuel, were measured and recorded in Table 4.12.

Table 4. 12 The pH values of diesel and TPO with the respective percentage of sodium carbonate used to extract it.

Fuel	pH Value
TPO 0.0 % sodium carbonate	6.93
TPO 1.5 % sodium carbonate	7.91
TPO 2.5 % sodium carbonate	8.11
TPO 5.0 % sodium carbonate	8.12
TPO 7.5 % sodium carbonate	7.60
TPO 10.0 % sodium carbonate	6.98
Diesel fuel	4.44

The results in Table 4.12 were used to plot a graph of the variation of the pH value of TPO with the percentage of sodium carbonate as shown in Figure 4.17.

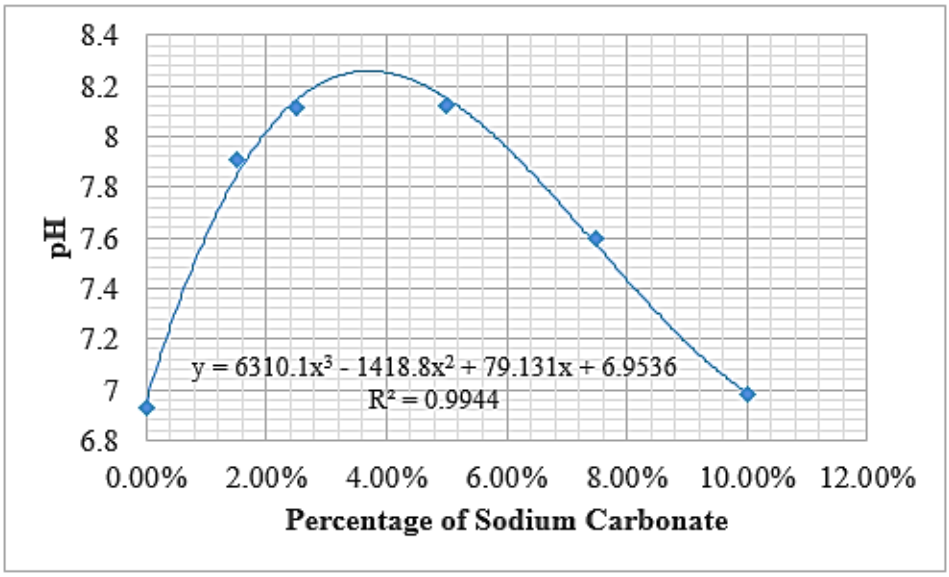

Figure 4. 17 Variation of pH value of TPO with the percentage of sodium carbonate.

The pH number of TPO was found to be 6.93 (without sodium carbonate) and that of diesel fuel was found to be 4.44. This indicated the TPO to be neutral and the diesel to be acidic. There was an increase in pH number with an increase in sodium carbonate up to 4 % and then a decrease in pH with an increase in sodium carbonate. All the samples of TPO were found to be close to a neutral condition. Whereas Martinez *et al.* [81] found the pH of TPO to be 7.5, proving it to be alkaline, Islam *et al.* [22] found it to be 4.3, which was acidic.

A pH value of 6.93 and 6.98 for the oil samples at 0 and 10 % sodium carbonate, respectively, indicated that the oil had a low concentration of hydrogen ions. The values that

were above pH number seven indicated the presence of hydroxide ions in the oil. They increased with an increase in sodium carbonate and started to decrease with an increase in sodium carbonate beyond 4 %. If the oil samples are used on metallic surfaces, the level of corrosion they can cause is less compared to diesel, which was found to be more acidic.

4.4.7 Cetane Index

Table 4.13 shows the distillation data. The Cetane index value of TPO with respect to the percentage of sodium carbonate and diesel fuel were calculated and recorded in Table 4.14.

Table 4. 13 Distillation for 50% recovery temperatures

Fuel	Distillation temperatures
TPO 0.0 % sodium carbonate	210
TPO 1.5 % sodium carbonate	208
TPO 2.5 % sodium carbonate	206
TPO 5.0 % sodium carbonate	204
TPO 7.5 % sodium carbonate	202
TPO 10.0 % sodium carbonate	200
Diesel fuel	250

Table 4. 14 The Cetane index values of diesel and TPO with respect to the percentage of sodium carbonate used to extract it.

Fuel	Cetane Index
TPO 0.0 % sodium carbonate	12.72
TPO 1.5 % sodium carbonate	10.51
TPO 2.5 % sodium carbonate	9.43
TPO 5.0 % sodium carbonate	7.15
TPO 7.5 % sodium carbonate	5.51
TPO 10.0 % sodium carbonate	3.66
Diesel fuel	47.00

The results in Table 4.14 were used to plot a graph of the variation of Cetane index value of TPO with the percentage of sodium carbonate as shown in Figure 4.18.

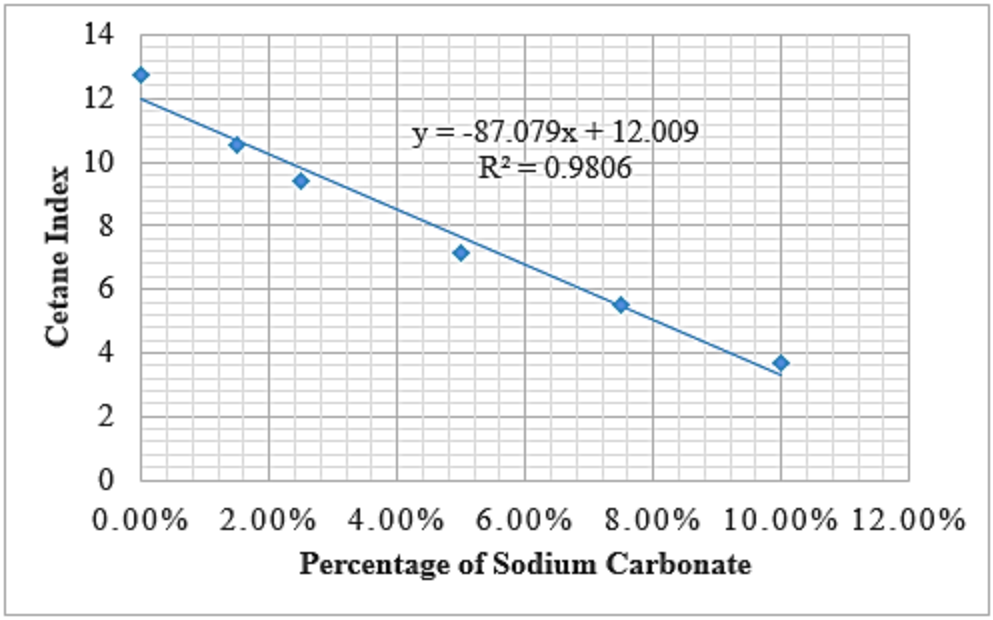

Figure 4. 18 Variation of Cetane index of TPO with the percentage of sodium carbonate.

The TPO Cetane index was found to be 12.71 in agreement with what Williams *et al.* [74] reported. In the case of diesel fuel, a Cetane index value of 47 was obtained, in comparison to the recommended Cetane index for diesel fuel value of 40. Figure 4.18 shows that the value of TPO's Cetane index decreases with an increase in the amount of sodium carbonate in the feed material of tyre pyrolysis oil. TPO had hydrocarbons which were unsaturated and branched, and the intensity of these properties increased with a corresponding increase in the catalyst used in pyrolysis, resulting in a decrease in the Cetane number and poor combustion [182]. An increase in branching also results in a decrease in the recovery temperature and an increase in specific gravity, hence lowering the Cetane index number [143], [187]. The inclusion of sodium carbonate as a catalyst acted as a contaminant/inhibitor of the TPO's ability to auto ignite.

Using TPO only to run the diesel engine can be problematic. This is due to its low Cetane index which indicates that the fuel will take a long time to ignite after its injection into the cylinder [181]. Even though the recovery temperature of TPO is less compared to diesel fuel, the specific gravity of TPO is higher than diesel fuel which makes its cetane index to be lower than the recommended. Therefore, the TPO may need to be blended with diesel fuel in order to approach the minimum required Cetane index or use appropriate additives which will

improve its Cetane index. The required mixture of TPO (without sodium carbonate) and diesel is 20 % and 80 % respectively to attain a Cetane index of 40.142, which is the appropriate value for the normal operation of a diesel engine. The TPO can be reduced to 16 % (for 10 % sodium carbonate to get 40.066) and diesel can be increased to 84 % for diesel engine operation.

4.4.8 Fourier transformation infrared analysis (FTIR)

The FT-IR may not be the best analytical technique for detecting saturated, aromatic, and polar components [27], [73], [84], [106]. This analysis, on the other hand, is based on the fact that most molecules absorb infrared light, which aids in determining the chemical properties of the liquid [27]. Using this principle, various functional groups in TPO were identified. Apart from monatomic (Argon, Helium, Neon, etc.) and homopolar diatomic (Oxygen, Hydrogen, Nitrogen, etc.) molecules that do not absorb infrared light, other chemical molecules in the TPO respond to infrared light by bond stretching and contracting in a specific wavelength range independent of other molecules' structures. The FT-IR transmittance spectra for diesel fuel in Figure 4.19 and pyrolysis oils (thermal and catalyzed) are shown in Figures 4.20 to 4.25 and Figure 4.26 shows the FTIR overlay transmittance spectrum. The functional groups in tyre pyrolysis oils and diesel fuel are presented in Table 4.14.

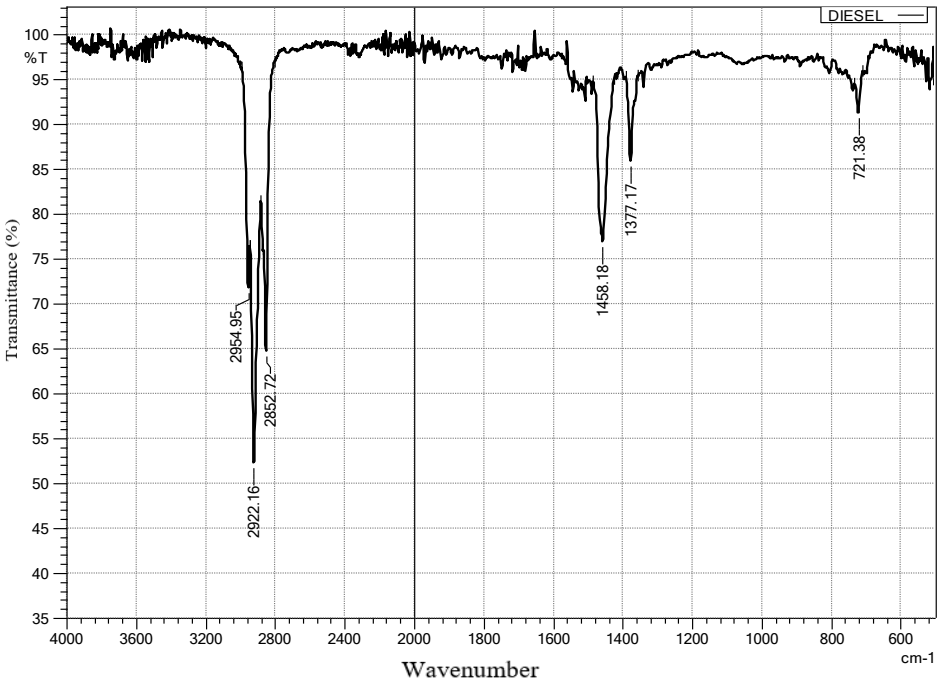

Figure 4. 19 FTIR transmittance spectrum for diesel fuel.

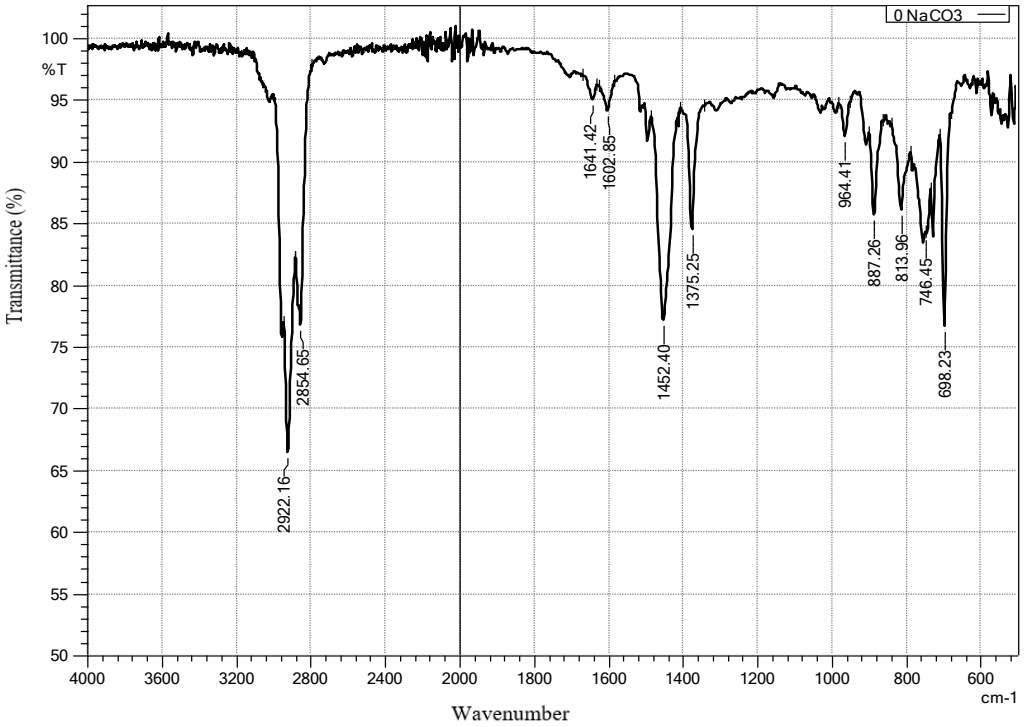

Figure 4. 20 FTIR transmittance spectrum for tyres pyrolytic oil without catalyst.

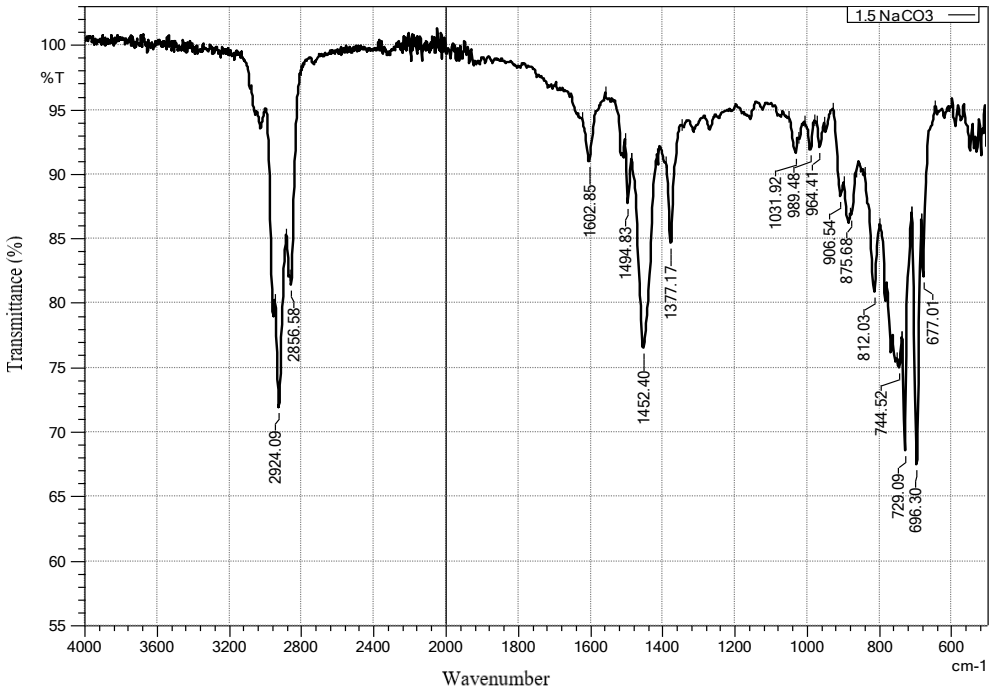

Figure 4. 21 FTIR transmittance spectrum for TPO with 1.5% catalyst.

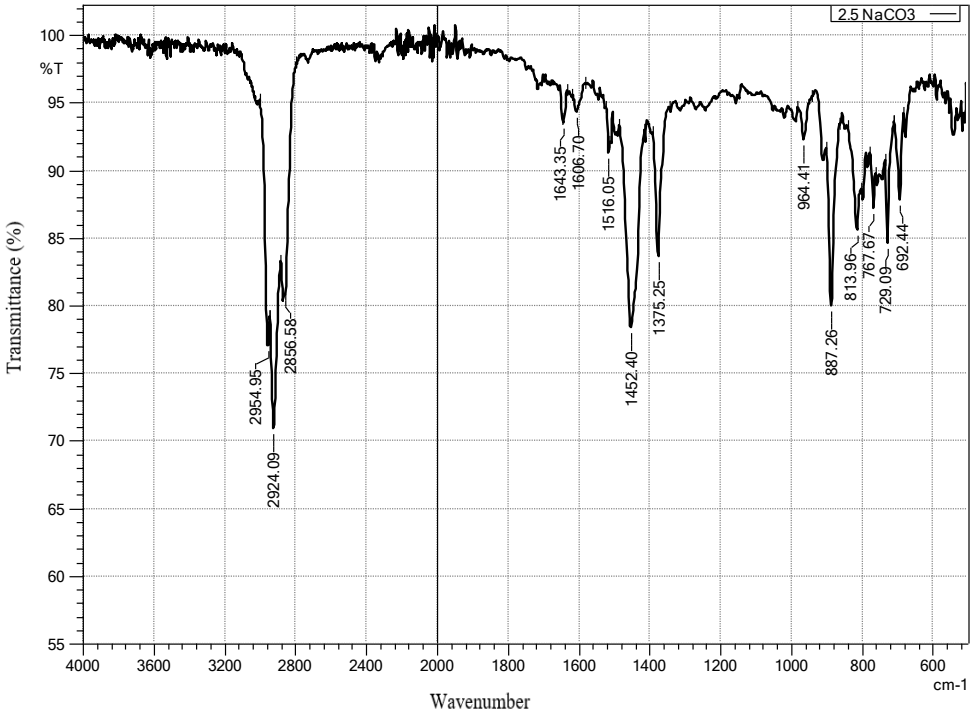

Figure 4. 22 FTIR transmittance spectrum for tyres pyrolytic oil with 2.5 % catalyst.

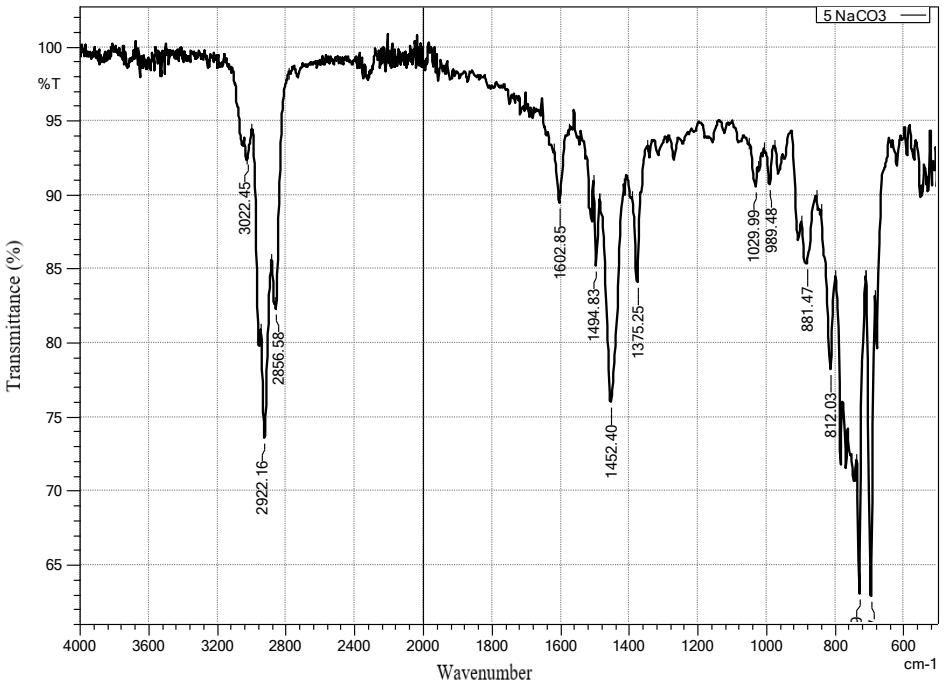

Figure 4. 23 FTIR transmittance spectrum for used tyres pyrolytic oil with 5 % catalyst.

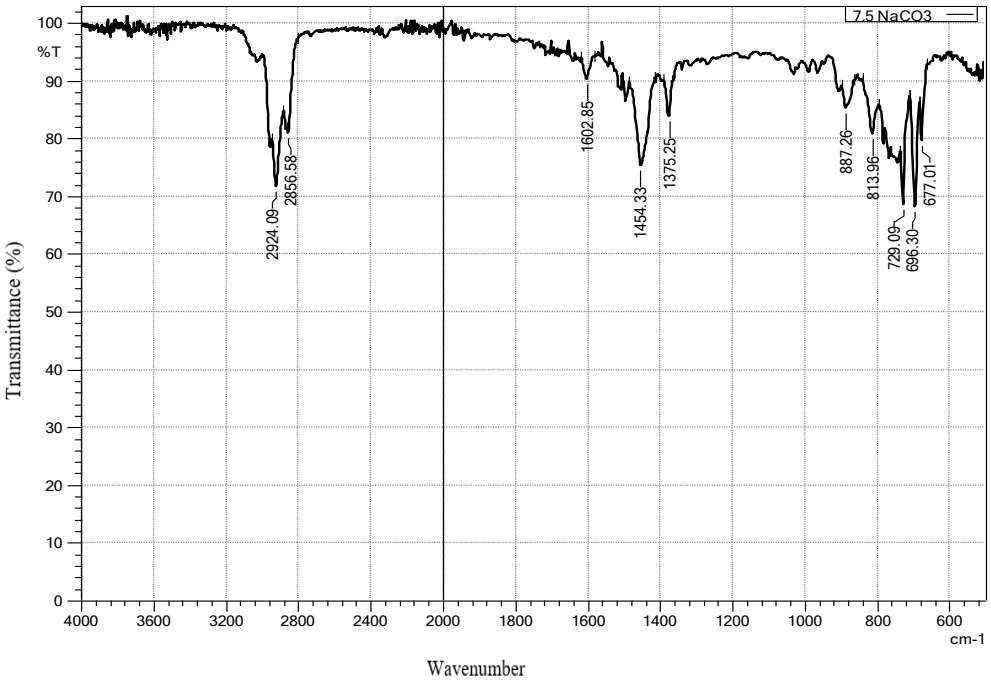

Figure 4. 24 FTIR transmittance spectrum for used tyres pyrolytic oil with 7.5 % catalyst.

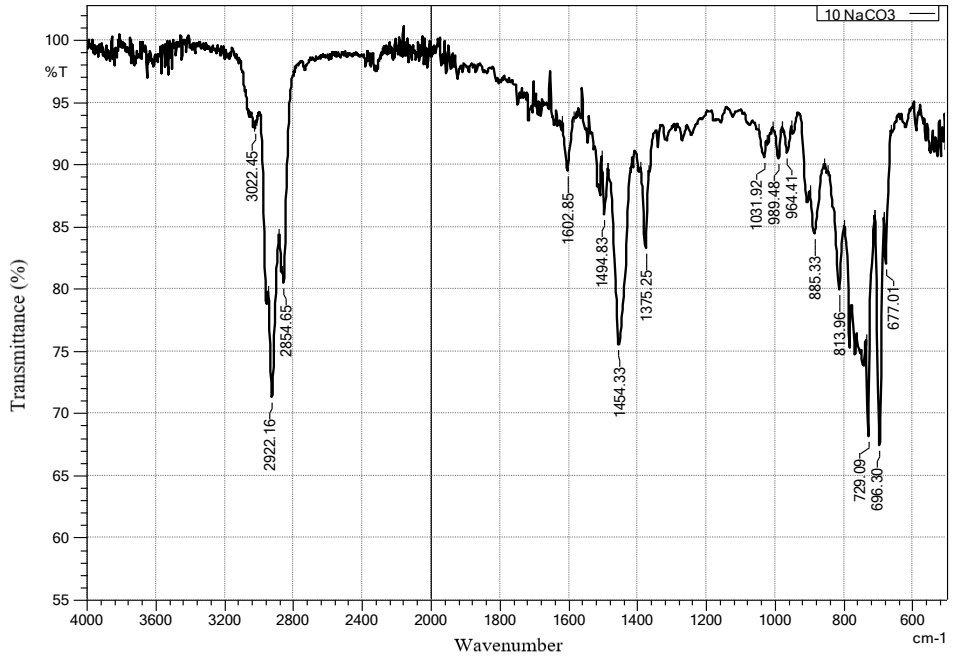

Figure 4. 25 FTIR transmittance spectrum for used tyres pyrolytic oil with 10 % catalyst.

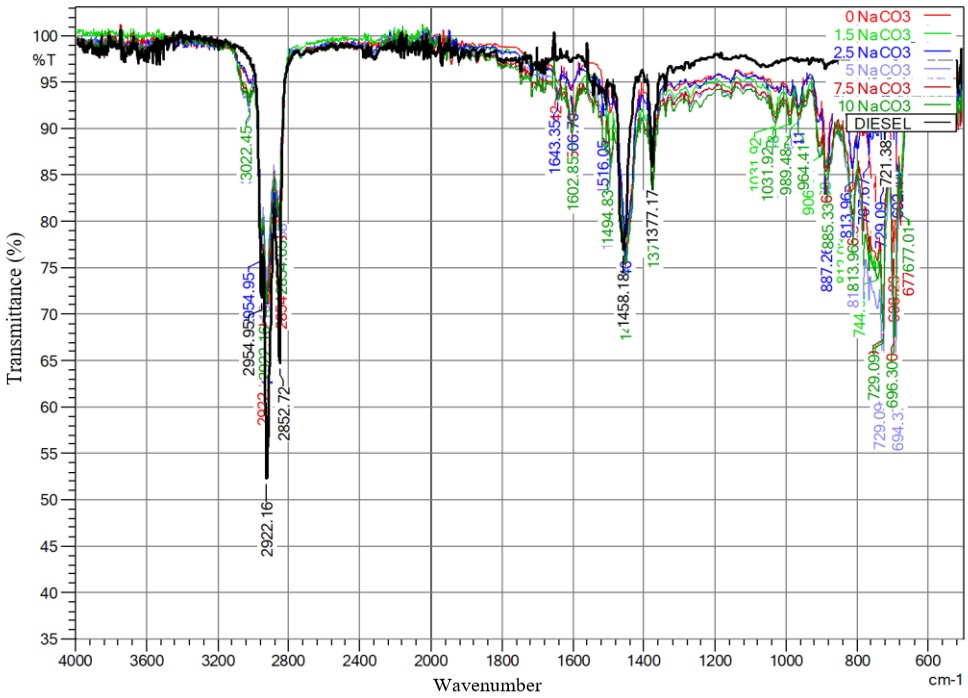

Figure 4. 26 The FTIR overlay transmittance spectrum

Table 4. 15 The indicated functional groups in tyre pyrolysis oils and diesel fuel

0 %	1.5 %	2.5 %	5 %	7.5 %	10 %	Diesel	Functional group	Class of compound
3100-3000	3100-3000	3100-3000	3100-3000	3100-3000	3100-3000	-	C–H stretching	Alkenes
3000-2700	3000-2720	3000-2780	3000-2780	3000-2720	3000-2780	3000-2760	C-H stretching	Alkanes.
1650-1580	1640-1560	1650-1580	1650-1560	1650-1560	1650-1580	-	C=C stretching	Alkenes.
1520-1400	1520-1400	1500-1400	1520-1400	1560-1400	1560-1400	1550-1400	Carbon-carbon stretching	Aromatic compound
1400-1300	1400-1300	1400-1340	1400-1320	1400-1350	1400-1340	1400-1360	C-H bending	Alkanes.
1050-1000	1100-1000	1060-1000	1100-1000	1080-1000	1100-1000	-	C-H in plane bending	Aromatic compound
960-860	980-920	940-860	920-850	940-850	980-800	-	C=C stretching	Alkenes.
840-650	860-650	860-650	800-660	800-670	720-650	800-680	C-H out of plane bending	Aromatic compounds.

In general, the tyre pyrolysis oil comprises of mainly aliphatic (alkane and alkene groups), aromatic compounds (alkyl aromatics with rings) hydroxyl compounds, and other hydrocarbon compounds that may be present in low proportions. This depends on the composition of the tyres used. The hydrocarbons present in TPO (Refer to Figs 4.20 to 4.26 and Table 4.15) as identified in this study were also reported by González *et la.* [73], Islam *et al.* [22] Conesa *et al.* [25], and Aguado *et al.* [110]. When comparing diesel fuel and tyre pyrolysis oils, functional group composition analysis revealed that diesel fuel contained both aliphatic (alkane groups) compounds and aromatic compounds. All the oil samples and diesel fuel appeared to contain the C-H aliphatic stretch (about 2922 and 2852 cm^{-1}), C-H bending (about 1377 cm^{-1}), and carbon-carbon stretching (about 1458 cm^{-1}). The presence of saturated and unsaturated hydrocarbons (C=C stretching at about 1602 cm^{-1} and 885 cm^{-1}) in tyre pyrolysis oil was detected, whereas diesel included mainly saturated hydrocarbons.

An FTIR spectral library search was performed and the functional groups found in the 0 percent, 1.5 percent, 5 percent, and 10 percent runs were mostly comparable to Styrene/Ethlylene-Buthylene, whereas the 2.5 percent and 7.5 percent runs were mostly comparable to Paraffin and for diesel were comparable to Liquid Paraffin. This indicates that the TPO samples are combustible and can be used as fuel [212]. When sodium carbonate catalyst was used, there was active alkylation, isomerization, hydrogenation, and reactions involving the introduction of heteroatoms and the migration of the double bonds in unsaturated compounds, resulting in the variation of functional groups in TPO molecules [128], [129].

4.4.9 Gas chromatography and mass spectrometry (GC-MS)

The pyrolysis oil samples were subjected to GC-MS analysis in order to determine the nature and type of hydrocarbons present. Table 4.16 indicates the Peak Report TIC for TPO samples and table 4.17 indicates the Peak Report TIC for diesel fuel. The chromatogram peaks of the various samples of TPO-derived chemicals are displayed in Figure 4.27 to 4.32 and Figure 4.33 is for diesel fuel. The peaks obtained were analyzed with NIST search software to identify the different compounds present.

Table 4. 16 Peak Report TIC for TPO for various percentages of sodium carbonates used.

R. Time	0.0%	1.5%	2.5%	5.0%	7.5%	10.0%	Name
3.922	1.32	8.38	1.35	9.02	7.20	4.05	Benzene
7.184	9.40	22.66	8.94	23.97	20.35	16.75	Toluene
10.319	35.47	24.80	26.47	21.43	24.15	25.96	2-Pentanone, 4-hydroxy-4-methyl-
10.905	4.59	6.19	-	5.39	4.71	2.97	Ethylbenzene
11.278	4.36	11.98	10.75	8.42	12.57	-	Benzene, 1,3-dimethyl-
11.280	-	-	-	-	-	7.66	o-Xylene
12.208	-	7.58	-	-	5.69	-	Benzenepropanoyl bromide
12.212	-	-	-	7.51	-	6.67	Styrene
14.518	-	-	2.50	-	-	-	Cyclobutane, 1,2-bis(1-methylethenyl)-, trans-
15.674	-	-	-	-	1.19	-	Benzene, 1-ethyl-3-methyl-
15.875	-	-	-	-	0.62	-	Benzene, 1-ethyl-2-methyl-
16.019	-	-	-	-	1.01	-	Mesitylene
17.059	4.09	2.32	3.02	-	1.62	-	Benzene, 1-methyl-3-(1-methylethyl)-
17.158	22.76	4.08	31.71	2.27	4.59	5.29	D-Limonene
17.938	-	-	-	2.87	-	2.05	1H-Indene, 1-chloro-2,3-dihydro-
17.964	-	-	-	-	0.97	-	Indene
18.741	-	-	1.23	-	-	-	Cyclohexene, 1-methyl-4-(1-methylethylidene)-
18.897	-	-	1.08	-	-	-	-Isopropenyltoluene
19.076	-	-	-	-	0.75	-	2-Methylindene
19.787	-	4.43	-	9.53	4.67	-	Azulene
20.097	-	-	-	-	-	8.69	Naphthalene
20.855	-	-	-	3.27	1.56	2.94	Naphthalene, 2-methyl-
21.018	6.26	-	-	-	-	-	Eicosane
21.036	-	7.57	12.94	5.17	6.16	15.47	9-Octadecenamide, (Z)-
21.519	4.49	-	-	-	-	-	Silane, trichlorooctadecyl-
21.787	-	-	-	-	0.21	-	3-(2-Methyl-propenyl)-1H-indene
22.167	1.52	-	-	-	-	-	Eicosane, 10-methyl-
22.189	-	-	-	-	0.41	-	Dodecane, 2,6,11-trimethyl-
22.631	5.73	-	-	-	-	-	2-methyloctacosane
23.089	-	-	-	1.17	0.73	-	Phenanthrene
24.809	-	-	-	-	0.84	-	Tetradecanamide

Table 4. 17 Peak Report TIC for diesel fuel.

Peak #	R. Time	Area%	Name
1	10.328	5.49	2-Pentanone, 4-hydroxy-4-methyl-
2	12.191	0.71	Nonane, 2-methyl-
3	15.916	1.29	Undecane
4	18.855	2.52	Undecane
5	19.993	3.22	Dodecane
6	20.676	4.92	Dodecane
7	21.031	2.46	Hexadecane, 2,6,10,14-tetramethyl-
8	21.146	8.12	Tetradecane
9	21.365	3.37	Tetradecane, 4-methyl-
10	21.519	10.15	Pentadecane
11	21.848	10.21	Hexadecane
12	21.985	2.91	Pentadecane, 2,6,10-trimethyl-
13	22.168	10.06	Heptadecane
14	22.512	9.48	Heptadecane
15	22.900	6.95	Eicosane, 10-methyl-
16	23.361	6.32	Eicosan
17	23.930	5.13	Heneicosane
18	24.649	3.88	Heptadecane
19	25.571	2.81	Tricosane

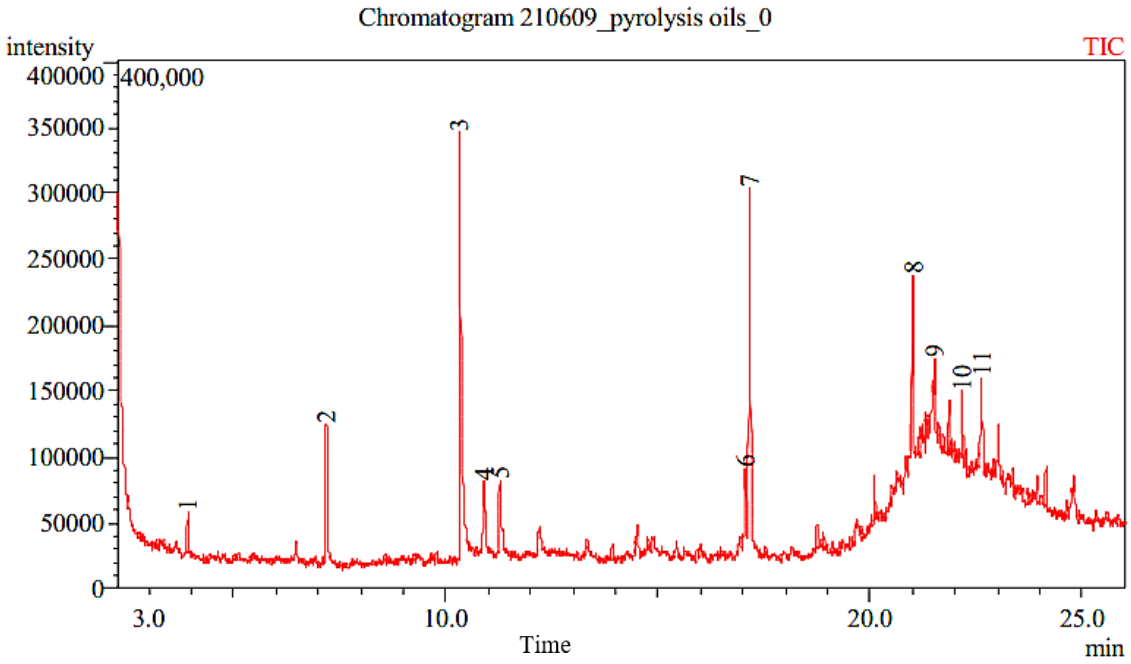

Figure 4. 27 GC-MS chromatogram for tyre pyrolysis oil without catalyst.

It was found that the components of thermal pyrolysis oil from tyres were; 4-hydroxy-4-methyl-2-Pentanone (35.47 %), D-Limonene (22.76 %), Toluene (9.40 %), benzene, methyl-, ethyl-, 1,3-dimethyl-, 1,2-dimethyl-, 1,4-dimethyl-, 1,3-dimethyl-, 1,2-dimethyl-, ethyl-, 1-methyl-3-(1-methylethyl)-, 2-ethyl-1,3-dimethyl-, 1-ethyl-2,4-dimethyl- and 1-methyl-4-(1-methylethyl)-benzene (14.36 %), eicosane, 1-iodo- and 10-methylicosane (13.51 %), trichlorooctadecyl- and Octadecyltrichlorosilane (4.49 %).

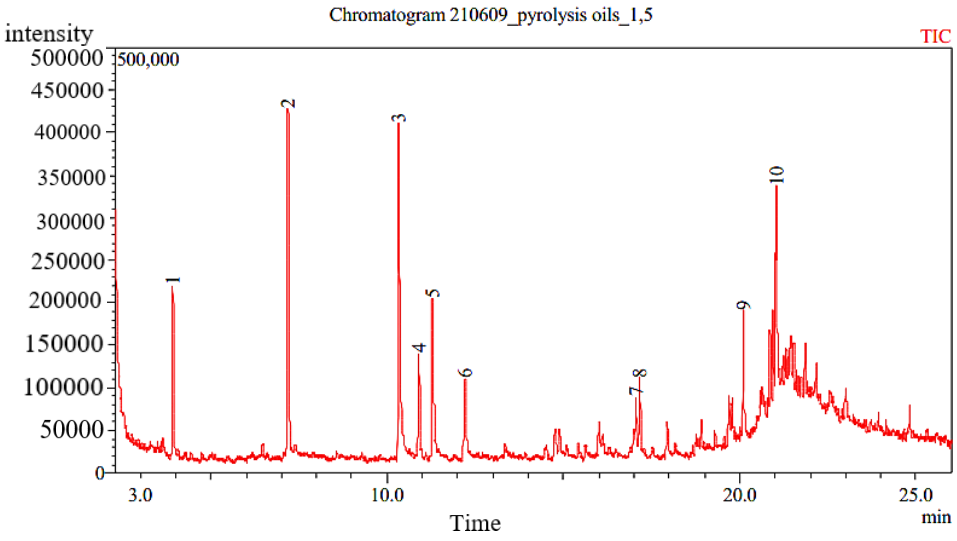

Figure 4. 28 GC-MS chromatogram for tyre pyrolysis oil with 1.5 % catalyst.

It was found that at 1.5 % catalytic pyrolysis TPO components were; 4-hydroxy-4-methyl-2-Pentanone (24.80 %), Toluene (22.66 %), Benzene, methyl-, Ethyl-, 1,3-dimethyl-, 1,2-dimethyl-, 1,4-dimethyl-, 1,3-dimethyl-, 1,2-dimethyl-, 1,4-dimethyl-, 1-ethyl-2,4-dimethyl-, 1-methyl-3-(1-methylethyl)-, 1-methyl-4-(1-methylethyl)-, 2-ethyl-1,3-dimethyl- and 4-ethyl-1,2-dimethylbenzene (28.87 %), Benzenepropanoyl bromide (7.58 %), 9-Octadecenamide, (Z)-(7.57), Azulene (4.43 %) and D-Limonene (4.08 %).

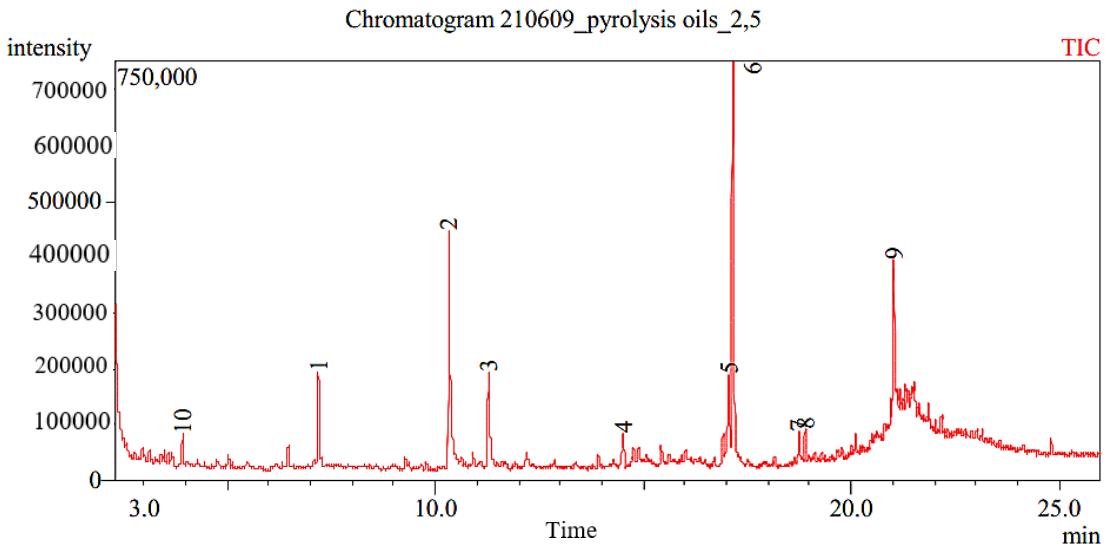

Figure 4. 29 GC-MS chromatogram for tyre pyrolysis oil with 2.5 % catalyst.

At 2.5 % catalytic pyrolysis TPO components were; D-Limonene (31.71), 4-hydroxy-4-methyl-2-Pentanone (26.47 %), methyl, 1,3-dimethyl-,1,2-dimethyl-, 1,4-dimethyl-, ethyl-, 1-methyl-3-(1-methylethyl)-, 1-ethyl-2,4-dimethyl-, 2-ethyl-1,3-dimethyl-, 1-methyl-4-(1-methylethyl)-, 1-methyl-4-(1-methylethenyl)-, 2-ethenyl-1,4-dimethyl-, 2-methyl-1-propenyl-, 1-methyl-3-(10-methylethenyl)-benzene (15.12%), toluene (8.94%) and 9-Octadecenamide, (Z)- (12.94 %). There were also smaller quantities of 1,2-bis(1-methylethenyl)-, trans-, 1,3-diisopropenyl-, trans, Cyclobutane (2.5%), 1-methyl-4-(1-methylethenyl)-, (R)-, 1-methyl-4-(1-methylethenyl)-, (S)-, 4-ethenyl-1,4-dimethyl-, 1-methyl-4-(1-methylethenyl)-, (R)-, 1-methyl-4-(1-methylethenyl)-, 1-methyl-5-(1-methylethenyl)-, 3-methyl-6-(1-methylethylidene)-, 4-methyl-3-(1-methylethylidene)-cyclohexene (1.23 %) o-Isopropenyltoluene (1.08).

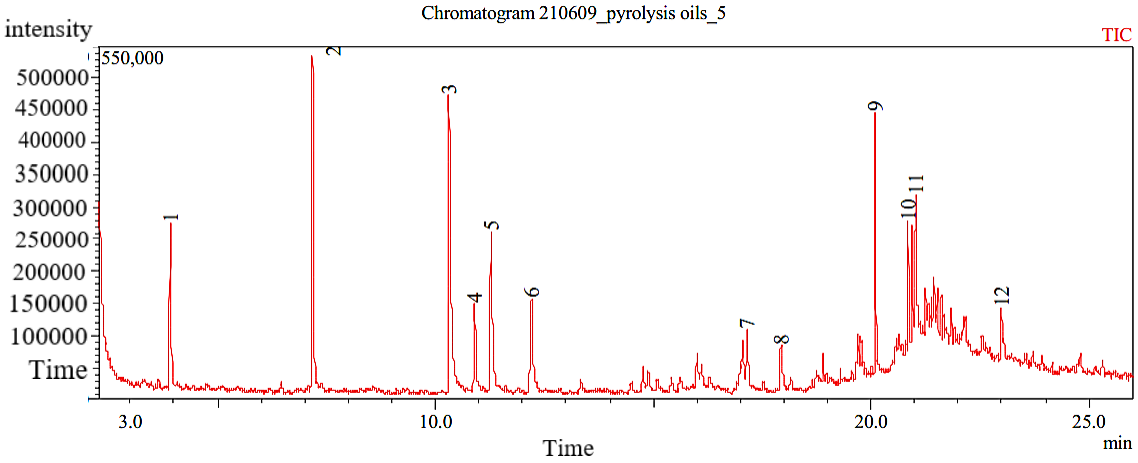

Figure 4. 30 GC-MS chromatogram for tyre pyrolysis oil with 5 % catalyst.

In the case of the 5 % catalytic pyrolysis, the TPO components obtained were; Benzene, methyl-, ethyl-, 1,2-dimethyl-, 1,4-dimethyl-, 1,3-dimethyl-, ethenyl-, 2-nitroethyl-, 1-propynyl-, 1-ethynyl-3-methyl- and 2-Propynyl- (30.34 %), Toluene (23.97 %), 4-hydroxy-4-methyl-2-Pentanone (21.43 %), D-Limonene (2.27 %), 1H-Indene, 1-chloro-2,3-dihydro-, 1-methylene- and 1-ethylidene-1H –Indene (2.87 %), Azulene and Benz[a]azulene (9.53 %), Naphthalene, 2-methyl-, 1-methyl-, 1,4-dihydro- and Paranaphthalene (3.27 %), 9-Octadecenamide, (Z)- (5.17 %), Phenanthrene (1.17 %).

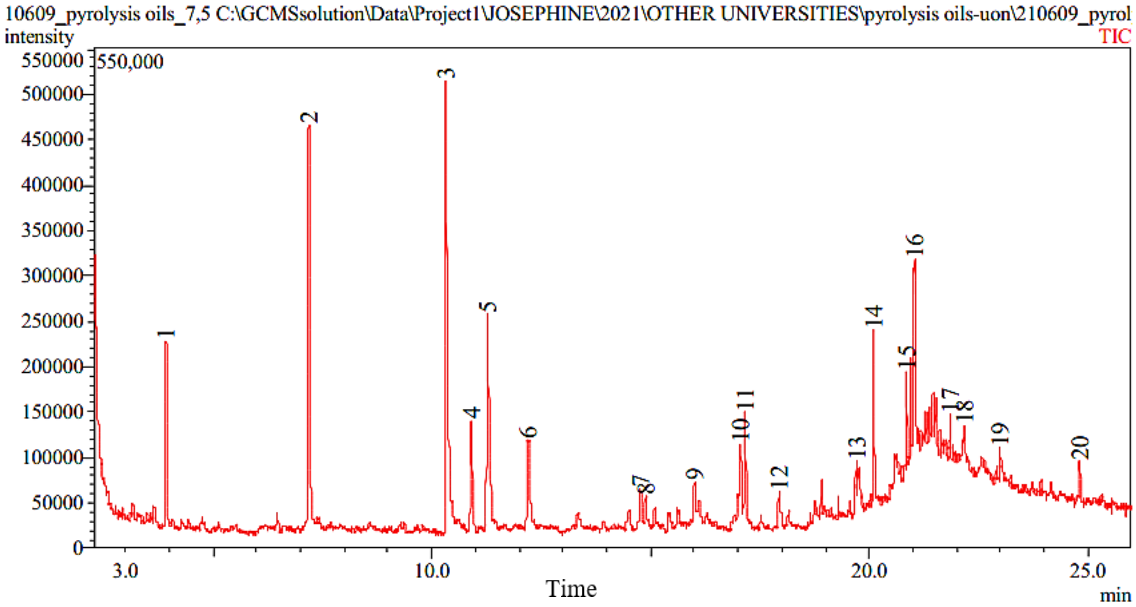

Figure 4. 31 GC-MS chromatogram for tyre pyrolysis oil with 7.5 % catalyst.

It was found that at 7.5 % catalytic pyrolysis TPO components were; Benzene, methyl-, ethyl-, 1,2-dimethyl-, 1,3-dimethyl-, 1,4-dimethyl-, Benzenepropanoyl bromide, 1-ethyl-3-methyl-, 1-ethyl-2-methyl-, 1-ethyl-4-methyl-, 1,2,3-trimethyl-, 1,2,4-trimethyl-, 1-ethyl-2-methyl-, 1-ethyl-4-methyl-, 1-methylethyl-, 1,3,5-trimethyl-, 1-methyl-3-(1-methylethyl)-, 1-methyl-4-(1-methylethyl)-, 1-ethyl-2,4-dimethyl-, 2-ethyl-1,3-dimethyl-, 1-propynyl-, 1-ethynyl-3-methyl-, 2-Propynyl-, 1-methyl-1,2-propadienyl- (54.96 %), 4-hydroxy-4-methyl-2-Pentanone (24.15). There were also smaller quantities of D-Limonene (4.59), 1H-Indene, 1-chloro-2,3-dihydro-, 3-methyl-,1-methylene-,1-ethylidene-, 2-methyl-, 3-(2-Methyl-propenyl)-1H-Indene (1.93 %), Azulene, 4,6,8-trimethyl-, Benz[a]azulene (4.67 %), Naphthalene, 4a,8a-(Methaniminomethano)naphthalene-9,11-dione, 10-phenyl-, 2-methyl-, 1-methyl-, 2,3,6-trimethyl-, 1,4-dihydro-, Paranaphthalene (1.56 %), 9-Octadecenamide, (Z)-(6.16 %), 2,6,11-trimethyl-, 2-methyl-6-propyldodecane (0.41 %), Phenanthrene(0.73), Tetradecanamide (0.84 %),

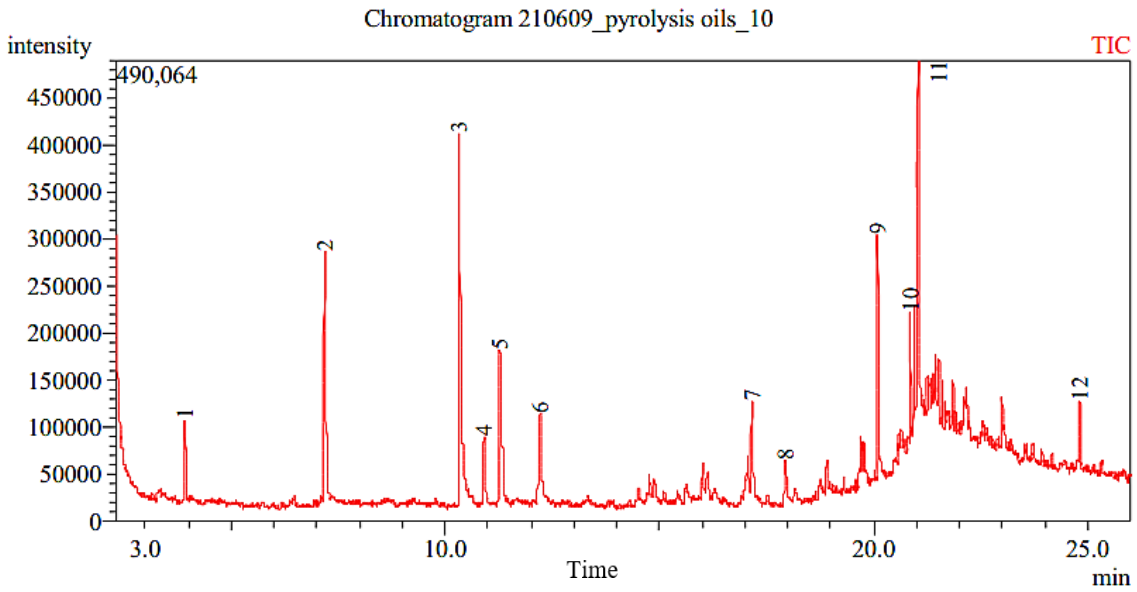

Figure 4. 32 GC-MS chromatogram for tyre pyrolysis oil with 10 % catalyst.

TPO components obtained for the 10 % catalytic pyrolysis were; Benzene, Benzenemethanimine, methyl-, ethyl-, 1,2-dimethyl-, 1,4-dimethyl-, 1,3-dimethyl-, ethenyl-, 1-ethynyl-3-methyl-, 1-propynyl-, 2-Propynylbenzene (38.10 %), 4-hydroxy-4-methyl-2-Pentanone (25.96 %), D-Limonene (5.29 %), Indene, 1-chloro-2,3-dihydro-, 1-methylene-, 1-ethylidene1H-Indene (2.05 %), 4a,8a-(Methaniminomethano)naphthalene-9,11-dione, 10-phenyl-, 2-methyl-, 1-methyl-, 1,4-dihydronaphthalene (11.63 %), 9-Octadecenamide, (Z)-, Octadecanamide (16.97 %).

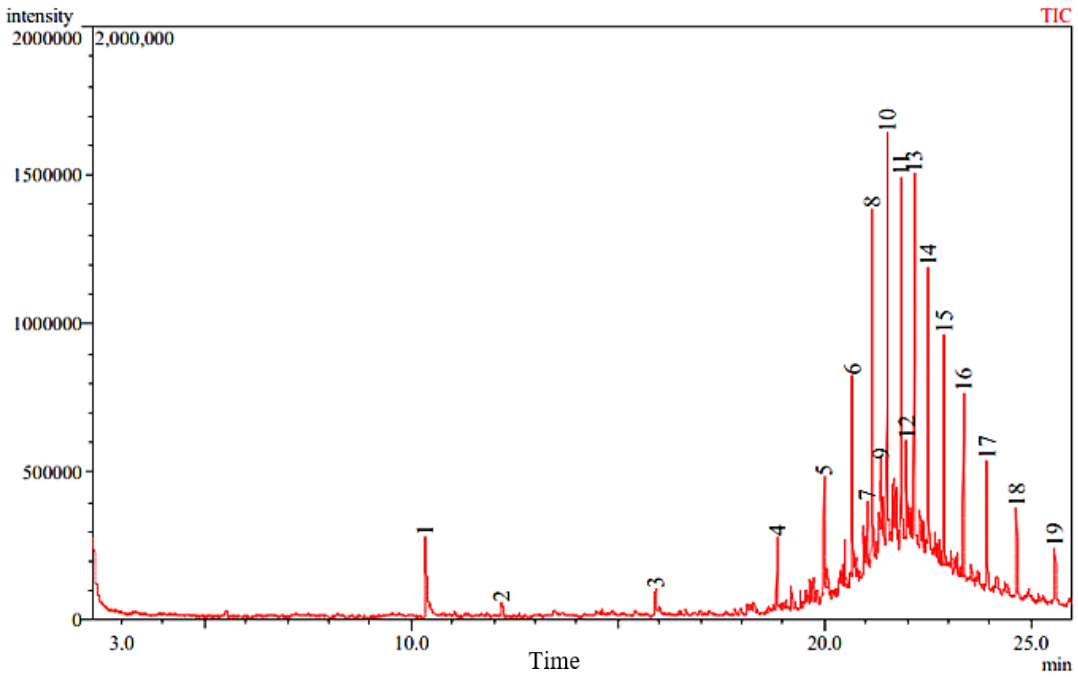

Figure 4. 33 GC-MS chromatogram for diesel fuel.

For comparison, the components present in diesel were also identified using GC-MS as follows; 4-hydroxy-4-methyl- 2-Pentanone (5.49), 2-methyl-, 1-Iodo-2-methylnonane (0.71 %), Undecane (3.81 %), Dodecane, 2-methyl-, 2,6,11-trimethyl-, 2,7,10-trimethyl-, 4-methyl-, 2-methyl-6-propyldodecane (8.14 %), hexadecane, 7-methyl-, 2,6,10,14-tetramethyl-, 2,6,11,15-tetramethylhexadecane (12.67 %), tetradecane, 4-methyltetradecane (11.49 %), Pentadecane, 2,6,10-Trimethyl-, 7-methylpentadecane (13.06 %), Heptadecane, 2,6-dimethyl-, 7-Methylheptadecane (23.42 %), Eicosane, 10-methyl-, 7-hexylicosane (13.27 %), Heneicosane (5.13 %), Tricosane (2.81 %).

As shown in Figures 4.26 to 4.32, it is clear that tyre pyrolysis oil obtained by both thermal and catalytic processes was a complex combination dominated by various aromatic and aliphatic components. Some of the substances identified were alkanes, alkynes, alkenes, naphthalene, benzene and its derivatives, and compounds that contained nitrogen and oxygen. TPO is considered a fuel since it contains alkanes, cycloalkanes, and Toluene, which are combustible and can be used as fuel [212].

The hydrocarbons in TPO had some branching which was attributed to the formation of benzene rings. There was an increase in branching which was witnessed from TPO without a catalyst that contained single ring benzene, as the number of rings formed increased to form

three rings for paranaphthalene and polycyclic aromatic hydrocarbons with an increase in catalyst. This is in agreement with Miandad *et al.*, [141]. The present compounds consisted of saturated and unsaturated hydrocarbons. Since TPO contains unsaturated hydrocarbons, it is susceptible to oxidation when kept, which can lead to loss of TPO's fuel qualities [135]. The TPO was found to contain aliphatic compounds that were similar to the ones contained in diesel fuel, indicating that the TPO contained diesel. Table 4.18 shows the proportions of aromatics and aliphatic compounds in diesel fuel and tyre pyrolysis oils.

Table 4. 18 Proportions of aromatics and aliphatic compounds in diesel fuel and tyre pyrolysis oils

Fuel Sample	Percentage of Aromatics compounds	Percentage of Aliphatic compounds
TPO 0.0 % sodium carbonate	53.47	46.52
TPO 1.5 % sodium carbonate	32.37	67.62
TPO 2.5 % sodium carbonate	31.91	68.08
TPO 5.0 % sodium carbonate	26.60	73.42
TPO 7.5 % sodium carbonate	31.56	68.44
TPO 10.0 % sodium carbonate	42.93	57.07
Diesel fuel	0	100

Generally, the results presented in Table 4.18 show that the percentage of aromatic content for thermal pyrolysis oil was lower while aliphatic content was higher. The data compared well to results obtained by Mastral *et al.* [18], Laresgoiti *et al.* [38] and Rodriquez et al. [71], but Rofiqul *et al.* [27] found it to be less. This condition may be due to the tyre pyrolysis oil that was collected in this research consisting of oil that was collected at lower temperatures before the achievement of the temperature that was intended for pyrolysis, while Mastral *et al.* [18], Laresgoiti *et al.* [38] and Rodriquez *et al.* [71] may have collected oil at specified temperatures of pyrolysis only. Mastral *et al.* [18], Laresgoiti *et al.* [38] did pyrolysis at different temperatures and found that the amount of aromatics in the resulting tyre pyrolysis oil increases as the pyrolysis temperature rises. The carbon content ranged between

C_4-C_{45} and this closely agrees with Alsaleh *et al.* [17], also found the most abundant carbon content to be (C_6–C_{37}) chains.

Secondary reactions can occur in the reactor via Diels Alder type reactions involving alkenes and alkanes to form more aromatic and polycyclic aromatic hydrocarbons [97], [122], [123]. The amount of aromatics in the tyre pyrolysis oil can also be determined by the type of rubber component utilized [21], [117] for instance, polystyrene butadiene rubber (SBR) could be a source of extra benzene rings, resulting in a dehydrogenation process [71]. This is because SBR has a significant amount of aromatics, which means that when compared to natural rubber (NR) and butadiene rubber (BR) under the same conditions, SBR will yield oil with a greater aromatic concentration [73], [90], [94].

4.5 Summary of the Chapter

A batch type reactor was designed and fabricated. It was then used to extract tyre pyrolysis from waste tyres. The analysis of the physical and chemical properties of TPO indicated that they were deviating from the fuel requirements for a diesel engine. This is due to the presence of additional hydrocarbons which are contaminants to diesel fuel. This may require some blending of approximately 20 % TPO with 80 % diesel in order to achieve the required minimum properties. It was found from FTIR and GC-MS analyses, that the TPO samples extracted by both catalytic and thermal pyrolysis processes were complex mixtures of aliphatic, aromatics, nitrogen and oxygen containing compounds with carbon content ranging between C_4 and C_{45}. TPO proved to be a fuel since it contained alkanes, cycloalkanes and Toluene which can be used as fuel.

CHAPTER FIVE: CONCLUSIONS AND RECOMMENDATIONS

5.1 Conclusions

The objective of this research was achieved, using available time and resources, in that the extraction and evaluation of fuel properties of tyre pyrolysis oil was done. The specific objectives that were achieved and the following conclusions were made.

1. A batch type pyrolysis system was designed, fabricated and used to extract TPO from waste tyres.
2. The amount of TPO produced without a catalyst was 35 % and increased to 43 % when 10 % of the catalyst was used. It was black in colour.
3. The specific gravity of TPO was higher than that of diesel at all the tested temperatures and was increasing with the increase in sodium carbonate in the feed material.
4. The kinematic viscosity of TPO was higher than diesel. It started to decrease when sodium carbonate was used and started increasing when sodium carbonate exceeded 2.5 % of the feed material with an increase in sodium carbonate.
5. The calorific value of TPO was 40.431 MJ/kg and reduced to 39.182 when 10% of sodium carbonate was used, whereas that of diesel fuel was 43.144 MJ/kg.
6. The flash point of TPO was 51 ^{0}C while that of diesel was 62 ^{0}C. The flash point of TPO decreased with the increase of the catalyst, up to 32^{0}C when 10 % of the catalyst was used.
7. The sulphur content in TPO was 8443 mg/kg and the use of sodium carbonate was found to reduce the sulphur content in TPO by approximately 80 % when 10 % of sodium carbonate was used.
8. The pH value of TPO was close to the neutral position where it fluctuated between 6.93 and 8.12 while that of diesel was 4.44 which was slightly acidic.
9. The Cetane index of TPO was 12.71 and decreased to 3.66 with a 10 % catalyst.
10. FTIR analysis indicated that the functional groups that were contained in TPO were both saturated and unsaturated.
11. GC-MS analysis indicated that the TPO was made up of hydrocarbons that were similar when compared to diesel fuel (aliphatic), with additional hydrocarbons that were unsaturated (aromatics).

Sodium carbonate is a catalyst in branching and it is also alkaline in nature. When it was used, it reacted with sulfur, which resulted in the formation of sodium sulfate (in a solid state) and was retained in the reactor as part of the char resulting to sulphur reduction in oil. Its effect on branching and unsaturation resulted interference of the other fuel properties. Hence, not suitable for use in a diesel engine in its form.

5.2 Recommendations

1. A cyclone can be introduced along the connection tube to ensure that the sediments from the reactor are trapped so that they don't get to the condenser to block the tubes.
2. If possible, a mixer can be installed at the reactor to enhance heat transfer within the feed material.
3. A cheaper means of reducing high sulphur content in the TPO should be devised to achieve the recommended level for diesel fuel and assessment of the effects on fuel properties.
4. A research study to find appropriate additions that can improve the properties of TPO can be done, e.g. density, viscosity, flash point and Cetane index.
5. Ways of saturating or reducing unsaturated hydrocarbons in the TPO fuel can be studied.

REFERENCES

[1] R. K. Kimilu, J. A. Nyang'aya, and J. M. Onyari, "The effects of temperature and blending on the specific gravity and viscosity of Jatropha methyl ester," *ARPN J. Eng. Appl. Sci.*, vol. 6, no. 12, pp. 97–105, 2011.

[2] S. Samuel and L. Á. Garcia, "Fuel from waste tyres and particulate matter emitted from the process," *Int. J. Sustain. Eng.*, vol. 7, no. 4, pp. 293–306, 2014, doi: 10.1080/19397038.2013.848954.

[3] M. Sienkiewicz, H. Janik, K. Borzędowska-Labuda, and J. Kucińska-Lipka, "Environmentally friendly polymer-rubber composites obtained from waste tyres: A review," *J. Clean. Prod.*, vol. 147, pp. 560–571, 2017, doi: 10.1016/j.jclepro.2017.01.121.

[4] A. Demirbas, B. O. Al-Sasi, and A.-S. Nizami, "Conversion of waste tires to liquid products via sodium carbonate catalytic pyrolysis," *Energy Sources, Part A Recover. Util. Environ. Eff.*, vol. 38, no. 16, pp. 2487–2493, 2016, doi: 10.1080/15567036.2015.1052598.

[5] A. Ciesielski, *An Introduction to Rubber Technology*. Rapra Technology Limited, 1999.

[6] V. H. L. Rodrigo, T. U. K. Silva, and E. S. Munasinghe, "Improving the spatial arrangement of planting rubber (Hevea brasiliensis Muell. Arg.) for long-term intercropping," *F. Crop. Res.*, vol. 89, no. 2–3, pp. 327–335, 2004, doi: 10.1016/j.fcr.2004.02.013.

[7] S. M. Najam, "Investigation of Mesoporous silica (KIT-6 and SBA- 15-S) effect on property balance of Natural Rubber nanocomposites," M.Sc. Thesis, Institute of Information Technology Lahore, 2017.

[8] J. B. Omwoyo, R. K. Kimilu, and J. M. Onyari, "Catalytic pyrolysis and composition evaluation of tire pyrolysis oil," *Chem. Eng. Commun.*, vol. 0, no. 0, pp. 1–11, 2022,

doi: 10.1080/00986445.2022.2053681.

[9] M. Arabiourrutia, G. Lopez, M. Artetxe, J. Alvarez, J. Bilbao, and M. Olazar, “Waste tyre valorization by catalytic pyrolysis – A review,” *Renew. Sustain. Energy Rev.*, vol. 129, pp. 1–24, 2020, doi: 10.1016/j.rser.2020.109932.

[10] D. Czajczyńska, R. Krzyżyńska, H. Jouhara, and N. Spencer, “Use of pyrolytic gas from waste tire as a fuel: A review,” *Energy*, vol. 134, pp. 1121–1131, 2017, doi: 10.1016/j.energy.2017.05.042.

[11] P. T. Williams, “Pyrolysis of waste tyres: A review,” *Waste Manag.*, vol. 33, no. 8, pp. 1714–1728, 2013, doi: 10.1016/j.wasman.2013.05.003.

[12] I. Vassura, A. Santini, F. Passarini, G. Pecci, and L. Morselli, “Tyres recovery with thermodynamic cracking technology,” *Environ. Eng. Manag. J.*, vol. 12, no. 11, pp. 61–64, 2013.

[13] M. Sienkiewicz, J. Kucinska-Lipka, H. Janik, and A. Balas, “Progress in used tyres management in the European Union: A review,” *Waste Manag.*, vol. 32, no. 10, pp. 1742–1751, 2012, doi: 10.1016/j.wasman.2012.05.010.

[14] J. B. Omwoyo, R. K. Kimilu, and J. M. Onyari, “Effects of temperature and catalytic reduction of sulfur content on kinematic viscosity and specific gravity of tire pyrolysis oil,” *Chem. Eng. Commun.*, vol. 0, no. 0, pp. 1–8, 2021, doi: 10.1080/00986445.2021.2015339.

[15] C. Marculescu, G. Antonini, A. Badea, and T. Apostol, “Pilot installation for the thermo-chemical characterisation of solid wastes,” *Waste Manag.*, vol. 27, no. 3, pp. 367–374, 2007, doi: 10.1016/j.wasman.2006.02.011.

[16] M. Juma, Z. Koreňová, J. Markoš, L. Jelemensky, and M. Bafrnec, “Pyrolysis and combustion of scrap tire,” *Pet. Coal*, vol. 48, no. 1, pp. 15–26, 2006, doi: 10.1002/pat.811.

[17] A. Alsaleh and M. L. Sattler, “Waste Tire Pyrolysis: Influential Parameters and

Product Properties," *Curr. Sustain. Energy Reports*, vol. 1, no. 4, pp. 129–135, 2014, doi: 10.1007/s40518-014-0019-0.

[18] A. M. Mastral, R. Murillo, M. S. Callen, and T. Garcia, "Optimisation of scrap automotive tyres recycling into valuable liquid fuels," *Resour. Conserv. Recycl.*, vol. 29, no. 4, pp. 263–272, 2000, doi: 10.1016/S0921-3449(00)00051-3.

[19] R. Murillo, E. Aylo, M. V Navarro, M. S. Calle, A. Aranda, and A. M. Mastral, "The application of thermal processes to valorise waste tyre," *Fuel Process. Technol.*, vol. 87, no. 2, pp. 143–147, 2006, doi: 10.1016/j.fuproc.2005.07.005.

[20] T. I. Ogedengbe, O. Oroye, and A. O. Akinola, "Modelling the products ' yield of used tyre pyrolyzed in fixed bed reactor," *Leonardo Electron. J. Pract. Technol.*, no. 32, pp. 103–118, 2018.

[21] S. Ucar, S. Karagoz, A. R. Ozkan, and J. Yanik, "Evaluation of two different scrap tires as hydrocarbon source by pyrolysis," *Fuel*, vol. 84, no. 14–15, pp. 1884–1892, 2005, doi: 10.1016/j.fuel.2005.04.002.

[22] M. R. Islam, M. Parveen, H. Haniu, and M. R. I. Sarker, "Innovation in Pyrolysis Technology for Management of Scrap Tire: a Solution of Energyand Environment," *Int. J. Environ. Sci. Dev.*, vol. 1, no. 1, pp. 89–96, 2010, doi: 10.7763/ijesd.2010.v1.18.

[23] J. D. Martínez, J. Rodríguez-Fernández, J. Sánchez-Valdepeñas, R. Murillo, and T. García, "Performance and emissions of an automotive diesel engine using a tire pyrolysis liquid blend," *Fuel*, vol. 115, pp. 490–499, 2014, doi: 10.1016/j.fuel.2013.07.051.

[24] W. Kaminsky and C. Mennerich, "Pyrolysis of synthetic tire rubber in a fluidised-bed reactor to yield 1,3-butadiene, styrene and carbon black," *J. Anal. Appl. Pyrolysis*, vol. 58–59, pp. 803–811, 2001, doi: 10.1016/S0165-2370(00)00129-7.

[25] J. A. Conesa, R. Font, and A. Marcilla, "Gas from the pyrolysis of scrap tires in a

fluidized bed reactor," *Energy and Fuels*, vol. 10, no. 1, pp. 134–140, 1996, doi: 10.1021/ef950152t.

[26] J. D. Martínez, M. Lapuerta, R. García-Contreras, R. Murillo, and T. García, "Fuel properties of tire pyrolysis liquid and its blends with diesel fuel," *Energy and Fuels*, vol. 27, no. 6, pp. 3296–3305, 2013, doi: 10.1021/ef400602e.

[27] I. M. Rofiqul, H. Haniu, and A. B. M. Rafiqul, "Limonene-Rich Liquids from Pyrolysis of Heavy Automotive Tire Wastes," *J. Environ. Eng.*, vol. 2, no. 4, pp. 681–695, 2007, doi: 10.1299/jee.2.681.

[28] A. B. Tabinda, F. Arshed, A. Yasar, M. Afzaal, and A. Iqbal, "Comparative analysis of desulphurization methods of tyre pyrolysis oil," *Int. J. Environ. Sci. Technol.*, vol. 16, pp. 4013–4018, 2019, doi: 10.1007/s13762-018-1898-1.

[29] R. Serefentse, W. Ruwona, G. Danha, and E. Muzenda, "A review of the desulphurization methods used for pyrolysis oil," in *Procedia Manufacturing*, 2019, vol. 35, pp. 762–768, doi: 10.1016/j.promfg.2019.07.013.

[30] S. Ahmad, M. I. Ahmad, K. Naeem, M. Humayun, Sebt-E-Zaeem, and F. Faheem, "Oxidative Desulfurization of Tire," *Chem. Ind. Chem. Eng.*, vol. 22, no. 3, pp. 249–254, 2016, doi: 10.2298/CICEQ150609038A.

[31] M. R. Islam, M. U. H. Joardder, S. M. Hasan, K. Takai, and H. Haniu, "Feasibility study for thermal treatment of solid tire wastes in Bangladesh by using pyrolysis technology," *Waste Manag.*, vol. 31, no. 9–10, pp. 2142–2149, 2011, doi: 10.1016/j.wasman.2011.04.017.

[32] S. Frigo, M. Seggiani, M. Puccini, and S. Vitolo, "Liquid fuel production from waste tyre pyrolysis and its utilisation in a Diesel engine," *Fuel*, vol. 116, pp. 399–408, 2014, doi: 10.1016/j.fuel.2013.08.044.

[33] N. Nkosi and E. Muzenda, "A review and discussion of waste tyre pyrolysis and derived products," in *Proceeding of the World Congress on Engineering*, 2014, vol. 2,

pp. 979–985.

[34] C. Díez, O. Martínez, L. F. Calvo, J. Cara, and A. Morán, “Pyrolysis of tyres. Influence of the final temperature of the process on emissions and the calorific value of the products recovered,” *Waste Manag.*, vol. 24, no. 5, pp. 463–469, 2004, doi: 10.1016/j.wasman.2003.11.006.

[35] M. Olazar, M. Arabiourrutia, G. Lôpez, R. Aguado, and J. Bilbao, “Effect of acid catalysts on scrap tyre pyrolysis under fast heating conditions,” *J. Anal. Appl. Pyrolysis*, vol. 82, no. 2, pp. 199–204, 2008, doi: 10.1016/j.jaap.2008.03.006.

[36] A. Chaala and C. Roy, “Production of coke from scrap tire vacuum pyrolysis oil,” *Fuel Process. Technol.*, vol. 46, no. 3, pp. 227–239, 1996, doi: https://doi.org/10.1016/0378-3820(95)00065-8.

[37] T. Kan, V. Strezov, and T. Evans, “Fuel production from pyrolysis of natural and synthetic rubbers,” *Fuel*, vol. 191, pp. 403–410, 2017, doi: 10.1016/j.fuel.2016.11.100.

[38] M. F. Laresgoiti, B. M. Caballero, I. De Marco, A. Torres, M. A. Cabrero, and M. J. Chomón, “Characterization of the liquid products obtained in tyre pyrolysis,” *J. Anal. Appl. Pyrolysis*, vol. 71, no. 2, pp. 917–934, 2004, doi: 10.1016/j.jaap.2003.12.003.

[39] E. Yazdani, S. H. Hashemabadi, and A. Taghizadeh, “Study of waste tire pyrolysis in a rotary kiln reactor in a wide range of pyrolysis temperature,” *Waste Manag.*, vol. 85, pp. 195–201, 2019, doi: 10.1016/j.wasman.2018.12.020.

[40] Fred W. Barlow, *Rubber compounding: principles, materials, and techniques*, Second edi. Taylor & Francis, 1993.

[41] K. Unapumnuk, “A study of the pyrolysis of tire derived fuels and an analysis of derived chars and oils,” PhD. Thesis, University of Cincinnati, 2006.

[42] J. E. Mark, B. Erman, and F. R. Eirich, *Science and Technology of Rubber*, Third. Burlington: Elsevier Academic Press, 2005.

[43] P. T. Williams and D. T. Taylor, “Aromatization of tyre pyrolysis oil to yield polycyclic aromatic hydrocarbons,” *Fuel*, vol. 72, no. 11, pp. 1469–1474, 1993, doi: 10.1016/0016-2361(93)90002-J.

[44] A. Quek and R. Balasubramanian, “Liquefaction of waste tires by pyrolysis for oil and chemicals - A review,” *J. Anal. Appl. Pyrolysis*, vol. 101, pp. 1–16, 2013, doi: 10.1016/j.jaap.2013.02.016.

[45] N. Jasminská, T. Brestovič, and M. Čarnogurská, “The effect of temperature pyrolysis process of used tires on the quality of output products,” *Acta Mech. Autom.*, vol. 7, no. 1, pp. 20–25, 2013, doi: 10.2478/ama-2013-0004.

[46] D. A. Khalaf, Z. N. Abudi, and S. M. Dhaher, “Bio Oil Production by Thermal and Catalytic Pyrolysis of Waste Tires,” *J. Ecol. Eng. J.*, vol. 22, no. 8, pp. 189–199, 2021.

[47] M. S. N. Awang *et al.*, “Effect of blending local plastic pyrolytic oil with diesel fuel on lubricity,” *J. Tribol.*, vol. 27, pp. 143–157, 2020.

[48] S. C. Moldoveanu, *Analytical pyrolysis of other natural organic polymers*. 2021.

[49] D. Supramono, E. Kusrini, and H. Yuana, “Yield and composition of bio-oil from Co-pyrolysis of corn cobs and plastic waste of HDPE in a fixed bed reactor,” *J. Japan Inst. Energy*, vol. 95, no. 8, pp. 621–628, 2016, doi: 10.3775/jie.95.621.

[50] S. C. Moldoveanu, *Pyrolysis of Organic Molecules with Applications to Health and Environmental Issues - Techniques and Instrumentation in Analytical Chemistry 28*, vol. 28. 2010.

[51] P. Parthasarathy *et al.*, “Influence of process conditions on product yield of waste tyre pyrolysis- A review,” *Korean J. Chem. Eng.*, vol. 33, no. 8, pp. 2268–2286, 2016, doi: 10.1007/s11814-016-0126-2.

[52] M. N. Islam and M. R. Nahian, “Improvement of Waste Tire Pyrolysis Oil and Performance Test with Diesel in CI Engine,” *J. Renew. Energy*, vol. 2016, pp. 1–8, 2016, doi: 10.1155/2016/5137247.

[53] J. Singh, “A review paper on pyrolysis process of waste tyre,” *Int. J. Appl. Res.*, vol. 1, no. 13, pp. 258–262, 2017.

[54] P. Basu, *Biomass gasification and pyrolysis*, First edit. Elsevier Inc., 2012.

[55] R. C. Brown and K. Wang, *Fast Pyrolysis of Biomass Advances in Science and Technology*. 2017.

[56] J. Akhtar and N. S. Amin, “A review on operating parameters for optimum liquid oil yield in biomass pyrolysis,” *Renew. Sustain. Energy Rev.*, vol. 16, pp. 5101–5109, 2012, doi: 10.1016/j.rser.2012.05.033.

[57] E. Salehi, J. Abedi, and T. Harding, “Bio-oil from Sawdust: Pyrolysis of Sawdust in a Fixed-Bed System,” *Energy & Fuels*, vol. 23, no. 7, pp. 3767–3772, 2009.

[58] T. Kan, V. Strezov, and T. J. Evans, “Lignocellulosic biomass pyrolysis : A review of product properties and effects of pyrolysis parameters,” *Renew. Sustain. Energy Rev.*, vol. 57, pp. 1126–1140, 2016, doi: 10.1016/j.rser.2015.12.185.

[59] A. V. Bridgwater and S. A. Bridge, “A Review of Biomass Pyrolysis and Pyrolysis Technologies,” *Biomass Pyrolysis Liq. Upgrad. Util.*, pp. 11–92, 1991, doi: 10.1007/978-94-011-3844-4_2.

[60] S. Boxiong, W. Chunfei, L. Cai, G. Binbin, and W. Rui, “Pyrolysis of waste tyres: The influence of USY catalyst/tyre ratio on products,” *J. Anal. Appl. Pyrolysis*, vol. 78, no. 2, pp. 243–249, 2007, doi: 10.1016/j.jaap.2006.07.004.

[61] N. Antoniou and A. Zabaniotou, “Features of an efficient and environmentally attractive used tyres pyrolysis with energy and material recovery,” *Renew. Sustain. Energy Rev.*, vol. 20, pp. 539–558, 2013, doi: 10.1016/j.rser.2012.12.005.

[62] J. Shah, M. R. Jan, and F. Mabood, “Recovery of value-added products from the catalytic pyrolysis of waste tyre,” *Energy Convers. Manag.*, vol. 50, no. 4, pp. 991–994, 2009, doi: 10.1016/j.enconman.2008.12.017.

[63] W. M. Lewandowski, K. Januszewicz, and W. Kosakowski, “Efficiency and proportions of waste tyre pyrolysis products depending on the reactor type—A review,” *J. Anal. Appl. Pyrolysis*, vol. 140, pp. 25–53, 2019, doi: 10.1016/j.jaap.2019.03.018.

[64] H. Huang and L. Tang, “Pyrolysis treatment of waste tire powder in a capacitively coupled RF plasma reactor,” *Energy Convers. Manag.*, vol. 50, no. 3, pp. 611–617, 2009, doi: 10.1016/j.enconman.2008.10.023.

[65] N. P. Cheremisinoff, *Handbook of Solid Waste Management and Waste Minimization Technologies*. elsevier, 2003.

[66] D. M. Money and G. Harrison, “Liquefaction of scrap automobile tyres in different solvents and solvent mixes,” *Fuel*, vol. 78, pp. 1729–1736, 1999.

[67] S. Uçar, S. Karagöz, J. Yanik, M. Saglam, and M. Yuksel, “Copyrolysis of scrap tires with waste lubricant oil,” *Fuel Process. Technol.*, vol. 87, no. 1, pp. 53–58, 2005, doi: 10.1016/j.fuproc.2005.06.001.

[68] R. Font, J. A. Conesa, and I. Martin-gullo, “Rubber tire thermal decomposition in a used oil environment,” *J. Anal. Appl. Pyrolysis*, vol. 74, pp. 265–269, 2005, doi: 10.1016/j.jaap.2004.09.002.

[69] F. A. López, M. I. Martín, F. J. Alguacil, J. M. Rincón, T. A. Centeno, and M. Romero, “Thermolysis of fibreglass polyester composite and reutilization of the glass fibre residue to obtain a glass–ceramic material,” *J. Anal. Appl. Pyrolysis*, vol. 93, pp. 104–112, 2012, doi: 10.1016/j.jaap.2011.10.003.

[70] G. Lopez, M. Olazar, M. Amutio, R. Aguado, and J. Bilbao, “Influence of tire formulation on the products of continuous pyrolysis in a conical spouted bed reactor,” *Energy and Fuels*, vol. 23, no. 11, pp. 5423–5431, 2009, doi: 10.1021/ef900582k.

[71] I. M. Rodriguez, M. F. Laresgoiti, M. A. Cabrero, A. Torres, M. J. Chomon, and B. Caballero, “Pyrolysis of scrap tyres,” *Fuel Process. Technol.*, vol. 72, pp. 9–22, 2001.

[72] P. T. Williams and R. P. Bottrill, “Sulfur-polycyclic aromatic hydrocarbons in tyre pyrolysis oil,” *Fuel*, vol. 74, no. 5, pp. 736–742, 1995, doi: 10.1016/0016-2361(94)00005-C.

[73] J. F. González, J. M. Encinar, J. L. Canito, and J. J. Rodríguez, “Pyrolysis of automobile tyre waste. Influence of operating variables and kinetics study,” *J. Anal. Appl. Pyrolysis*, vol. 58, no. 59, pp. 667–683, 2001, doi: 10.1016/S0165-2370(00)00201-1.

[74] P. T. Williams, S. Besler, and D. T. Taylor, “The Batch Pyrolysis of Tyre Waste - Fuel Properties of the Derived Pyrolytic Oil and Overall Plant Economics,” in *Proceedings of the Institution of Mechanical Engineers, Part A: Journal of Power and Energy*, 1993, vol. 207, no. 1, pp. 55–63, doi: 10.1243/PIME_PROC_1993_207_007_02.

[75] A. A. Zabaniotou and G. Stavropoulos, “Pyrolysis of used automobile tires and residual char utilization,” *J. Anal. Appl. Pyrolysis*, vol. 70, no. 2, pp. 711–722, 2003, doi: 10.1016/S0165-2370(03)00042-1.

[76] C. Roy, A. Chaala, and H. Darmstadt, “Vacuum pyrolysis of used tires end-uses for oil and carbon black products,” *J. Anal. Appl. Pyrolysis*, vol. 51, no. 1, pp. 201–221, 1999, doi: 10.1016/S0165-2370(99)00017-0.

[77] D. Mohan, C. U. Pittman, and P. H. Steele, “Pyrolysis of wood/biomass for bio-oil: A critical review,” *Energy and Fuels*, vol. 20, no. 3, pp. 848–889, 2006, doi: 10.1021/ef0502397.

[78] M. R. Islam, M. N. Islam, N. N. Mustafi, M. A. Rahim, and H. Haniu, “Thermal recycling of solid tire wastes for alternative liquid fuel: The first commercial step in Bangladesh,” in *Procedia Engineering*, 2013, vol. 56, pp. 573–582, doi: 10.1016/j.proeng.2013.03.162.

[79] P. T. Williams and A. J. Brindle, “Aromatic chemicals from the catalytic pyrolysis of scrap tyres,” *J. Anal. Appl. Pyrolysis*, vol. 67, pp. 143–164, 2003.

[80] J. D. Martínez, Á. Ramos, O. Armas, R. Murillo, and T. García, “Potential for using a tire pyrolysis liquid-diesel fuel blend in a light duty engine under transient operation,” *Appl. Energy*, vol. 130, pp. 437–446, 2014, doi: 10.1016/j.apenergy.2014.05.056.

[81] J. D. Martínez, R. Murillo, T. García, and A. Veses, “Demonstration of the waste tire pyrolysis process on pilot scale in a continuous auger reactor,” *J. Hazard. Mater.*, vol. 261, pp. 637–645, 2013, doi: 10.1016/j.jhazmat.2013.07.077.

[82] A. M. Cunliffe and P. T. Williams, “Composition of oils derived from the batch pyrolysis of tyres,” *J. Anal. Appl. Pyrolysis*, vol. 44, pp. 131–152, 1998.

[83] M. Banar, V. Akyildiz, A. Özkan, Z. Çokaygil, and Ö. Onay, “Characterization of pyrolytic oil obtained from pyrolysis of TDF (Tire Derived Fuel),” *Energy Convers. Manag.*, vol. 62, pp. 22–30, 2012, doi: 10.1016/j.enconman.2012.03.019.

[84] M. R. Islam, H. Haniu, and M. R. A. Beg, “Liquid fuels and chemicals from pyrolysis of motorcycle tire waste: Product yields, compositions and related properties,” *Fuel*, vol. 87, no. 13–14, pp. 3112–3122, 2008, doi: 10.1016/j.fuel.2008.04.036.

[85] E. R. Umeki, C. F. De Oliveira, R. B. Torres, and R. G. dos Santos, “Physico-chemistry properties of fuel blends composed of diesel and tire pyrolysis oil,” *Fuel*, vol. 185, pp. 236–242, 2016, doi: 10.1016/j.fuel.2016.07.092.

[86] E. Hürdoğan, C. Ozalp, O. Kara, and M. Ozcanli, “Experimental investigation on performance and emission characteristics of waste tire pyrolysis oil–diesel blends in a diesel engine,” *Int. J. Hydrogen Energy*, vol. 42, no. 36, pp. 23373–23378, 2017, doi: 10.1016/j.ijhydene.2016.12.126.

[87] R. D. Wankhade, “Studies on Compatibility of Tyre Pyrolysis Oil as Fuel for Diesel Engine,” PhD. Thesis, G. B. Pant University of Agriculture and Technology, 2017.

[88] A. Undri, S. Meini, L. Rosi, M. Frediani, and P. Frediani, “Microwave pyrolysis of polymeric materials: Waste tires treatment and characterization of the value-added products,” *J. Anal. Appl. Pyrolysis*, vol. 103, pp. 149–158, 2013, doi:

10.1016/j.jaap.2012.11.011.

[89] C. Leonard, “Development of an Innovative Pyrolysis Plant for the Production of Secondary Raw Materials,” PhD. Thesis, Università di Bologna, 2015.

[90] M. Kyari, A. Cunliffe, and P. T. Williams, “Characterization of oils, gases, and char in relation to the pyrolysis of different brands of scrap automotive tires,” *Energy and Fuels*, vol. 19, no. 3, pp. 1165–1173, 2005, doi: 10.1021/ef049686x.

[91] J. D. Martínez, N. Puy, R. Murillo, T. García, M. V. Navarro, and A. M. Mastral, “Waste tyre pyrolysis - A review,” *Renew. Sustain. Energy Rev.*, vol. 23, pp. 179–213, 2013, doi: 10.1016/j.rser.2013.02.038.

[92] S. John and W. Kaminsky, “Feedstock Recycling and Pyrolysis of WastePlastics: Converting Waste Plastics into Diesel and Other Fuels,” First., John Wiley & Sons, 2006, pp. 85–96.

[93] M. D. Grau, J. M. Nougués, and L. Puigjaner, “Comparative study of two chemical reactions with different behaviour in batch and semibatch reactors,” *Chem. Eng. J.*, vol. 88, no. 1–3, pp. 225–232, 2002, doi: 10.1016/S1385-8947(02)00027-X.

[94] M. M. Barbooti, T. J. Mohamed, A. A. Hussain, and F. O. Abas, “Optimization of pyrolysis conditions of scrap tires under inert gas atmosphere,” *J. Anal. Appl. Pyrolysis*, vol. 72, no. 1, pp. 165–170, 2004, doi: 10.1016/j.jaap.2004.05.001.

[95] D. Chen, L. Yin, H. Wang, and P. He, “Pyrolysis technologies for municipal solid waste: A review,” *Waste Manag.*, vol. 34, no. 12, pp. 2466–2486, 2014, doi: 10.1016/j.wasman.2014.08.004.

[96] Y. Uemichi, J. Nakamura, T. Itoh, M. Sugioka, A. A. Garforth, and J. Dwyer, “Conversion of polyethylene into gasoline-range fuels by two-stage catalytic degradation using silica-alumina and HZSM-5 zeolite,” *Ind. Eng. Chem. Res.*, vol. 38, no. 2, pp. 385–390, 1999, doi: 10.1021/ie980341+.

[97] P. T. Williams and E. A. Williams, “Fluidised bed pyrolysis of low density

polyethylene to produce petrochemical feedstock," *J. Anal. Appl. Pyrolysis*, vol. 51, no. 1–2, pp. 107–126, 1999, doi: 10.1016/S0165-2370(99)00011-X.

[98] Q. Cao, L. Jin, W. Bao, and Y. Lv, "Investigations into the characteristics of oils produced from co-pyrolysis of biomass and tire," *Fuel Process. Technol.*, vol. 90, no. 3, pp. 337–342, 2009, doi: 10.1016/j.fuproc.2008.10.005.

[99] Y. Suleiman *et al.*, "Design and Fabrication of Fluidized-bed Reactor," *Int. J. Eng. Comput. Sci.*, vol. 2, no. 5, pp. 1595–1605, 2013, [Online]. Available: www.ijecs.in.

[100] X. Dai, X. Yin, C. Wu, W. Zhang, and Y. Chen, "Pyrolysis of waste tires in a circulating fluidized-bed reactor," *Energy*, vol. 26, no. 4, pp. 385–399, 2001, doi: 10.1016/S0360-5442(01)00003-2.

[101] M. Arabiourrutia, G. Lopez, G. Elordi, M. Olazar, R. Aguado, and J. Bilbao, "Product distribution obtained in the pyrolysis of tyres in a conical spouted bed reactor," *Chem. Eng. Sci.*, vol. 62, no. 18–20, pp. 5271–5275, 2007, doi: 10.1016/j.ces.2006.12.026.

[102] J. M. Arandes *et al.*, "Transformation of Several Plastic Wastes into Fuels by Catalytic Cracking," *Ind. Eng. Chem. Res.*, vol. 36, no. 11, pp. 4523–4529, 1997, doi: 10.1021/ie970096e.

[103] G. M. Alwan, S. B. Aradhya, and M. H. Al-Dahhan, "Study of Solids and Gas Distribution in Spouted Bed Operated In Stable and Unstable Conditions," *J. Eng. Res. Appl.*, vol. 4, no. 2, pp. 2248–9622, 2014, [Online]. Available: www.ijera.com.

[104] S. Zinchik *et al.*, "Evaluation of fast pyrolysis feedstock conversion with a mixing paddle reactor," *Fuel Process. Technol.*, vol. 171, pp. 124–132, 2018, doi: 10.1016/j.fuproc.2017.11.012.

[105] M. Day, Z. Shen, and J. D. Cooney, "Pyrolysis of auto shredder residue: experiments with a laboratory screw kiln reactor," *J. Anal. Appl. Pyrolysis*, vol. 51, no. 1, pp. 181–200, 1999, doi: 10.1016/S0165-2370(99)00016-9.

[106] M. R. Islam, M. S. H. K. Tushar, and H. Haniu, "Production of liquid fuels and

chemicals from pyrolysis of Bangladeshi bicycle/rickshaw tire wastes," *J. Anal. Appl. Pyrolysis*, vol. 82, no. 1, pp. 96–109, 2008, doi: 10.1016/j.jaap.2008.02.005.

[107] D. Pradhan and R. K. Singh, "Thermal Pyrolysis of Bicycle Waste Tyre Using Batch Reactor," *Int. J. Chem. Eng. Appl.*, vol. 2, no. 5, pp. 332–336, 2011, doi: 10.7763/ijcea.2011.v2.129.

[108] C. Ilkiliç and H. Aydin, "Fuel production from waste vehicle tires by catalytic pyrolysis and its application in a diesel engine," *Fuel Process. Technol.*, vol. 92, no. 5, pp. 1129–1135, 2011, doi: 10.1016/j.fuproc.2011.01.009.

[109] S. Murugan, M. C. Ramaswamy, and G. Nagarajan, "The use of tyre pyrolysis oil in diesel engines," *Waste Manag.*, vol. 28, no. 12, pp. 2743–2749, 2008, doi: 10.1016/j.wasman.2008.03.007.

[110] R. Aguado, M. Olazar, D. Ve´lez, M. Arabiourrutia, and J. Bilbao, "Kinetics of scrap tyre pyrolysis under fast heating conditions," *J. Anal. Appl. Pyrolysis*, vol. 73, pp. 290–298, 2005, doi: 10.1016/j.jaap.2005.02.006.

[111] X. Zhang, T. Wang, L. Ma, and J. Chang, "Vacuum pyrolysis of waste tires with basic additives," *Waste Manag.*, vol. 28, no. 11, pp. 2301–2310, 2008, doi: 10.1016/j.wasman.2007.10.009.

[112] C. Roy, B. Labrecque, and B. de Caumia, "Recycling of scrap tires to oil and carbon black by vacuum pyrolysis," *Resour. Conserv. Recycl.*, vol. 4, no. 3, pp. 203–213, 1990, doi: 10.1016/0921-3449(90)90002-L.

[113] A. M. Mastral, R. Murillo, T. García, M. V. Navarro, M. S. Callen, and J. M. López, "Study of the viability of the process for hydrogen recovery from old tyre oils," *Fuel Process. Technol.*, vol. 75, no. 3, pp. 185–199, 2002, doi: 10.1016/S0378-3820(02)00004-8.

[114] T. Soni and A. Gaikwad, "Waste pyrolysis tire oil as alternative fuel for diesel engines," *Int. J. Mech. Prod. Eng. Res. Dev.*, vol. 7, no. 6, pp. 271–278, 2017, doi:

10.24247/ijmperddec201730.

[115] C. Berrueco, E. Esperanza, F. J. Mastral, J. Ceamanos, and García-Bacaicoa P., "Pyrolysis of waste tyres in an atmospheric static-bed batch reactor: Analysis of the gases obtained," *J. Anal. Appl. Pyrolysis*, vol. 74, no. 1–2, pp. 245–253, 2005, doi: 10.1016/j.jaap.2004.10.007.

[116] I. D. Marco, B. M. Caballero, M. A. Cabrero, M. F. Laresgoiti, A. Torres, and M. J. Chomón, "Recycling of automobile shredder residues by means of pyrolysis," *J. Anal. Appl. Pyrolysis*, vol. 79, no. 1–2, pp. 403–408, 2007, doi: 10.1016/j.jaap.2006.12.002.

[117] J. I. Osayi, S. Iyuke, M. O. Daramola, P. Osifo, I. J. Van Der Walt, and S. E. Ogbeide, "Evaluation of pyrolytic oil from used tires and natural rubber (Hevea brasiliensis)," *Chem. Eng. Commun.*, vol. 205, no. 6, pp. 805–821, 2018, doi: 10.1080/00986445.2017.1422493.

[118] L. Ding, Z. Zhou, Q. Guo, W. Huo, and G. Yu, "Catalytic effects of Na2CO3 additive on coal pyrolysis and gasification," *Fuel*, vol. 142, pp. 134–144, 2015, doi: 10.1016/j.fuel.2014.11.010.

[119] A. Oyedun, K. Lam, M. Fittkau, and C. Hui, "Optimisation of particle size in waste tyre pyrolysis," *Fuel*, vol. 95, pp. 417–424, 2012, doi: 10.1016/j.fuel.2011.09.046.

[120] H. Haykiri-Acma, "The role of particle size in the non-isothermal pyrolysis of hazelnut shell," *J. Anal. Appl. Pyrolysis*, vol. 75, pp. 211–216, 2006, doi: 10.1016/j.jaap.2005.06.002.

[121] G. López, M. Olazar, R. Aguado, and J. Bilbao, "Continuous pyrolysis of waste tyres in a conical spouted bed reactor," *Fuel*, vol. 89, no. 8, pp. 1946–1952, 2010, doi: 10.1016/j.fuel.2010.03.029.

[122] R. Cypres, "Aromatic hydrocarbons formation during coal pyrolysis," *Fuel Process. Technol.*, vol. 15, pp. 1–15, 1987, doi: 10.1016/0378-3820(87)90030-0.

[123] D. Depeyre, C. Flicoteaux, and C. Chardalre, "Pure n-Hexadecane Thermal Steam

Cracking," *Ind. Eng. Chem. Process Des. Dev.*, vol. 24, no. 4, pp. 1251–1258, 1985, doi: 10.1021/i200031a059.

[124] M. L. Boroson, J. B. Howard, J. P. Longwell, and W. A. Peters, "Product Yields and Kinetics from the Vapor Phase Cracking of Wood Pyrolysis Tars," *AIChE J.*, vol. 35, no. 1, pp. 120–128, 1989.

[125] S. Önenç, M. Brebu, C. Vasile, and J. Yanik, "Copyrolysis of scrap tires with oily wastes," *J. Anal. Appl. Pyrolysis*, vol. 94, pp. 184–189, 2012, doi: 10.1016/j.jaap.2011.12.006.

[126] T. Popa, M. Fan, M. D. Argyle, R. B. Slimane, D. A. Bell, and B. F. Towler, "Catalytic gasification of a Powder River Basin coal," *Fuel*, vol. 103, pp. 161–170, 2013, doi: 10.1016/j.fuel.2012.08.049.

[127] J. Shah, M. R. Jan, and F. Mabood, "Catalytic conversion of waste tyres into valuable hydrocarbons," *J. Polym. Environ.*, vol. 15, no. 3, pp. 207–211, 2007, doi: 10.1007/s10924-007-0062-7.

[128] G. Kabir and B. H. Hameed, "Recent progress on catalytic pyrolysis of lignocellulosic biomass to high-grade bio-oil and bio-chemicals," *Renew. Sustain. Energy Rev.*, vol. 70, pp. 945–967, 2017, doi: 10.1016/j.rser.2016.12.001.

[129] J. Shah, M. Rasul Jan, and F. Mabood, "Catalytic pyrolysis of waste tyre rubber into hydrocarbons via base catalysts," *Iran. J. Chem. Chem. Eng.*, vol. 27, no. 2, pp. 103–109, 2008.

[130] H. Hattori, "Solid base catalysts: Fundamentals and their applications in organic reactions," *Appl. Catal. A Gen.*, vol. 504, pp. 103–109, 2015, doi: 10.1016/j.apcata.2014.10.060.

[131] H. Hattori, "Solid base catalysts: Generation of basic sites and application to organic synthesis," *Appl. Catal. A Gen.*, vol. 222, no. 1–2, pp. 247–259, 2001, doi: 10.1016/S0926-860X(01)00839-0.

[132] H. Ukei *et al.*, “Catalytic degradation of polystyrene into styrene and a design of recyclable polystyrene with dispersed catalysts,” *Catal. Today*, vol. 62, no. 1, pp. 67–75, 2000, doi: 10.1016/S0920-5861(00)00409-0.

[133] K. Chen, C. Chen, and J. Huang, “Optimal parameter study of waste tyre pyrolysis modulation for green diesel production,” *J. Inf. Optim. Sci.*, vol. 39, no. 3, pp. 749–758, 2018, doi: 10.1080/02522667.2018.1427743.

[134] S. Q. Li, Q. Yao, Y. Chi, J. H. Yan, and K. F. Cen, “Pilot-scale pyrolysis of scrap tires in a continuous rotary kiln reactor,” *Ind. Eng. Chem. Res.*, vol. 43, no. 17, pp. 5133–5145, 2004, doi: 10.1021/ie030115m.

[135] O. W. Otta, “Two-stage chemical and enzymatic strategies for the preparation of biodiesel from croton megalocarpus oil and evaluation of its engine performance and oxidation stability,” PhD. Thesis, University of Nairobi, 2016.

[136] F. Luis and G. Moncayo, *Alternative Fuels and Advanced Vehicle Technologies for Improved Environmental Performance*. Woodhead Publishing Limited, 2014.

[137] G. W. Balich and C. R. Aschenbach, *The Gasoline 4-Stroke Engine for Automobiles*. 2004.

[138] J. V. Gerpen, B. Shanks, R. Pruszko, D. Clements, and G. Knothe, “Biodiesel Production Technology,” 2004.

[139] C. Wongkhorsub and N. Chindaprasert, “A Comparison of the Use of Pyrolysis Oils in Diesel Engine,” *Energy Power Eng.*, vol. 05, no. 04, pp. 350–355, 2013, doi: 10.4236/epe.2013.54b068.

[140] H. Aydın and C. Ilkılıç, “Optimization of fuel production from waste vehicle tires by pyrolysis and resembling to diesel fuel by various desulfurization methods,” *Fuel*, vol. 102, pp. 605–612, 2012, doi: 10.1016/j.fuel.2012.06.067.

[141] R. Miandad, M. A. Barakat, M. Rehan, A. S. Aburiazaiza, J. Gardy, and A. S. Nizami, “Effect of advanced catalysts on tire waste pyrolysis oil,” *Process Saf. Environ. Prot.*,

vol. 116, pp. 542–552, 2018, doi: 10.1016/j.psep.2018.03.024.

[142] F. A. Razmi *et al.*, “Production and characterization of diesel-like fuel by catalytic upgrading of scrap tire pyrolysis oil using basic catalyst derived from blood cockle shell (Anadara Granosa),” *Materials Today: Proceedings*. Elsevier Ltd, pp. 2–7, 2021, doi: 10.1016/j.matpr.2021.02.805.

[143] A. A. Refaat, “Correlation between the chemical structure of biodiesel and its physical properties,” *Int. J. Env. Sci. Technol*, vol. 6, no. 4, pp. 677–694, 2009, doi: 10.1007/bf03326109.

[144] L. F. Ramírez-Verduzco, J. E. Rodríguez-Rodríguez, and A. D. R. Jaramillo-Jacob, “Predicting cetane number, kinematic viscosity, density and higher heating value of biodiesel from its fatty acid methyl ester composition,” *Fuel*, vol. 91, no. 1, pp. 102–111, 2012, doi: 10.1016/j.fuel.2011.06.070.

[145] M. J. Pratas, S. Freitas, M. B. Oliveira, S. C. Monteiro, Á. S. Lima, and J. A. P. Coutinho, “Densities and Viscosities of Fatty Acid Methyl and Ethyl Esters,” *J. Chem. Eng. Data*, vol. 55, no. 9, pp. 3983–3990, 2011, doi: 10.1021/je1012235.

[146] A. Gopinath, K. Sairam, R. Velraj, and G. Kumaresan, “Effects of the properties and the structural configurations of fatty acid methyl esters on the properties of biodiesel fuel: A review,” *Proc. Inst. Mech. Eng. Part D J. Automob. Eng.*, vol. 229, no. 3, pp. 357–390, 2015, doi: 10.1177/0954407014541103.

[147] Y. Ali, M. A. Hanna, and S. L. Cuppett, “Fuel properties of tallow and soybean oil esters,” *J. Am. Oil Chem. Soc.*, vol. 72, no. 12, pp. 1557–1564, 1995, doi: 10.1007/BF02577854.

[148] C. E. Ejim, B. A. Fleck, and A. Amirfazli, “Analytical study for atomization of biodiesels and their blends in a typical injector: Surface tension and viscosity effects,” *Fuel*, vol. 86, no. 10–11, pp. 1534–1544, 2007, doi: 10.1016/j.fuel.2006.11.006.

[149] W. Yang, M. Jia, K. Sun, and T. Wang, “Influence of density ratio on the secondary

atomization of liquid droplets under highly unstable conditions," *Fuel*, vol. 174, pp. 25–35, 2016, doi: 10.1016/j.fuel.2016.01.078.

[150] X. Jiang, G. A. Siamas, K. Jagus, and T. G. Karayiannis, "Physical modelling and advanced simulations of gas-liquid two-phase jet flows in atomization and sprays," *Prog. Energy Combust. Sci.*, vol. 36, no. 2, pp. 131–167, 2010, doi: 10.1016/j.pecs.2009.09.002.

[151] R. Kiplimo, E. Tomita, N. Kawahara, and S. Yokobe, "Effects of spray impingement, injection parameters, and EGR on the combustion and emission characteristics of a PCCI diesel engine," *Appl. Therm. Eng.*, vol. 37, pp. 165–175, 2012, doi: 10.1016/j.applthermaleng.2011.11.011.

[152] R. Kiplimo, "Combustion and Engine – out Emission Characteristics of a PCCI Diesel Engine," Ph.D. Okayama University, 2012.

[153] K. Sivaramakrishnan and P. Ravikumar, "Determination of cetane number of biodiesel and it's influence on physical properties," *ARPN J. Eng. Appl. Sci.*, vol. 7, no. 2, pp. 205–211, 2012.

[154] Y. Yang *et al.*, "Characterisation of waste derived intermediate pyrolysis oils for use as diesel engine fuels," *Fuel*, vol. 103, pp. 247–257, 2013, doi: 10.1016/j.fuel.2012.07.014.

[155] P. I. Lacey and S. A. Howell, "Fuel Lubricity Reviewed," *J. FUELS Lubr.*, vol. 107, no. 4, pp. 1461–1479, 1998.

[156] M. Lackner, Á. B. Palotás, and F. Winter, *Combustion From Basics to Applications*. Wiley-VCH Verlag GmbH & Co., 2013.

[157] C. Haşimoğlu, M. Ciniviz, I. Özsert, Y. Içingür, A. Parlak, and M. S. Salman, "Performance characteristics of a low heat rejection diesel engine operating with biodiesel," *Renew. Energy*, vol. 33, no. 7, pp. 1709–1715, 2008, doi: 10.1016/j.renene.2007.08.002.

[158] M. S. Graboski and R. L. McCormick, “Combustion of Fat and Vegetable Oil Derived Fuels in Diesel Engines,” *Prog. Energy Combust. Sci.*, vol. 24, no. 2, pp. 125–164, 1998.

[159] S. Pinzi, D. Leiva, G. Arzamendi, L. M. Gandia, and M. P. Dorado, “Multiple response optimization of vegetable oils fatty acid composition to improve biodiesel physical properties,” *Bioresour. Technol.*, vol. 102, no. 15, pp. 7280–7288, 2011, doi: 10.1016/j.biortech.2011.05.005.

[160] A. Demirbas, *Biodiesel A Realistic Fuel Alternative for Diesel Engines*. Springer, 2008.

[161] G. Knothe and K. R. Steidley, “Kinematic viscosity of biodiesel fuel components and related compounds. Influence of compound structure and comparison to petrodiesel fuel components,” *Fuel*, vol. 84, no. 9, pp. 1059–1065, 2005, doi: 10.1016/j.fuel.2005.01.016.

[162] A. J. Folayan, P. A. L. Anawe, A. E. Aladejare, and A. O. Ayeni, “Experimental investigation of the effect of fatty acids configuration, chain length, branching and degree of unsaturation on biodiesel fuel properties obtained from lauric oils, high-oleic and high-linoleic vegetable oil biomass,” *Energy Reports*, vol. 5, pp. 793–806, 2019, doi: 10.1016/j.egyr.2019.06.013.

[163] B. Freedman and M. O. Bagby, “Predicting cetane numbers of n-alcohols and methyl esters from their physical properties,” *J. Am. Oil Chem. Soc.*, vol. 67, no. 9, pp. 565–571, 1990, doi: 10.1007/BF02540768.

[164] G. Knothe, “Dependence of biodiesel fuel properties on the structure of fatty acid alkyl esters,” *Fuel Process. Technol.*, vol. 86, no. 10, pp. 1059–1070, 2005, doi: 10.1016/j.fuproc.2004.11.002.

[165] M. J. Pratas, S. Freitas, M. B. Oliveira, S. C. Monteiro, Á. S. Lima, and J. A. P. Coutinho, “Densities and viscosities of minority fatty acid methyl and ethyl esters present in biodiesel,” *J. Chem. Eng. Data*, vol. 56, no. 5, pp. 2175–2180, 2011, doi:

10.1021/je1012235.

[166] G. Knothe, "'Designer' Biodiesel: Optimizing Fatty Ester Composition to Improve Fuel Properties," *Energy & Fuels*, vol. 22, pp. 1358–1364, 2008, doi: 10.1016/j.bbrc.2011.08.056.

[167] I. Lee, L. A. Johnson, and E. G. Hammond, "Use of branched-chain esters to reduce the crystallization temperature of biodiesel," *J. Am. Oil Chem. Soc.*, vol. 72, no. 10, pp. 1155–1160, 1995, doi: 10.1007/BF02540982.

[168] D. Margaroni, "Fuel lubricity," *Ind. Lubr. Tribol.*, vol. 50, no. 3, pp. 108–118, 1998, doi: 10.4271/982567.

[169] L. M. V. Serrano, R. M. O. Câmara, V. J. R. Carreira, and M. C. Gameiro Da Silva, "Performance study about biodiesel impact on buses engines using dynamometer tests and fleet consumption data," *Energy Convers. Manag.*, vol. 60, no. 2012, pp. 2–9, 2012, doi: 10.1016/j.enconman.2011.11.029.

[170] S. M. Abbas and A. Elayaperumal, "Experimental investigation on the effect of ceramic coating on engine performance and emission characteristics for cleaner production," *J. Clean. Prod.*, vol. 214, pp. 506–513, 2019, doi: 10.1016/j.jclepro.2018.12.040.

[171] W. Wang, P. Li, S. Sheng, H. Tian, H. Zhang, and X. Zhang, "Influence of Hydrocarbon Base Oil Molecular Structure on Lubricating Properties in Nano-scale Thin Film," *Tribol. Lett.*, vol. 67, no. 4, pp. 1–9, 2019, doi: 10.1007/s11249-019-1222-3.

[172] J. Zhang, A. Tan, and H. Spikes, "Effect of Base Oil Structure on Elastohydrodynamic Friction," *Tribol. Lett.*, vol. 65, no. 13, pp. 1–24, 2017, doi: 10.1007/s11249-016-0791-7.

[173] F. Lujaji, A. Bereczky, L. Janosi, C. Novak, and M. Mbarawa, "Cetane number and thermal properties of vegetable oil, biodiesel, 1-butanol and diesel blends," *J. Therm.*

Anal. Calorim., vol. 102, no. 3, pp. 1175–1181, 2010, doi: 10.1007/s10973-010-0733-9.

[174] J. H. Kroll *et al.*, "Carbon oxidation state as a metric for describing the chemistry of atmospheric organic aerosol," *Nat. Chem.*, vol. 3, no. 2, pp. 133–139, 2011, doi: 10.1038/nchem.948.

[175] J. Liu, J. Wu, J. Zhu, Z. Wang, J. Zhou, and K. Cen, "Removal of oxygen functional groups in lignite by hydrothermal dewatering: An experimental and DFT study," *Fuel*, vol. 178, pp. 85–92, 2016, doi: 10.1016/j.fuel.2016.03.045.

[176] D. Pradhan, R. K. Singh, H. Bendu, and R. Mund, "Pyrolysis of Mahua seed (Madhuca indica) - Production of biofuel and its characterization," *Energy Convers. Manag.*, vol. 108, pp. 529–538, 2016, doi: 10.1016/j.enconman.2015.11.042.

[177] C. Y. Chun, C. W. Hsin, L. B. Jhih, C. J. Shu, and O. H. Chyuan, "Impact of torrefaction on the composition, structure and reactivity of a microalga residue," *Appl. Energy*, vol. 181, pp. 110–119, 2016, doi: 10.1016/j.apenergy.2016.07.130.

[178] M. H. Tahir *et al.*, "Fundamental investigation of the effect of functional groups on the variations of higher heating value," *Fuel*, vol. 253, pp. 881–886, 2019, doi: 10.1016/j.fuel.2019.05.079.

[179] O. M. Maube, "Performance Evaluation of Used Edible Oil Used as Diesel Fuel," M.Sc. Thesis, University of Nairobi, 2009.

[180] C. B. Khadka, "How Much Money Can an Equation Really Save? Standard Test Method for Calculating Cetane Index via Four Variable Equation," *Econ. J. Dev. Issues*, vol. 19, no. 1, pp. 60–76, 2017, doi: 10.3126/ejdi.v19i1-2.17702.

[181] K. W. Ragland and K. M. Bryden, *Handbook of Diesel Engines*. Springer, 2020.

[182] G. Knothe, A. C. Matheaus, and T. W. Ryan, "Cetane numbers of branched and straight-chain fatty esters determined in an ignition quality tester," *Fuel*, vol. 82, no. 8, pp. 971–975, 2003, doi: 10.1016/S0016-2361(02)00382-4.

[183] M. H. Keshavarz and M. Ghanbarzadeh, “Simple method for reliable predicting flash points of unsaturated hydrocarbons,” *J. Hazard. Mater.*, vol. 193, pp. 335–341, 2011, doi: 10.1016/j.jhazmat.2011.07.044.

[184] T. A. Albahri, “MNLR and ANN structural group contribution methods for predicting the flash point temperature of pure compounds in the transportation fuels range,” *Process Saf. Environ. Prot.*, vol. 93, pp. 182–191, 2015, doi: 10.1016/j.psep.2014.03.005.

[185] G. E. Totten, S. R. Westbrook, and R. J. Shah, *Fuels and Lubricants Handbook: Technology, Properties, Performance, and Testing*. West Conshohocken: ASTM International, 2003.

[186] S. K. Hoekman, A. Broch, C. Robbins, E. Ceniceros, and M. Natarajan, “Review of biodiesel composition, properties, and specifications,” *Renew. Sustain. Energy Rev.*, vol. 16, no. 1, pp. 143–169, 2012, doi: 10.1016/j.rser.2011.07.143.

[187] J. Yang *et al.*, “Solvent-free synthesis of C10 and C11 branched alkanes from furfural and methyl isobutyl ketone,” *ChemSusChem*, vol. 6, no. 7, pp. 1149–1152, 2013, doi: 10.1002/cssc.201300318.

[188] R. Platace, A. Adamovics, and I. Gulbe, “Evaluation of factors influencing calorific value of reed canary grass spring and autumn yield,” *Engineering for Rural Development*. pp. 521–525, 2013.

[189] E. Aylón, A. Fernández-Colino, R. Murillo, M. V. Navarro, T. García, and A. M. Mastral, “Valorisation of waste tyre by pyrolysis in a moving bed reactor,” *Waste Manag.*, vol. 30, no. 7, pp. 1220–1224, 2010, doi: 10.1016/j.wasman.2009.10.001.

[190] S. Timoshenko, *Strength of materials part I, Elementally theory and problems*, Second edi. D. Van Nostrand Company, Inc., 1940.

[191] S. Timoshenko, *Strength of Materials: Part II Advanced Theory and Problems*, Second edi. D. Van Nostrand Company, Inc., 1940.

[192] J. Lee, “Elevated-Temperature Properties of ASTM A992 Steel for Structural-Fire Engineering Analysis,” PhD. Thesis, The University of Texas at Austin, 2012.

[193] M. Ndaliman and A. Pius, “Behavior of Aluminum Alloy Castings under Different Pouring Temperatures and Speeds,” *Leonardo Electron. J. Pract. Technol.*, no. 11, pp. 71–80, 2007, [Online]. Available: http://lejpt.academicdirect.org/A11/071_080.htm.

[194] S. Boontein, W. Prukkanon, K. Puparatanapong, J. Kajornchaiyakul, and C. Limmaneevichitr, “Effect of Minor Sb Additions on SDAS, Age Hardening and Mechanical Properties of A356 Aluminium Alloy Casting,” *Mater. Sci. Forum*, vol. 519–521, pp. 537–542, 2006, doi: 10.4028/www.scientific.net/msf.519-521.537.

[195] A. M. A. Mohamed, F. H. Samuel, A. M. Samuel, and H. W. Doty, “Effects of individual and combined additions of Pb, Bi, and Sn on the microstructure and mechanical properties of Al-10.8Si-2.25Cu-0.3Mg alloy,” *Metall. Mater. Trans. A Phys. Metall. Mater. Sci.*, vol. 40, no. 1, pp. 240–254, 2009, doi: 10.1007/s11661-008-9692-1.

[196] N. T. Ngigi, “Effect of transition elements on microstructure and mechanical properties of secondary al-7Si-Mg cast aluminium,” M.Sc. Thesis, University of Nairobi, 2017.

[197] Y. A. Cengel, *Heat Transfer: A Practical Approach*. 2002.

[198] S. K. De, A. I. Isayeu, and Klementina Khait, *Rubber recyling*, First edit. CRC Press, 2005.

[199] K. K. Kuo, *Principles of Combustion*, Second edi. John Wiley and Sons incl., 2005.

[200] P. J. Pritchard and J. C. Leylegian, *Fox and McDonald’s Introduction To Fluid Mechanics*. 2011.

[201] J. P. Holman, *Heat Transfer*, Tenth edit. McGraw-Hill Companies, Inc., 2010.

[202] M. Vable, *Mechanics of materials*. Michigan Technological University press, 2009.

[203] J. E. Shigley and L. D. Mitchell, *Mechanical Engineering Design*, Fourth edi. Mc GrawHill Book Company, 1983.

[204] A. Ramirez-canon, "Decomposition of Used Tyre Rubber by Pyrolysis: Enhancement of the Physical Properties of the Liquid Fraction Using a Hydrogen Stream," *Environments*, vol. 5, no. 72, pp. 1–12, 2018, doi: 10.3390/environments5060072.

[205] M. E. Tat and J. H. Van Gerpen, "The Specific Gravity of Biodiesel and Its Blends with Diesel Fuel," *JAOCS*, vol. 77, no. 2, pp. 115–119, 2000.

[206] H. W. Kavunja, "Properties and performance testing of biodiesel from a mixture of jatropha curcas and croton megalocarpus blends," M.Sc. Thesis, University of Nairobi, 2010.

[207] J. Hannah and M. J. Hillier, *Applied Mechanics*. Longman, 1995.

[208] M. E. Mwangi, "A study of waste plastic oil as an alternative fuel to diesel in compression ignition engine," M.Sc. Thesis, University of Nairobi, 2018.

[209] T. C. Keener and W. T. Davis, "Study of the Reaction of S02 with NaHCO3 and Na2CO3," *JAPCA*, vol. 34, no. 6, pp. 651–654, 1984, doi: 10.1080/00022470.1984.10465793.

[210] S. Kimura and J. M. Smith, "Kinetics of the Sodium Carbonate-Sulfur Dioxide Reaction," *AIChE J.*, vol. 33, no. 9, pp. 1522–1532, 1987, doi: 10.1002/aic.690330912.

[211] D. C. Lee and C. Georgakis, "A Single , Particle-Size Model for Sulfur Retention in Fluidized Bed Coal Combustors," *AlChE J.*, vol. 27, no. 3, pp. 472–481, 1981, doi: 10.1002/aic.690270317.

[212] S. Dooley, J. Heyne, S. H. Won, P. Dievart, Y. Ju, and F. L. Dryer, "Importance of a cycloalkane functionality in the oxidation of a real fuel," *Energy and Fuels*, vol. 28, no. 12, pp. 7649–7661, 2014, doi: 10.1021/ef5008962.

LIST OF PUBLICATIONS FROM THIS RESEARCH

1. **Omwoyo J. B.,** Kimilu R. K. and Onyari J. M. (2021). Effects of temperature and catalytic reduction of sulfur content on kinematic viscosity and specific gravity of tire pyrolysis oil. *Chemical Engineering Communications*. https://doi.org/10.1080/00986445.2021.2015339
2. **Omwoyo J. B.,** Kimilu R. K. and Onyari J. M. (2022). Catalytic pyrolysis and composition evaluation of tire pyrolysis oil. *Chemical Engineering Communications*. https://doi.org/10.1080/00986445.2022.2053681

APPENDIX A TECHNICAL DRAWINGS

The orthographic projections of the designed components are indicated as shown below.

Table A1: Indicating list of designed components

Table A1 List of Component Numbers

Component number	Name of component
001	Reactor
002	Condenser
003	Condenser stand
004	Connection tube
005	Pressure gauge tube

Part 001

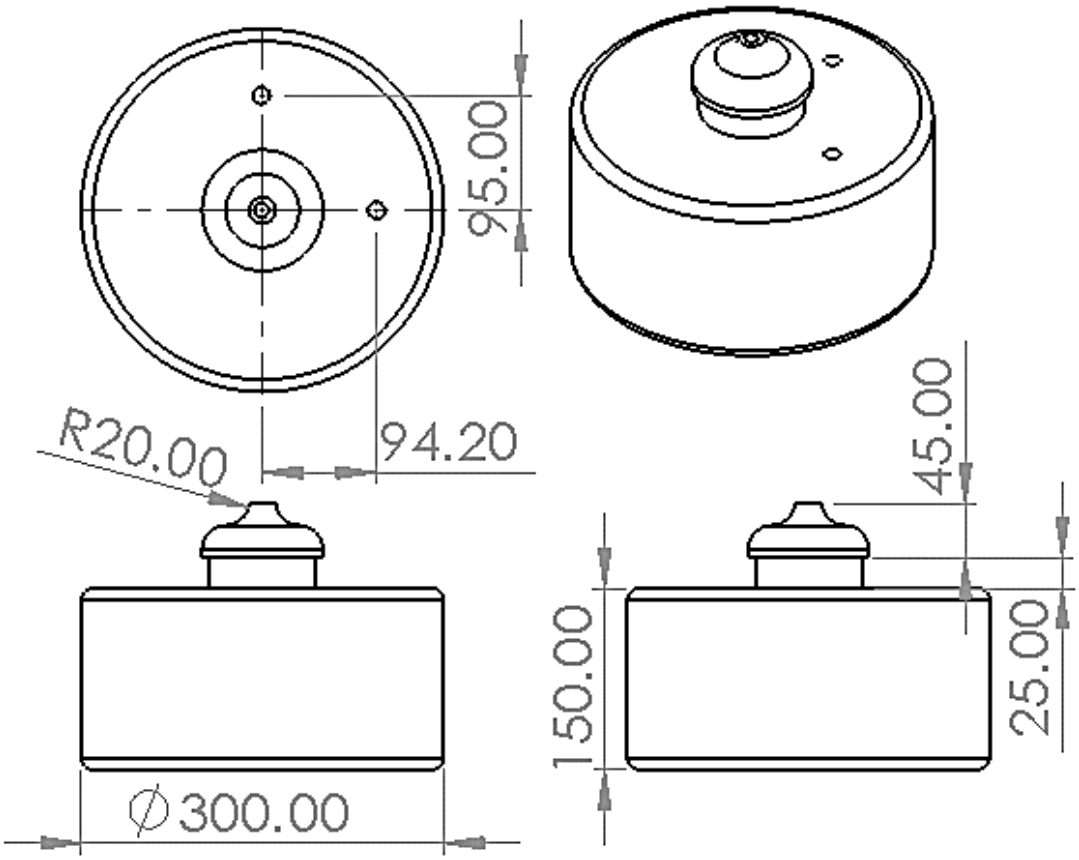

Part 002

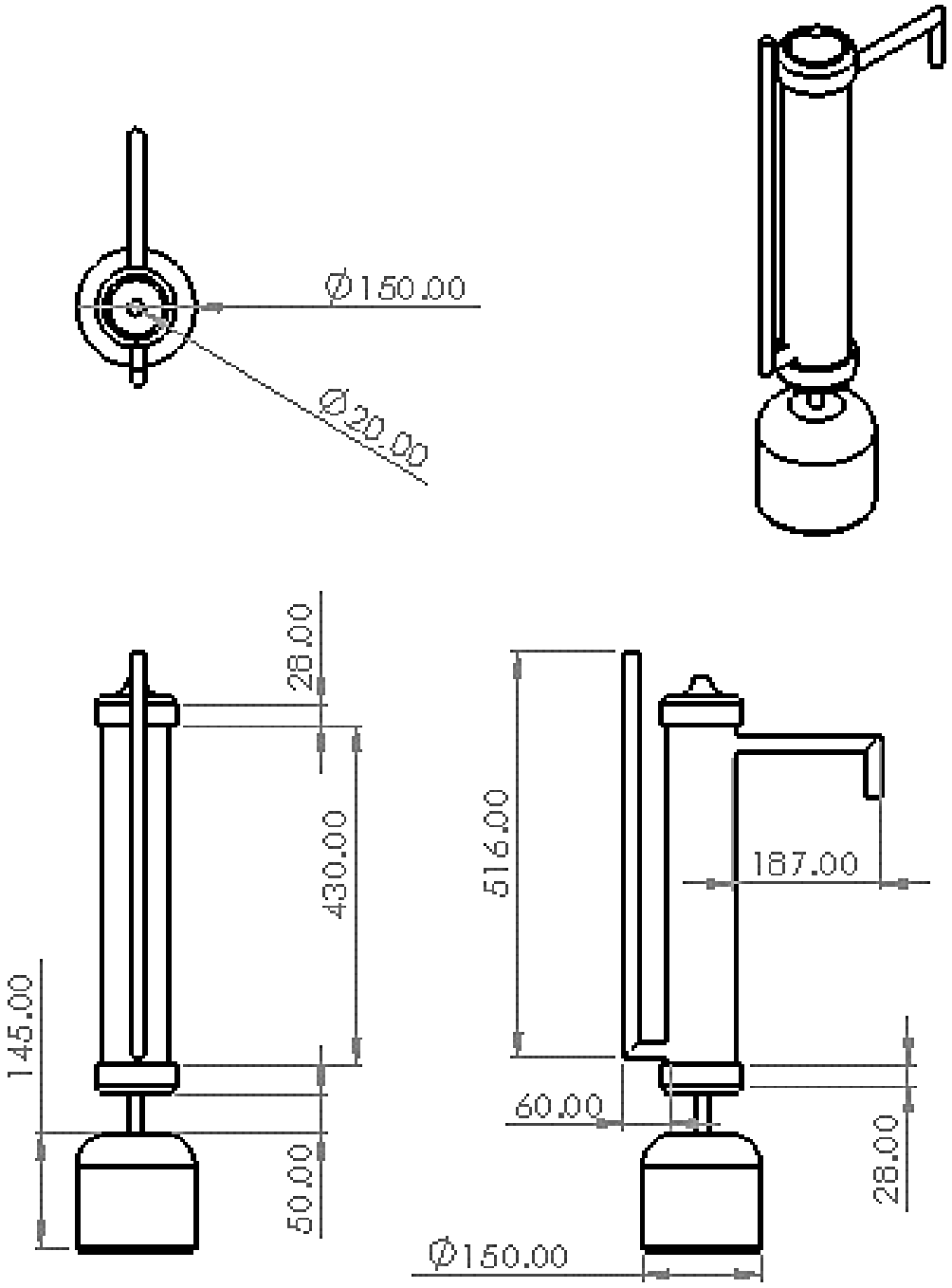
Ø150.00
Ø20.00
28.00
430.00
145.00
50.00
516.00
187.00
60.00
28.00
Ø150.00

Part 003

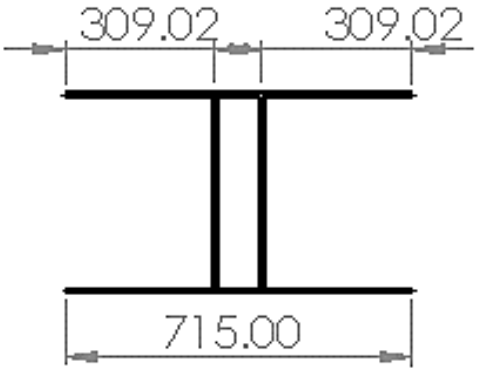

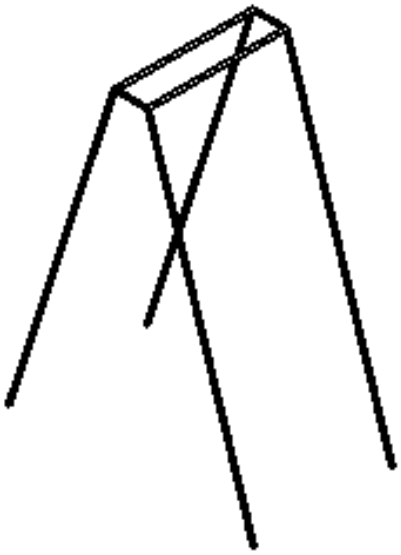

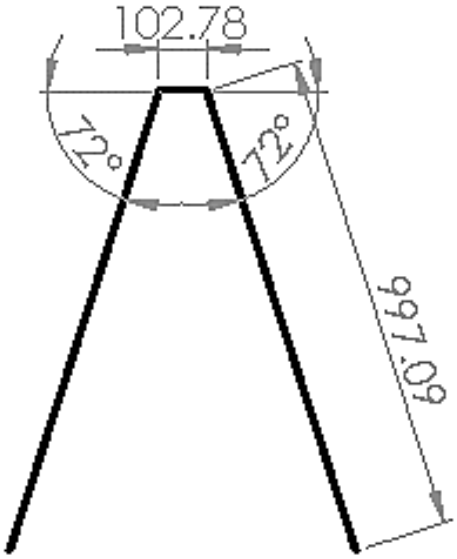

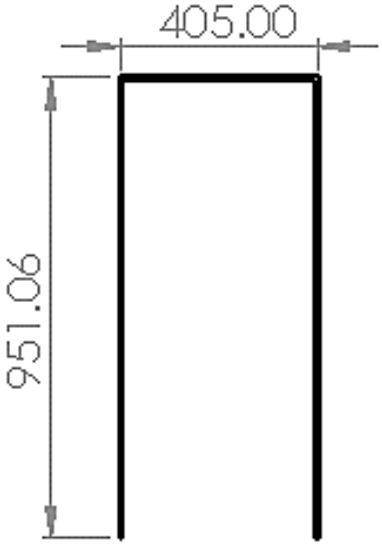

Part 004

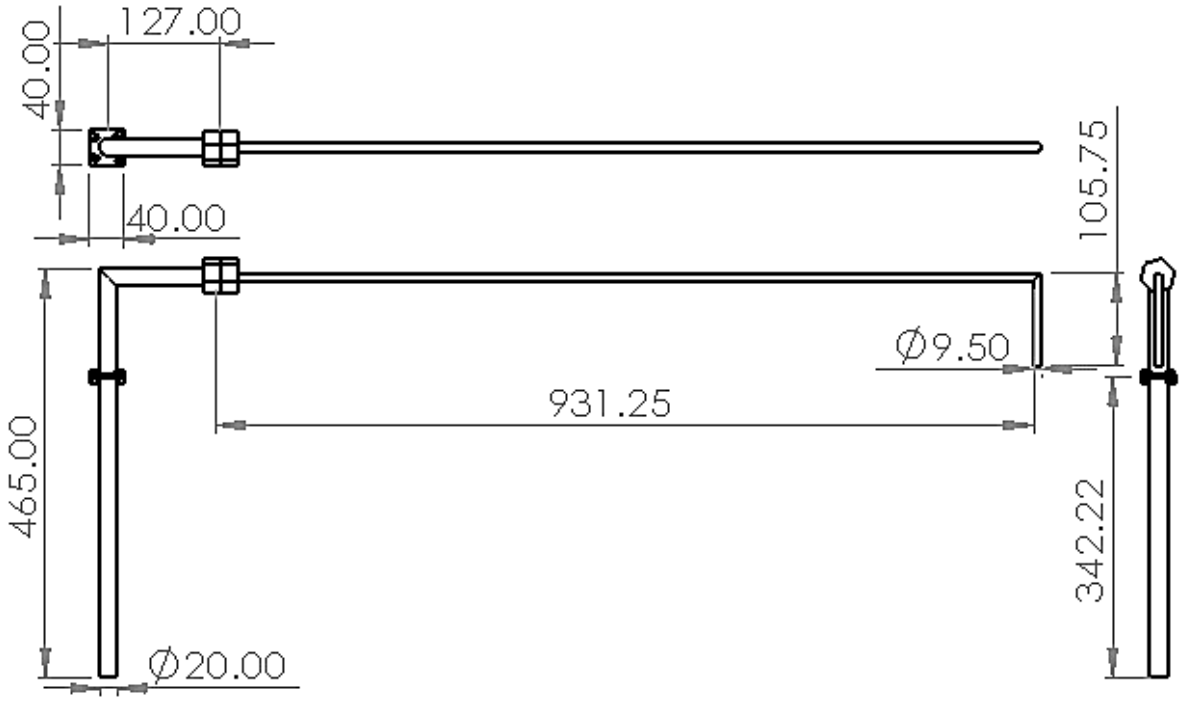

Part 005

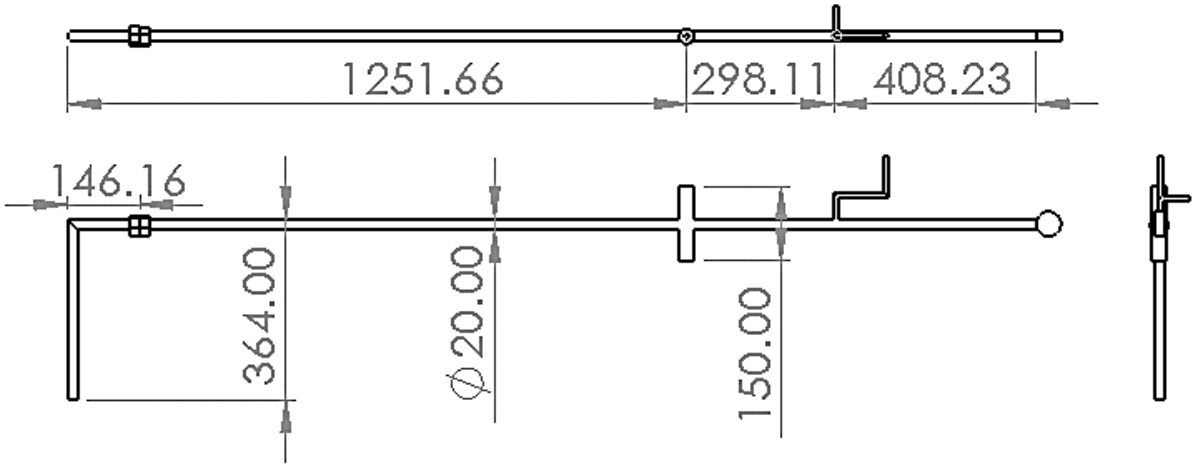

APPENDIX B FABRICATED COMPONENTS

Condenser

Reactor

Pyrolysis system

APPENDIX C GROSS COMBUSTION VALUES FOR SOME COMMONLY USED MATERIALS

Material		Gross Combustion Value (*Btu/lb*)
Carbon	C	14,093
Hydrogen	H_2	61,095
Carbon Monoxide	CO	4,347
Methane	CH_4	23,875
Ethane	C_2H_4	22,323
Propane	C_3H_8	21,669
n-Butane	C_4H_{10}	21,321
Isobutane	C_4H_{10}	21,271
n-Pentane	C_5H_{12}	21,095
Isopentane	C_5H_{12}	21,047
Neopentane	C_5H_{12}	20,978
n-Hexane	C_6H_{14}	20,966
Ethylene	C_2H_4	21,636
Propylene	C_3H_6	21,048
n-Butene	C_4H_8	20,854
Isobutene	C_4H_8	20,737
n-Pentene	C_5H_{10}	20,720
Benzene	C_6H_6	18,184
Toluene	C_7H_8	18,501
Xylene	C_8H_{10}	18,651
Acetylene	C_2H_2	21,502
Naphthalene	$C_{10}H_8$	17,303
Methyl alcohol	CH_3OH	10,258
Ethyl alcohol	C_2H_5OH	13,161
Ammonia	NH_3	9,667

Unit conversion

- 1 kJ/kg = 1 J/g = 10^{-3} GJ/tonne = 0.000278 kWh/kg = 0.4299 Btu/ lb_m = 0.23884 kcal/kg
- 1 Btu/lb_m = 2.326 kJ/kg = 0.55 kcal/kg
- 1 kcal/kg = 4.1868 kJ/kg = 1.8 Btu/lb_m

Source: The Engineering Toolbox

APPENDIX D OPERATION AND MAINTENANCE OF THE PYROLYSIS SYSTEM

Fire is a good servant but it can be master of chaos if not tamed properly. The process of pyrolysis involves generation of highly combustible products that may end up causing fire if not properly contained. A fraction of the resulting pyrolysis oil is petrol (hope everyone is aware of what petrol can cause when it comes into contact with fire). The non-condensable gases are flammable as well. If you are not sure or have no clue of what you want to do, ask and stopping justifying any guess work to contain any form of accuracy.

1 Operation

1. Check if there is any blockage along the connection tube and the pressure gauge tube before assembling the system.
2. Check and ensure that the pressure gauge is in its good working condition.
3. The system connection should be done properly and tightened to avoid any leakage that may occur during the process of pyrolysis.
4. Cooling water should be running before the reactor is fired.
5. The reactor will then be fired.
6. Keep on checking the pressure gauge to ensure that the reactor is as close as possible to the atmospheric pressure.
7. If there is any significant increase in pressure it is an indication of blockage along the connection duct and the process of heating should be stopped immediately and the pressure relieve valve was opened.
8. When the process of pyrolysis is complete, switch off the heating system, dismantle the system and empty the reactor.

2 Maintenance

Reactor

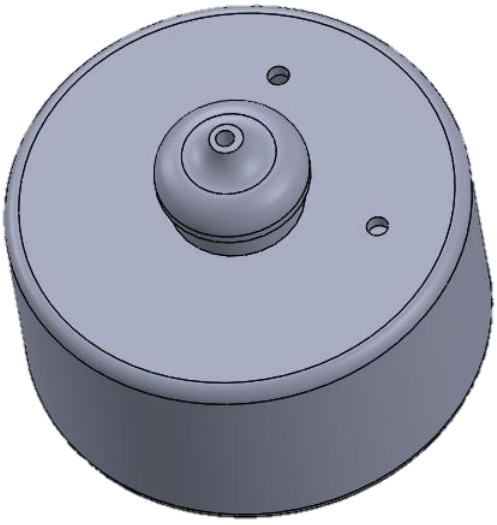

Batch type reactor.

1 It should be emptied after use and washed with hot water with soap to avoid corrosion.
2 It should be dried before storing it away from corrosive agents.
3 Check for any leakage before it is filled with feed material.

Condenser

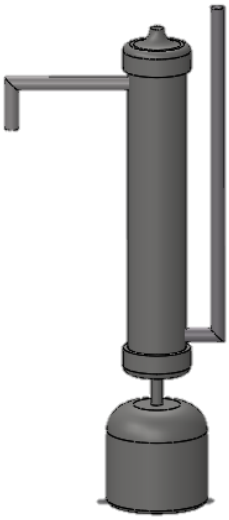

Water Cooled Condenser with oil collector.

1 Empty the cooling water immediately after use.
2 It should be cleaned along the oil path to get rid of any material that may cause corrosion or blockage during its operation.
3 Care should be taken not to avoid breaking the condenser tubes when cleaning.

4 Check for leakages along the tubes by running cooling water through it. If there is any water that the oil outlet of the condenser it indicates that there is a leakage from the shell into the tubes.

Connection tube

Connection Tube.

1 It should be cleaned using hot water with soap.
2 Make sure that there is no foreign material that may cause blockage during the process of pyrolysis.
3 It should be dried and stored after its cleaning.
4 Avoid bending it as this action may cause cracks which will lead to leakage during pyrolysis process.

Pressure gage tube

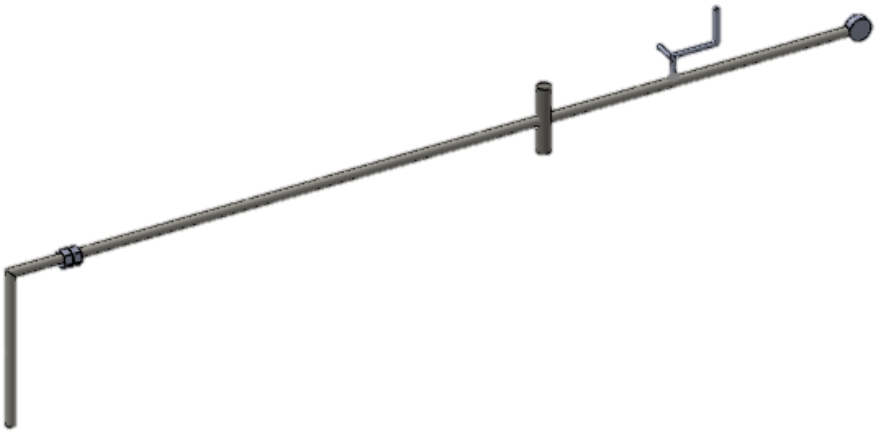

Pressure Gauge Tube.

1 It should be cleaned using hot water with soap.

2 Make sure that there is no any foreign material that may cause blockage giving the false pressure level at the pressure gauge.

3 It should be dried and stored after its cleaning.

Assembled pyrolysis system

The assembled pyrolysis system.

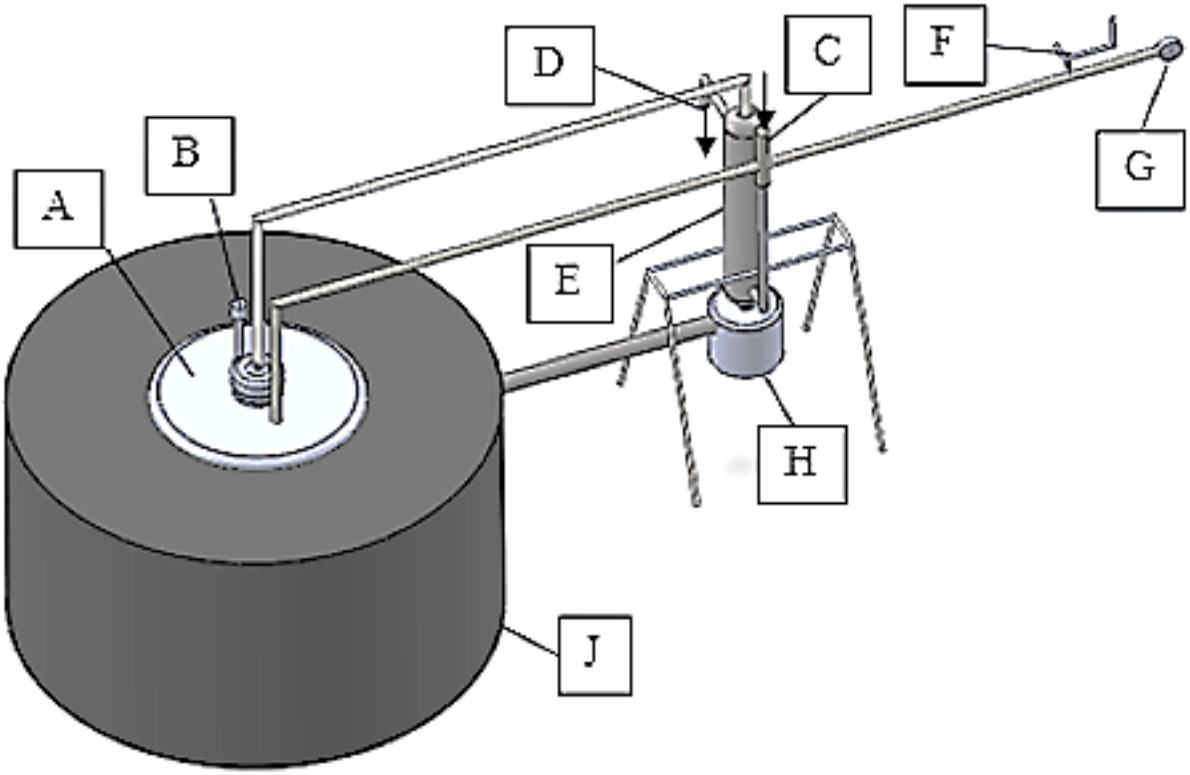

The assembled pyrolysis system.

The list of the labelled components in the assembled pyrolysis system is as follows;

- A – Reactor
- B – Thermocouple
- C – Water Inlet
- D – Water Outlet
- E – Condenser
- F – Pressure Relief Valve
- G – Pressure Gauge
- H – Oil Collector
- J – Heat Supplying Unit

APPENDIX E SAMPLE CALCULATIONS

The sample calculations consisted the determination fuel properties of tyre pyrolysis oil without a catalyst.

Specific Gravity

Specific gravity was calculated at a temperature of 25^0C

Mass of density bottle used was 36.89212g

The specific gravity was calculated as follows;

$$s.g. = \frac{M_O - M_e}{M_W - M_e}$$

Where $s.g = Specific\ Gravity$

$M_e = Mass\ of\ empty\ container$

$M_O = Mass\ of\ Oil + Mass\ of\ empty\ container$

$M_W = Mass\ of\ Water + mass\ of\ empty\ container$

$$Specific\ Gravity = \frac{82.70157 - 36.89212}{86.76034 - 36.89212} = \mathbf{0.91861}$$

Kinematic Viscosity

Viscosity of tyre pyrolysis oil at 25^0C

$$\upsilon_o = \frac{\upsilon_w t_o}{t_w}$$

Where υ_w– Kinematic viscosity of the oil

υ_o– Kinematic viscosity of water

t_o– Time taken for oil to flow.

t_w- Time taken for water to flow from.

Density of water at 25^0 C = 997 kg/m3

Dynamic viscosity of water at 25^0 C = 8.9 millipoise

Kinematic viscosity of water $= \frac{8.9 \times 10^2}{997} = 0.895$

Time taken for tyre pyrolysis oil to flow (t_o) = 177 seconds

Time taken for water to flow (t_w) = 33.5 seconds

$$kinematic\ viscosity\ of\ the\ oil = \frac{177 \times 0.895}{33.5} = \mathbf{4.69319}$$

Sulphur content

Amount of Sulphur content in for tyre pyrolysis oil was calculated as follows

$$Sulphur\ content = \frac{molecular\ mass\ of\ sulphur \times mass\ of\ BaSO_4}{molecular\ mass\ of\ \ BaSO_4 \times weight\ of\ fuel\ combusted}$$

$$Sulphur\ content = \frac{36.0365 \times 0.02156}{233.38 \times 0.3943} \times 10^6 = \mathbf{8443\ ppm\ or\ mg/kg}$$

Cetane index

ASTM D 976 Equation was used.

$$CI = 454.74\ - 1641.416D + 774.74D^2 - 0.544T_{50} + 97.803[log_{10}(T_{50})]^2$$

Where $CI = Cetane\ Index$

$D = Fuel\ Density\ at\ 15\ degrees\ centigrade$

$T_{50} = 50\%\ Recovery\ Temperature\ (degrees\ centigrade)$

$$CI = 454.74\ - 1641.416 \times 0.92395 + 774.74 \times 0.92395^2 - 0.544 \times 210 + 97.803[log_{10}(210)]^2$$

$CI = \mathbf{12.72}$

Calorific value

Calorific value was calculated as follows;

$$Energy\ (cal/g)\ = \frac{(\text{Energy due to the calorimeter} \times \Delta T) - Energy\ due\ to\ capsule}{mass\ of\ Oil}$$

$$\Delta T = (maximum\ temperature\ attained) - (temperature\ at\ firing)$$

Determination of energy due to calorimeter. A mass of 0.7381 g of naphthalene was used and resulted to a temperature increase of 2.977 ^{0}C. The specific enthalpy of combustion of naphthalene is $5160\frac{\text{KJ}}{\text{mol}}$.

$$Energy\ produced\ by\ 0.7381\ g\ naphthalene = 5160 \times 0.0078 \times 0.7381 = 29.707\ KJ$$

$$= 29.707 \times 0.239 = 7100\ cal$$

$$Energy\ due\ to\ calorimeter\left(\frac{cal}{deg}\right) = \frac{7100}{2.977} = 2385\ cal/deg$$

$$Enthalpy\ of\ combustion\ of\ capsule = 2385 \times 0.19 = 453.15\ cal.$$

The energy content was converted from cal. /g and expressed as MJ/Kg using the following converting factor; 1 calorie = 4.184 joules.

Calculation of calorific value was done as follows;

$$Energy\ \left(\frac{KJ}{kg}\right) = \frac{(2385 \times \Delta T) - Capsule\ Energy}{Mass\ of\ Oil} = \frac{(2385 \times 2.3969) - 453.15}{0.54469} \times 4.184 = \mathbf{40.431KJ/kg}$$